

**RADIONUCLIDE PROFILES AND NET SOIL CARBON ACCRUAL IN
MOIST ACIDIC TUNDRA NEAR TOOLIK LAKE, ALASKA**

by

Karyn DeFranco

A thesis submitted to the Faculty of the University of Delaware in partial fulfillment
of the requirements for the degree of Master of Science in Geology

Spring 2018

© 2018 Karyn DeFranco
All Rights Reserved

**RADIONUCLIDE PROFILES AND NET SOIL CARBON ACCRUAL IN
MOIST ACIDIC TUNDRA NEAR TOOLIK LAKE, ALASKA**

by

Karyn DeFranco

Approved: _____
Neil C. Sturchio, Ph.D.
Professor in charge of thesis on behalf of the Advisory Committee

Approved: _____
Neil C. Sturchio, Ph.D.
Chair of the Department of Geological Sciences

Approved: _____
Estella E. Atekwana , Ph.D.
Dean of the College of Earth, Ocean, and Environment

Approved: _____
Ann L. Ardis, Ph.D.
Senior Vice Provost for Graduate and Professional Education

ACKNOWLEDGMENTS

I would like to thank all of the people who contributed in some way to the work described in this thesis. I'd first like to thank my committee: my advisor Professor Neil C. Sturchio, Professor James E. Pizzuto, and Professor Adam F. Wallace for their interest, support, and guidance in my work. I would also like to thank the project principal investigator, Miquel Gonzalez-Meler for providing the samples and useful insight into the project and Michael P. Ricketts and Elana Blanc-Betes for collecting the samples that were used in this thesis.

A special thanks to my family and friends. Words cannot describe how grateful I am for the never-ending support from my mother and father. Thank you for teaching me to rise above any challenge I face with grace and poise. To my old advisor Dr. Holli Frey, thank you for teaching me how to be an independent thinker and perform quality science. You continue to be an amazing advisor, even after I graduated and I am extremely lucky to have learned under your supervision. To my best friend Sarah Kittross, thank you for always being there for me and liking rocks; without you I would have definitely lost all sanity.

Thank you to all the coffee baristas that literally fueled my motivation to complete this project. Thank you to Joe Biden for being the best thing that ever came out of Delaware, I'm sad that I did not get to meet you, despite all of the time I spent at *Brew HaHa!*, but the potential of meeting you was enough to keep me there and constantly caffeinated. Last, but certainly not least, a huge thanks to my dog for being a good boy.

TABLE OF CONTENTS

LIST OF TABLES	vi
LIST OF FIGURES	vii
ABSTRACT	viii

Chapter

1	INTRODUCTION	1
1.1	Importance of Arctic Climactic Modeling	1
1.2	Arctic Tundra Active Layer Importance to Climate Change	4
1.3	Objectives	6
2	METHODS AND MATERIALS	9
2.1	Site Description	9
2.2	Analytical Methods	15
3	RESULTS	18
3.1	Radionuclide Profiles	18
3.2	Soil Organic Carbon and % Carbon Through Soil Profile	21
3.3	Application of ^{210}Pb to Determine Net Carbon Uptake Rates with a Modified Model	24
3.4	Age Calculations	30
4	DISCUSSION	32
4.1	Toolik Soils and Organic Carbon	32
4.2	^7Be : Short-Term Soil Tracer	33
4.3	^{137}Cs : Widely Used Soil Tracer	34
4.4	^{210}Pb : Radionuclide Used for Estimation of Soil Mass Accumulation Rate	36
4.5	Carbon Accumulation Rates	37
4.6	Effect of Snow Depth on Ground Thermal Regime	39
4.7	Active Layer and Thermodynamics in Alaskan Continuous Permafrost Zone	41
4.8	Active Layer and Ecosystem Implications	43

5	SUMMARY AND CONCLUSIONS	47
5.1	Arctic Carbon Cycling	47
5.2	Future Work	49
	REFERENCES	51
Appendix		
	A. TABLES OF DATA MEASUREMENTS AND CALCULATIONS	55
	B. GRAPHS CREATED FOR ALL CORES ANALYZED	59

LIST OF TABLES

Table 1: Data measurements of depth corrected for compaction (cm), soil bulk density (g/cm ³), wt. % Carbon, carbon (g/cm ³), and radionuclide activity (Bq/kg) and corresponding errors (Bq/kg).....	55
Table 2: Table showing the post/pre or unaffected carbon accumulation rates and corresponding error.....	58

LIST OF FIGURES

Figure 1: Projected Temperature and Precipitation Changes by 2100.	2
Figure 2: Climate Change Impacts of the Arctic Carbon Cycle.	4
Figure 3: Four Main Types of Alaskan Arctic Tundra	6
Figure 4: Map of Alaskan Permafrost Zones and Aerial Photo of Site.	10
Figure 5: Soil Profile Photograph of Pit Dug Near Toolik Lake Site.	12
Figure 6: Diagram and Photograph of the Snow Fence Experimental Site.	13
Figure 7: Diagram Depicting Location of Cores in the Snow Fence Site.	14
Figure 8: Image of Core Holes and Core Field Processing.	15
Figure 9: Radionuclide Profile of 2016 INT-5 Core.	20
Figure 10: Graph of 2016 INT-5 Wt. Percent Carbon with Depth	22
Figure 11: Map of Approximate Soil Carbon Quantity in Toolik Lake Area.	23
Figure 12: Diagrams of Three Different Sedimentation Models Considered.	25
Figure 13: Graph of the Standard CIC Model Created for 2016 INT-5 Core.	27
Figure 14: Graph of Modified CIC Model Created for 2016 INT-5 Core.	29
Figure 15: Graph of 2016 INT-5 Calculated Calendar Year vs. Cumulative Dry Carbon.	31
Figure 16: Graph of Daily Recorded Air and Soil Temperatures Near Site.	42

ABSTRACT

The response of the Arctic terrestrial carbon cycle to climate change is one of the largest uncertainties affecting climate change predictions and research. Current models give a wide, varying estimate of the fate of currently frozen permafrost organic carbon with warming of the high-latitude climate. This study is an investigation of permafrost soil cores taken in 2012 and 2016 from a snow fence experiment installed in 1994 at Toolik Lake, AK. Data was acquired for depth profiles of radionuclides (^7Be , ^{137}Cs and ^{210}Pb), organic carbon contents, and carbon stable isotope ratios of permafrost active layer cores taken at locations that had different winter snow depths. Be-7 activities were measurable only in the top 1-3 cm, corresponding to the canopy thickness of current-year growth. Profiles of excess ^{210}Pb were normalized to cumulative dry mass vs. depth to obtain mass accumulation rates of the organic-rich horizon under a set of assumptions regarding initial ^{210}Pb activity in the accumulating material. The resulting age profiles were compared to the depth of the ^{137}Cs peak that was deposited in 1963, yielding agreement in some but not all cases. Previous studies have shown that ^{210}Pb deposition and accumulation is correlated with precipitation amounts, and also may be affected by local topography. Therefore, standard ^{210}Pb models do not accurately represent the conditions at the Toolik Lake snow fence site because of large variations in winter snow depth over a small distance. Normalization

of the ^{210}Pb activities to the organic carbon content of the cores gives historical information on the rate of net carbon uptake of the permafrost active layer, and an improved accounting of the response of the soil carbon system to changing snow depth that includes winter C loss, as a proxy for climate warming. Results from this method indicate substantial increases in rates of soil organic carbon accumulation following snow fence installation in the region of increased snow depth. Based on these results, increased winter precipitation in the Alaskan Arctic Continuous Permafrost Zone may be expected to cause increases in soil insulation, growing season, vegetation growth, and active layer thickness. This ultimately will lead to an increased organic carbon availability and general permafrost degradation with time. These changes may contribute positive feedback to the carbon cycle, and therefore promote the effects of current climate change predictions.

Chapter 1

INTRODUCTION

The escalating quantities of greenhouse gases in our atmosphere and their effect on climate is one of the fastest growing and most pressing topics of research in the field of environmental sciences. Global air temperature has risen significantly since the middle of the 19th century, with a strong warming trend since ~1980 (Alley et al. 2003). Simultaneously, Arctic amplification is occurring whereby the near-surface region of the northern high latitudes is warming at rates double that of lower latitudes (Cohen et al., 2014).

1.1 Importance of Arctic Climactic Modeling

Arctic regions are expected to experience the greatest changes in their ecosystems as climate warms (Fig. 1). Measurements of such changes in the Arctic regions may facilitate prediction of the larger, slower global responses to climate change (Garfinkel and Brubaker 1980; Lachenbruch and Marshall 1986). The major concern for Arctic climate change is that with warming, the permafrost active layers will deepen, possibly eliminating permafrost in some areas, and this will release stored organic carbon to the atmosphere in the form of greenhouse gases CO₂ and CH₄ (Walker et al., 2013). Current models give varying estimates of the fate of currently frozen permafrost carbon as the high-latitude climate warms, due to a lack of

information and understanding of spatial and temporal variability of Arctic carbon dynamics.

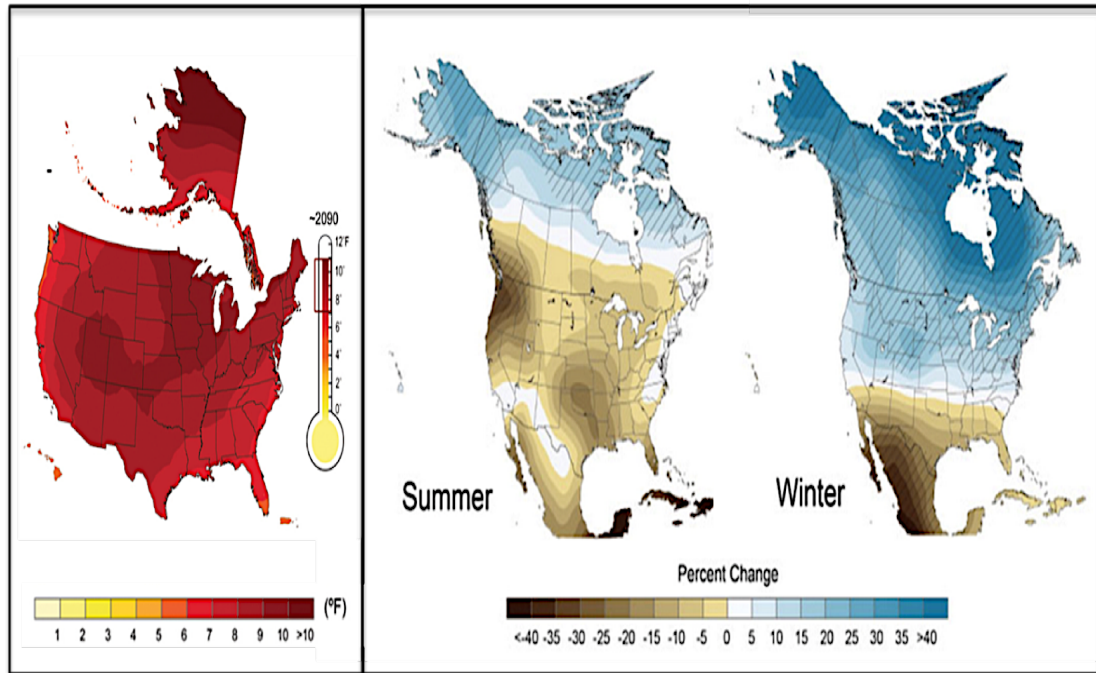


Figure 1: Projected temperature and precipitation changes by 2100 based on the highest GHG emissions scenario (Modified from EPA, 2010). Arctic regions are projected to be the most sensitive to changes in mean surface temperature and precipitation patterns. Image on left shows a projected temperature increase of $\sim 10^{\circ}\text{F}$; Image on right shows a projected increase in winter precipitation by 35% to $>40\%$.

Understanding the Arctic carbon cycle is essential for accurate assessment and prediction of short-term and long-term regional responses and associated feedbacks to climate change effects (Chapin et al., 2005). Studies indicate that during the 1990s, the Arctic region was on average a modest CO_2 sink of less than 0.5 Pg C/yr (McGuire et

al., 2012). In Arctic tundra systems, carbon cycling is a complex, but heavily reliant directly on precipitation, and its indirect effects, and permafrost stability/degradation (Fig. 2) with positive trends in carbon storage under colder and wetter conditions, and negative trends under drier and warmer conditions (McGuire et al., 2012; Thompson et al., 2006). As climate warming causes permafrost to thaw and precipitation to increase across the tundra, decomposition and respiration rates in Arctic ecosystems may change as a result of increased soil moisture availability. More specifically, the increase in moisture may lead to increased decomposition losses; once soil is thawed, soil temperature is a less important factor than soil moisture (Hicks et al., 2013). Arctic soil thawing can cause many different ecological, biological, and environmental effects (Fig. 2). Most of the predicted effects depend on the change in soil organic carbon, therefore it is essential to understand the magnitude of change that global warming will have on the organic carbon cycle in Arctic soils.

Global GHG Drivers of Arctic C Cycling

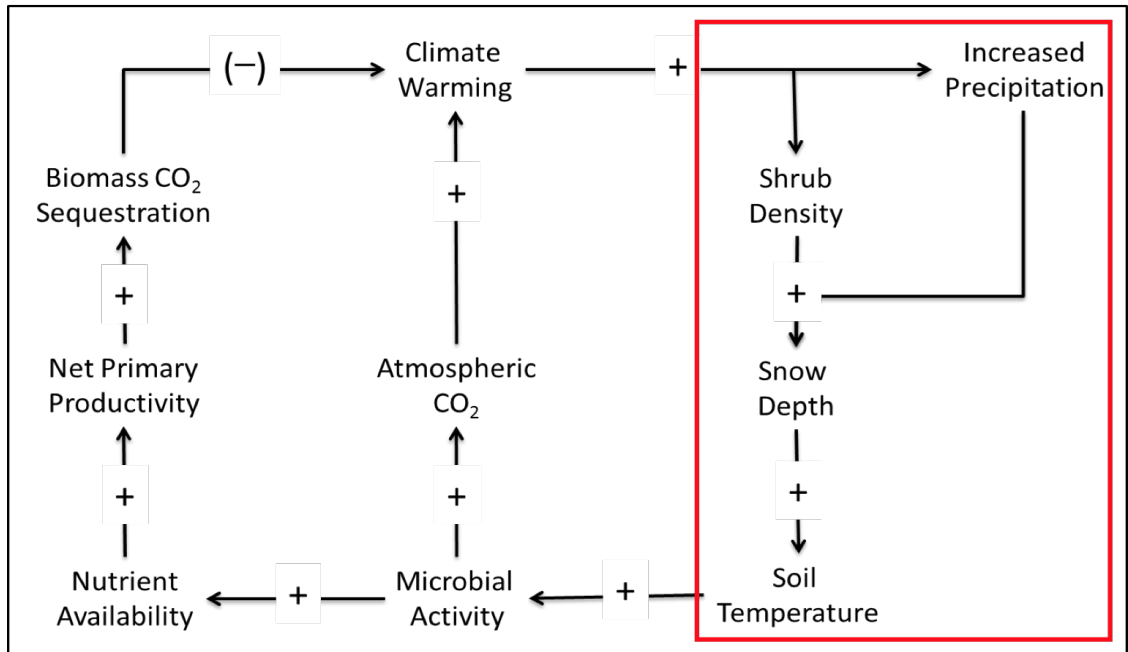


Figure 2: Simplified feedback loop hypotheses for climate change impacts of the Arctic C cycle; area of focus of this study is circled in red (Modified from Sturm et al., 2005). In this study we focused on increased precipitation and its effects on the areas enclosed in red, in order to understand the effect on carbon accumulation rates, and ultimately biomass CO₂ sequestration.

1.2 Arctic Tundra Active Layer Importance to Climate Change

Warming and thawing of the active soil layer in the Arctic could drive changes in the amount and type of organic matter and the mineral horizon. Field studies of Arctic soils indicate that warming and drying leads to higher soil respiration rates than warming alone (Oberbauer et al., 2007; Natali et al., 2015). Elberling et al. (2013) showed that permafrost soil carbon losses in laboratory incubations varied between 9% and 75%, depending on drainage conditions (higher drainage yielded greater carbon

loss), indicating that the rate of carbon mobilization will depend strongly on future soil moisture conditions, and also that carbon in near-saturated conditions may remain largely immobile. The Arctic is categorized into four main tundra types: Dry Tundra, Moist Tundra, Wet Tundra, and Aquatic Tundra based on a hierarchical tundra vegetation classification scheme developed by Walker (1983, 1985) (Fig.3). Projected climatic effects will vary between tundra types.

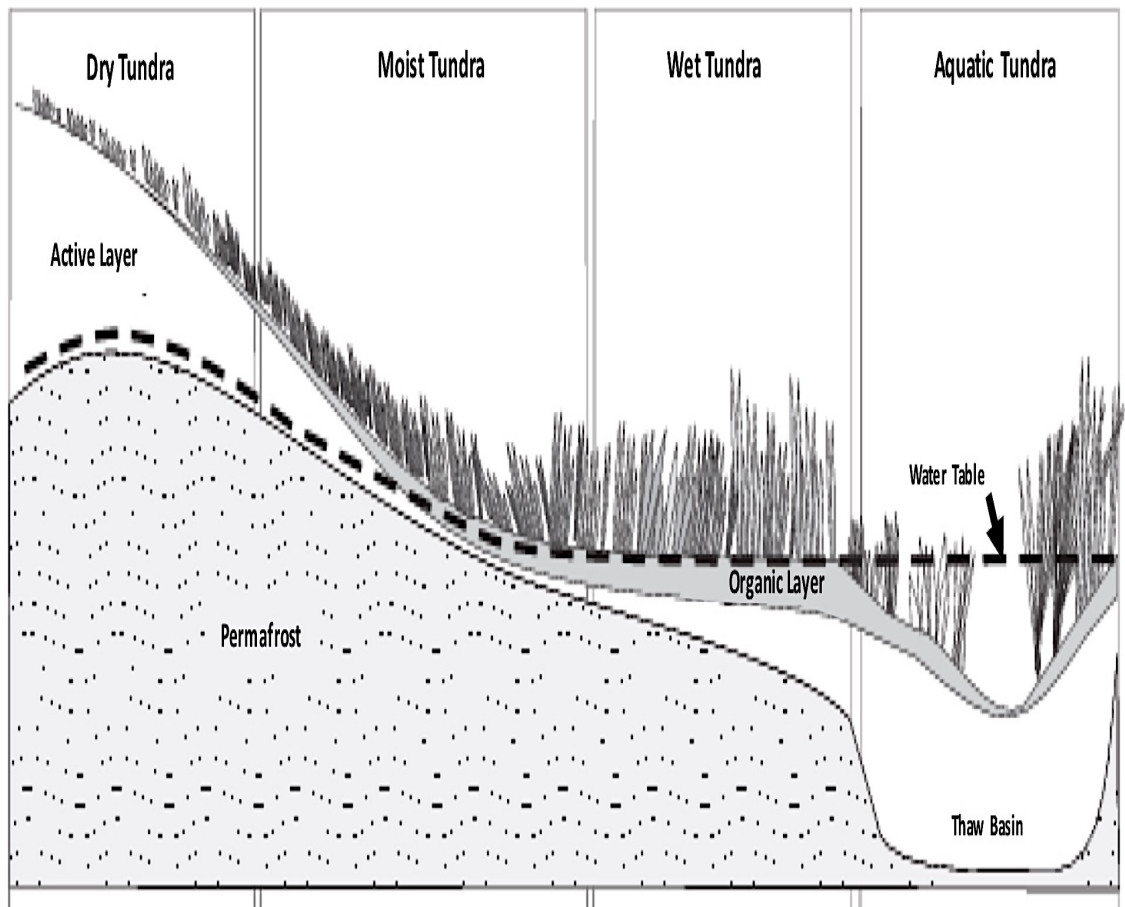


Figure 3: There are four main types of tundra classified based on the hierarchical tundra vegetation classification scheme developed by Walker (1983, 1985). Tundra environments can be especially sensitive to disturbances for several reasons: permafrost, short growing season, extreme winter wind, and cold temperatures. Our site is located in the Moist Tundra (Modified Walker et al., 1983).

1.3 Objectives

In this study we measured and compared the ^7Be , ^{137}Cs , and ^{210}Pb activity profiles, carbon contents, and carbon stable isotope ratios of permafrost soil cores taken from a snow-fence experiment in the moist acidic (tussock) tundra near Toolik Lake, Alaska in 2012 and 2016. ^{137}Cs has a half-life of 30.2 years, and has a known global

maximum deposition in 1963-1964. Therefore, the ^{137}Cs peak activity in soil profiles gives a reference horizon of known age, and the vertical distribution of ^{137}Cs can reflect annual or decadal deposition time and mechanical movement (Staunton *et al.*, 2002; Harden *et al.*, 2008; Klaminder *et al.*, 2014). Differences in ^{210}Pb activity among different soil plots leeward of the snow fence reflect variations in biotic (i.e. level of decomposition) (Bockheim *et al.*, 2003) and physical (i.e. soil compaction and/or consolidation) (Ruehlmann & Körschens, 2009) processes in response to treatment. Profiles of ^{210}Pb activity in soil cores were analyzed with a modification of the Constant Initial Concentration (CIC) model (Goldberg, 1963; Robbins, 1978; Appleby and Oldfield, 1983) to obtain estimates of apparent net carbon accrual rates during the pre-1994 (i.e., pre-snow fence) and post-1994 periods (i.e., post-snow fence), and to assess the effect of varying snow depth and soil temperature on these rates. The goal of this study is to better quantify the effects of climate change on soil carbon inventories in the Arctic, in the moist tussock tundra, and their potential impact on the global carbon cycle.

Lead-210 (half-life = 22.3 years) is a natural geogenic radioisotope of the ^{238}U decay series (Mabit *et al.*, 2008). ^{210}Pb is a decay product of ^{222}Rn within the soil, which in turn is produced by decay of its parent nuclide ^{226}Ra . Some of the ^{222}Rn produced by ^{226}Ra decay in soils diffuses into the atmosphere, however, where it decays to ^{210}Pb that is deposited to soil as atmospheric fallout. This results in soil ^{210}Pb activity in excess of that produced in-situ by decay of its parent ^{226}Ra , and this excess ^{210}Pb is generally referred to as “unsupported” or “excess” ^{210}Pb in the soil profile (Mabit *et al.*, 2008). Unsupported ^{210}Pb in undisturbed soils typically has a maximum activity at the surface of the soil profile, and decreases exponentially with

depth as it decays (Mabit et al., 2008). Unsupported ^{210}Pb is a useful tracer for long-term rates of soil redistribution and accumulation for up to 100 years (Mabit et al., 2008).

There are two common models used to calculate ^{210}Pb dates under varying sediment accumulation rates: the constant rate of ^{210}Pb supply (CRS) model, and the constant initial concentration (CIC) model (Goldberg, 1963; Robbins, 1978; Appleby and Oldfield, 1983). Both models assume a constant flux of ^{210}Pb from the atmosphere. The CRS model assumes that ^{210}Pb fallout from the atmosphere occurs at a constant rate, regardless of variations in the sediment accumulation rate, so that the initial unsupported ^{210}Pb activity of sediment may be variable. The CIC model assumes that the initial unsupported ^{210}Pb activity in sediment is constant regardless of variations in sediment accumulation rate (Appleby and Oldfield, 1983). The ^{210}Pb supply to the sediment is a complex combination of atmospheric deposition and ^{222}Rn exhalation from soil; however, in discontinuous and continuous permafrost Arctic tundra soils, the exhalation rate of ^{222}Rn is extremely low (Baskaran and Naidu, 1995). The results of the present study showed a clear near-surface ^{210}Pb activity maximum in all cores analyzed, supporting the findings that ^{210}Pb within Arctic soil is dominantly from atmospheric deposition. The low ^{226}Ra activity of the organic layer is due to its low mineral content, so the majority of ^{210}Pb within the organic layer is unsupported. However, varying snow depths after construction of the snow-fence in 1994 caused a change in the local annual deposition of ^{210}Pb downwind of the snow fence, which violates the key assumption of constant ^{210}Pb deposition rate of the CRS and CIC models. Therefore, we developed an alternative approach which is described in section III.

Chapter 2

METHODS AND MATERIALS

2.1 Site Description

The experimental site from which the active-layer soil cores were collected is located in the Arctic Foothills in the continuous permafrost zone of the Alaskan Arctic, near Toolik Lake, Alaska (68°38'N, 149°38'W; 760 m). The mean average air temperature of the region is -8°C, with summer temperatures averaging 10.5°C. The site is located near the Toolik Field Station, managed by the Institute of Arctic Biology at the University of Alaska Fairbanks (UAF), with cooperative agreement support from the Division of Polar Programs, Directorate for Geosciences at the National Science Foundation (NSF).

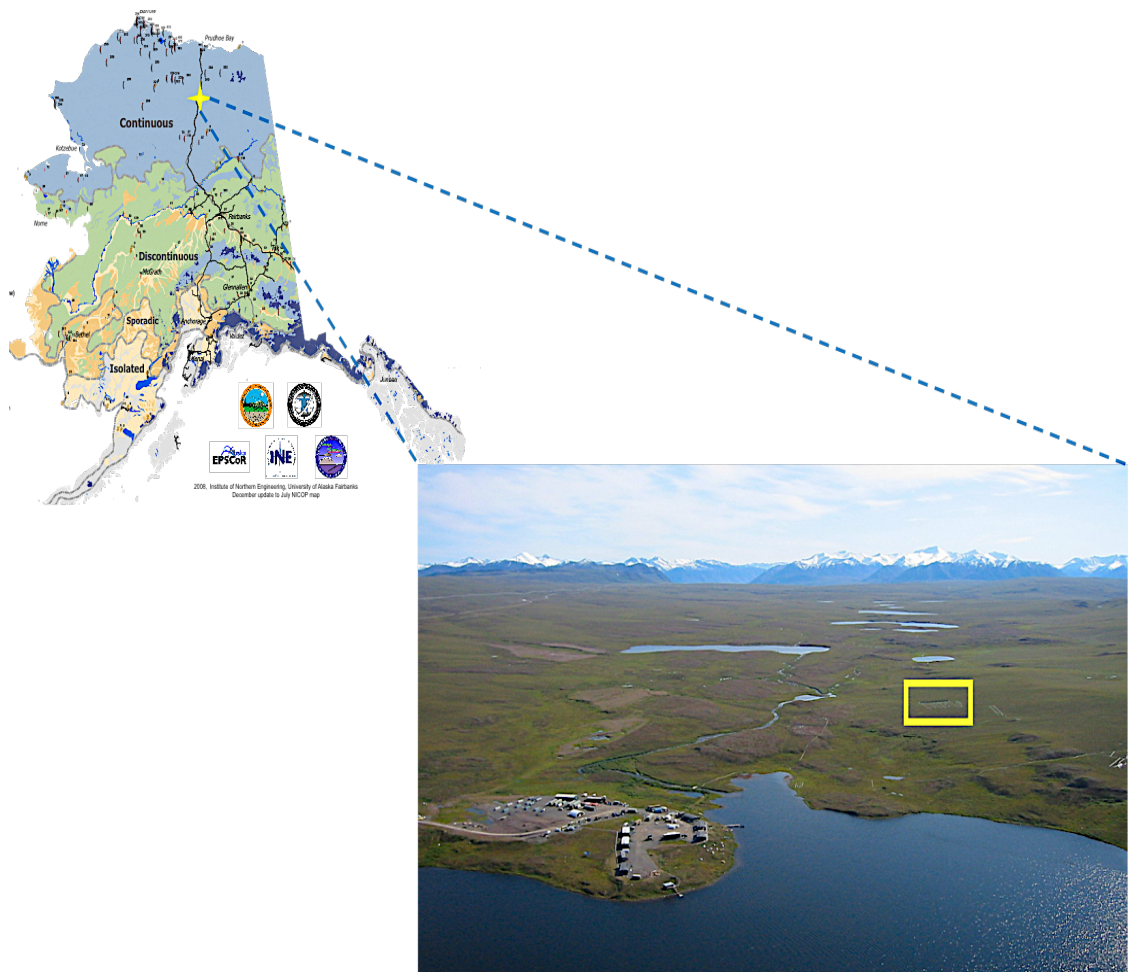


Figure 4: Map of the permafrost zones in Alaska (Modified from UAF, 2008) showing the location of Toolik Research station in the Continuous permafrost zone and an aerial photo of Toolik Lake, the research station, and the snow fence experimental site enclosed in yellow.

The active layer thickness averages ~30 cm during the growing season and reaches a maximum thaw depth of 45-50 cm by late August (Welker, Arctic LTER). Annual snow accumulation is 45-80 cm, with the snow-covered season typically running from mid-September to late May. Soils are classified as acidic, coarse-loamy, poorly-drained soils with shallow organic layers transitioning to organic-enriched

mineral layers with depth (Fig. 5) (Michaelson *et al.*, 1996; Ping *et al.*, 1997). The total organic carbon measured in these soils is essentially equal to the total organic carbon measured. This, combined with the acidity of the soils and negligible input of sedimentation from other input mechanisms (i.e. windblown), makes mineral content of the upper layers negligible. Vegetation is dominated by tussock forming sedges (*Eriophorum vaginatum*), and interspaced shrubs (*Betula nana*, *Salix pulchra*) and mosses (*Sphagnum sp.*) characteristic of moist acidic tundra across the Alaskan North Slope (Walker *et al.*, 1994; Wahren *et al.*, 2005).

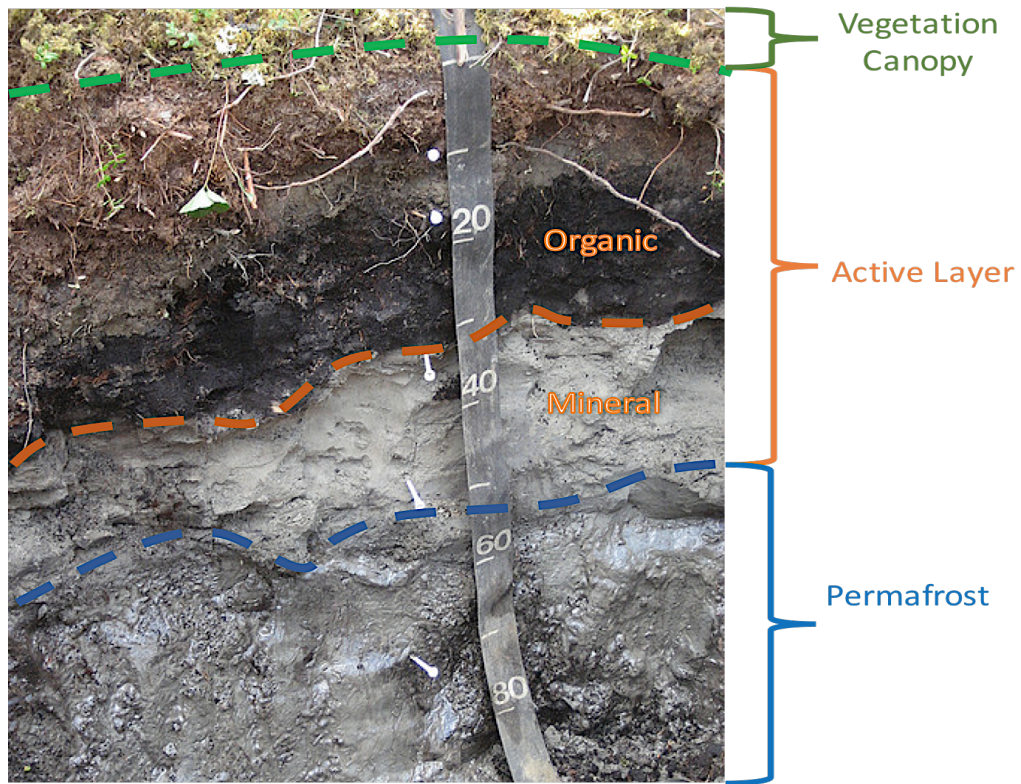


Figure 5: Pit dug in moist acidic tundra near Toolik Lake in August 2008, but not in the experimental snow fence site. Visible representation and thickness of vegetation canopy, organic and mineral layers of the active layer, and permafrost depth. Note the varying depth of each layer across the picture, showing site-specific natural variation.

Two 2.8x60 m snow fences were built perpendicular to prevailing winter winds near Toolik Lake, Alaska to artificially increase snow accumulation because anticipated future effects of global warming on the Arctic predicts an increase in winter precipitation (Fig. 2; Fig. 6). One snow fence was installed in 1994 (ITEX, International Tundra Experiment), and the other in 2006 (Walker *et al.*, 1999; Welker *et al.*, 2000; Blanc-Betes *et al.*, 2016).

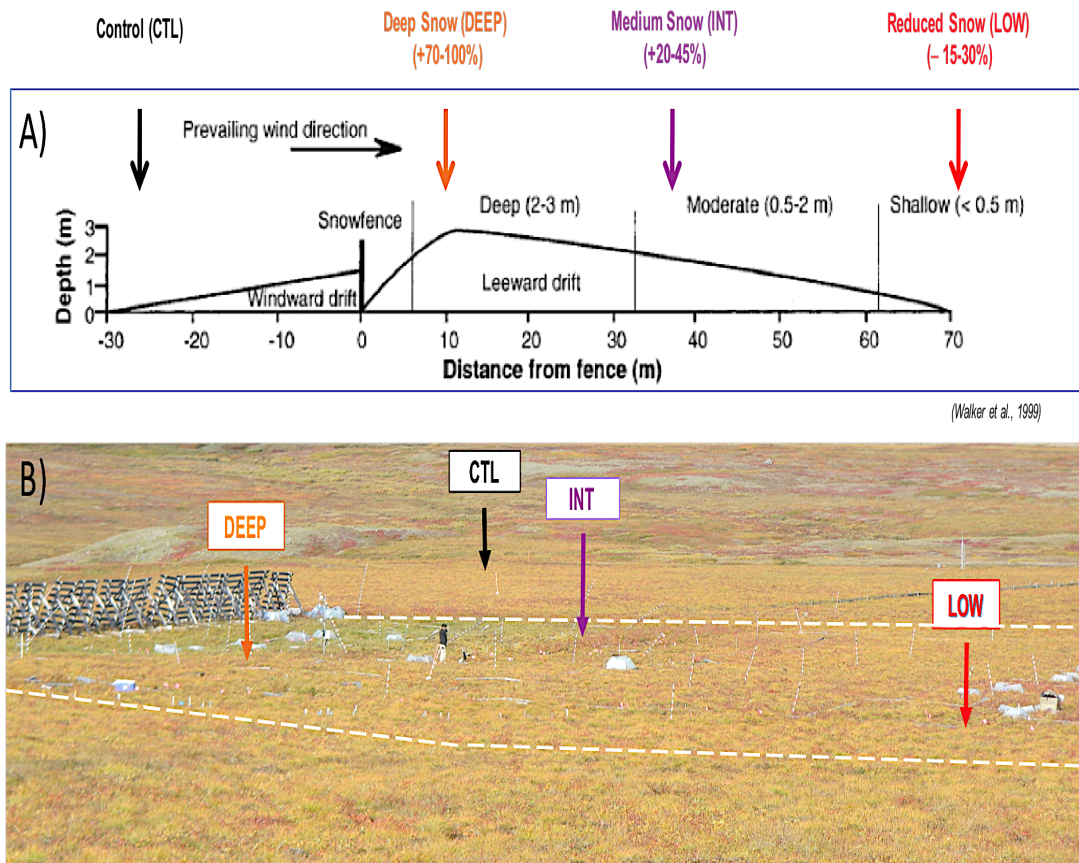


Figure 6: Figure of the snow fence experimental site near Toolik Lake where the cores were collected. **A)** Diagram of the snow fence showing estimated snow depth in meters, general snow depth locations in proximity to the snow fence, and prevailing wind direction (Modified from Walker et al., 1999). **B)** Photograph of the snow fence experimental site around the time of core collection, August 2016, with estimates on varying snow depth locations. Control plots are perpendicular and outside of the zone of influence of the snow fence. Deep, Intermediate, and Low plots are located parallel to the snow fence at varying distances (see Fig. 7).

Soil cores (4.8 cm diameter) were collected at each plot (Fig. 7) between 10am and 3pm over 4 days in early August of 2012 and 2016 to depths of ~30cm, wrapped in Al foil and plastic bags, and stored frozen until analysis (Fig. 8).

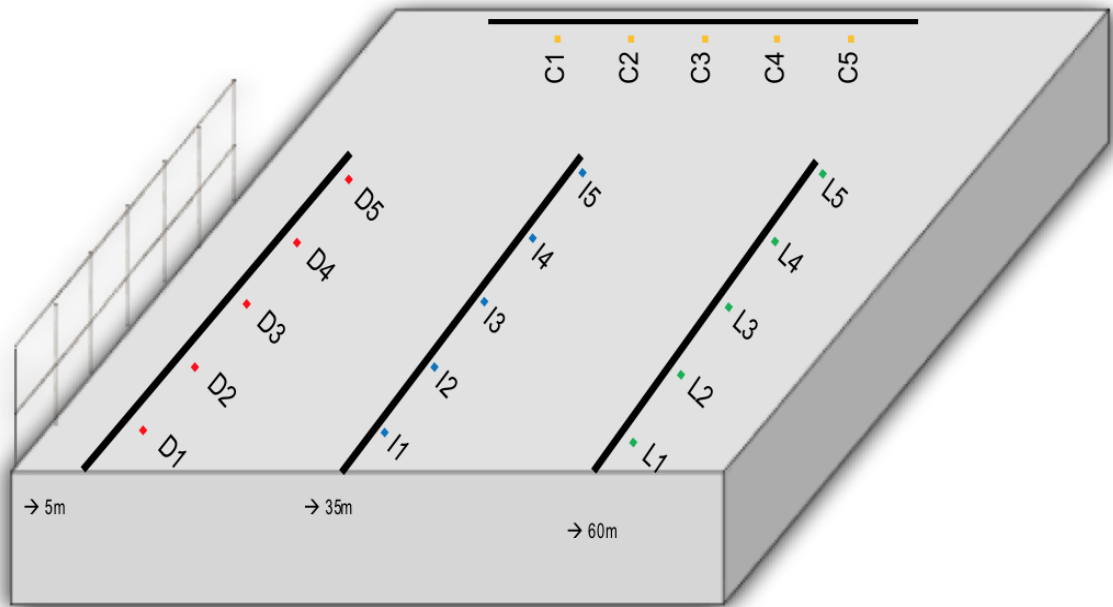


Figure 7: Diagram depicting the parallel rows of the cores and numerical locations along the plot in varying distances from the snow fence. Control cores are perpendicular to the snow fence and not directly in the zone of influence of the snow fence, but still in close proximity. Note: DEEP cores are ~5m, INT cores are ~35m, and LOW cores are ~60m from the snow fence.

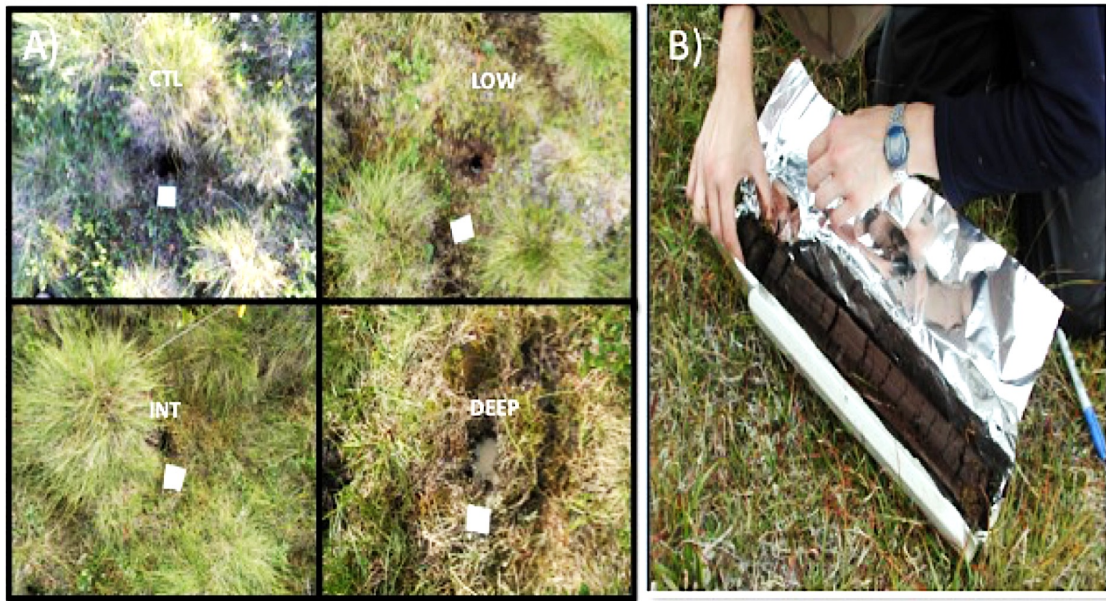


Figure 8: Image of core holes and core processing at site in August, 2016. **A)** Images of post-coring holes left in experimental site after cores were taken. Note the tussock vegetation; coring directly through the tussock vegetation patches was avoided. Note the DEEP core hole is filled with water and the ground surrounding the hole is disturbed; the DEEP plots were water logged soils and often completely saturated **B)** Image showing how the cores were wrapped in aluminum foil and packaged carefully at the site for later transport.

2.2 Analytical Methods

Cores were sectioned into 1-cm depth increments of known volume, weighed before drying, and then air-dried to a constant weight for the direct determination of soil water content and bulk dry density (g cm^{-3}) at the University of Illinois at Chicago. Aliquots (typically 2-3 g) of the homogenized dry samples were then analyzed at the University of Delaware for ^7Be , ^{137}Cs and ^{210}Pb using gamma spectrometry. Two high-purity Ge gamma spectrometers (Model GWL-170-15-LB-AWT with 15-mm well diameter, EG&G Ortec, Ametek, Inc.) were used to measure

gamma emissions. Radionuclide photopeaks quantified in this study were ^7Be (477.2 keV), ^{210}Pb (46.5 keV), ^{137}Cs (661.6 keV) and ^{226}Ra (186.2 keV). Gamma spectrometers were calibrated using efficiency equations based on measurements of certified radionuclide standards, including DL-1A (Reference Uranium-Thorium Ore, Canada Centre for Mineral and Energy Technology, Ontario, Canada) for ^{210}Pb and other U- and Th-series radionuclides, and NIST 4357 (Standard Reference Material 4357, National Institute of Standards and Technology, Gaithersburg, Maryland, USA) for ^{137}Cs adjusted for decay from the date of certification. The efficiency at the ^7Be energy was obtained by interpolation between the nearest large peaks of the U- and Th-series nuclides present in secular equilibrium in the DL-1A reference material. Specific activities and one sigma counting errors were calculated using standard counting techniques (Mook, 2001) and are reported in Becquerels per kilogram dry mass (Bq/kg). Reported activities were corrected for detector background and decay from time of sampling to the starting time of the gamma spectrometry measurement. Limits of quantification for radionuclides were defined as three times the standard deviation of the background under the peak used for the activity quantification, and values less than the limit of quantification are not reported.

Total C and N contents (wt. %) and stable isotopic compositions ($\delta^{13}\text{C}$ and $\delta^{15}\text{N}$) were determined by using a zero-blank Elemental Analyzer (Costech Analytical, EC4010; Valencia, CA, USA) coupled through a ConFlo III interface to a Thermo Finnigan Delta-Plus XL isotope-ratio mass spectrometer. Total C values are effectively equal to total soil organic C (SOC) because inorganic C is negligible in the moist acidic tundra active layer samples. Precision of C and N concentrations was \pm

1-2 wt. %, and that of $\delta^{13}\text{C}$ and $\delta^{15}\text{N}$ values was in the range of $\pm 0.3\text{-}0.5\text{‰}$, based on replicate analyses of samples and standards.

Chapter 3

RESULTS

3.1 Radionuclide Profiles

Seven cores collected in Summer 2016 were measured for ^7Be , ^{137}Cs and ^{210}Pb (Appendix I: Table 1). These cores include CTL-5, CTL-4, CTL-2, INT-5, INT-3, DEEP-4, and LOW-2, named according to depth of snow and grid location downwind of the snow fence (Fig.7). One core collected in Summer 2012, CTL-2, was also measured for ^7Be , ^{137}Cs and ^{210}Pb . Core profiles of the measured radionuclides were compared and showed contrasting results depending on location (Table 1; Appendix II).

Depths of maximum ^{137}Cs and ^{210}Pb activities varied significantly between core sites. Core LOW-2 had measurable values for ^7Be activity between 0-4 cm depth, maximum ^{137}Cs activity at 6-7 cm, and maximum ^{210}Pb activity in the upper-most portion of the core, that decreased with increasing depth (Table 1; Appendix II). Core INT-3 had measurable values for ^7Be activity between 0-2 cm depth, maximum ^{137}Cs activity at 2-3 cm, and maximum ^{210}Pb activity at 1-2 cm (Fig. TBD). Core DEEP-4 had measurable values for ^7Be activity between 0-4 cm depth, maximum ^{137}Cs activity at 4-5 cm, and maximum ^{210}Pb activity in the upper-most portion of the core that decreased with increasing depth (Table 1; Appendix II). Core CTL-5 had measurable

values for ^7Be activity between 0-3 cm depth, maximum ^{137}Cs activity at 8-9 cm, and maximum ^{210}Pb activity in the upper-most portion of the core that decreased with increasing depth (Table 1; Appendix II).

Maximum activities of the three radionuclides vary between cores. Core INT-3 has the lowest maximum ^{137}Cs activity at 122.4 Bq/kg, core DEEP-4 has the highest maximum activity of ^{210}Pb at 1335 Bq/kg, and core CTL-5 had the lowest maximum ^7Be activity at 16.9 Bq/kg (Table 1). General trends include decreasing ^{210}Pb activities with increasing depth; deeper ^{137}Cs peaks in control cores and those from low snow cover; and deeper maximum ^{210}Pb activities in areas of intermediate/deep snow cover.

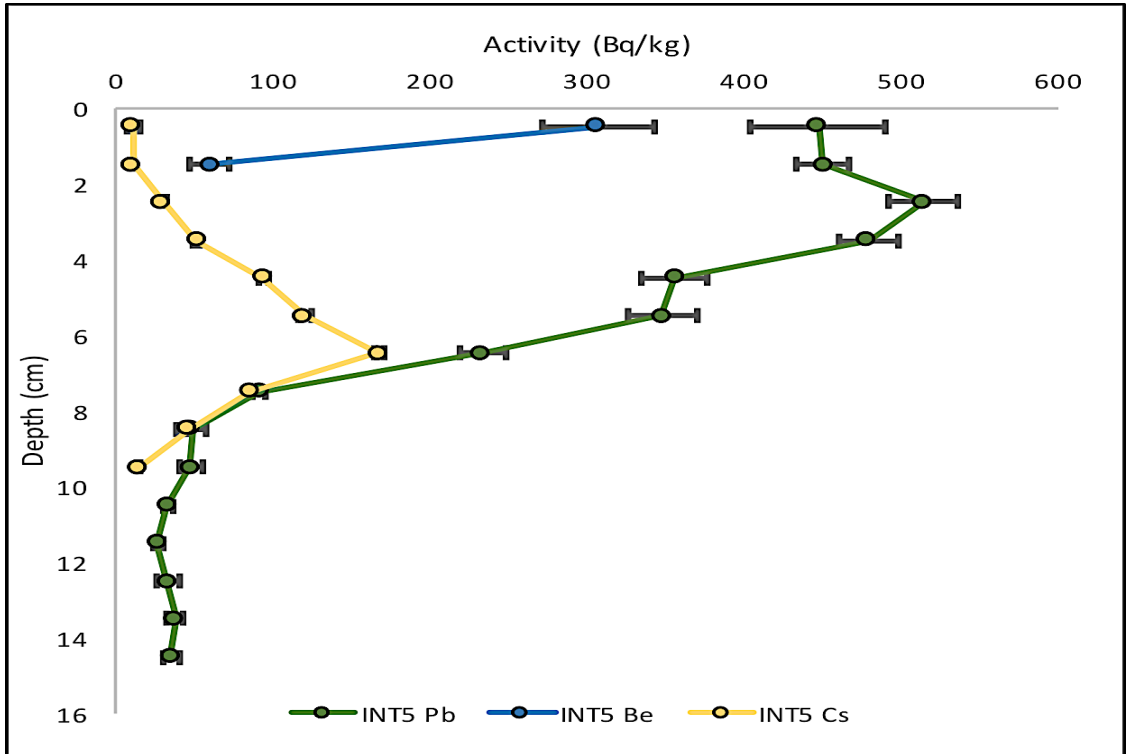


Figure 9: Radionuclide profile of 2016 INT-5. All radionuclide activity was measured in Bq/kg dry mass. ^{210}Pb is represented in green, ^7Be is represented in blue, and ^{137}Cs is represented in yellow. The radionuclide profiles with depth for the other core locations can be found in the Appendix II.

The top of some cores consisted of mostly canopy segments, such as 2012 CTL-2, 2016 INT-5, 2016 INT-3, and 2016 DEEP-4 (Fig. 9; Appendix II). The vegetation canopy is the vegetation that forms in the growing season (exists for approximately 60 days/year and is dominated by tussock forming sedges (*Eriophorum vaginatum*), interspaced shrubs (*Betula nana*, *Salix pulchra*) and mosses (*Sphagnum* sp.). The canopy segments are easily identified in their radionuclide profiles by the presence of measurable ^7Be (for cores collected in 2016 and measured quickly) in the upper-most few segments, and increasing excess ^{210}Pb activities with depth in the segments having measurable ^7Be (Table 1; Appendix II). When formulating the

modified CIC models for determination of apparent net carbon accrual rates (discussed below), the canopy segments were excluded from calculations to regulate age calculations from the natural variation in thickness of vegetation between cores, and the segment immediately below the canopy layer was considered to have the initial activity of unsupported ^{210}Pb based on the assumption that the annual snow cover compressed and consolidated the previous growth season's canopy to become the top part of the soil organic horizon.

3.2 Soil Organic Carbon and % Carbon Through Soil Profile

All cores had SOC concentrations in the 40-48 wt.% range for the upper-most segments, with wt. % C decreasing with depth (Fig. 10; Table 1; Appendix II). All cores had more than 10 wt. % carbon in the top 12 cm of the core, where most of the radionuclide activity also occurred.

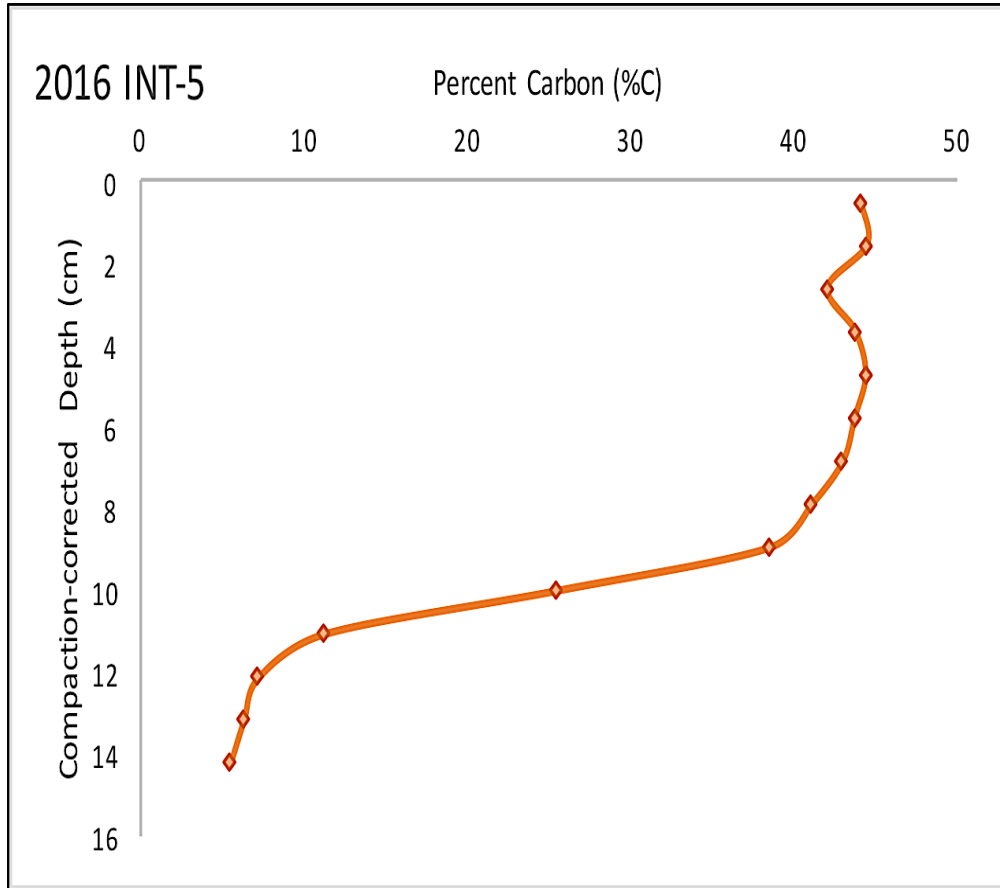


Figure 10: Graph of 2016 INT-5 percent carbon with depth. Wt. % carbon is calculated with relative errors of 2%, and significantly decreases with depth below approximately 10 cm, where biologically-driven carbon decomposition and respiration is likely occurring. All cores, despite snow depth location had similar %C vs depth graphs. The %C vs depth graphs for the other core locations can be found in the Appendix II.

Based on measured carbon weight percentage (Fig. 10; Table 1; Appendix II) in the cores collected, total carbon measured being almost equal to total organic carbon values, the soils being acidic, and recorded terrestrial soil carbon inventories in the area (Fig. 11), the carbon in our cores is almost entirely pure organic carbon.

Therefore, in this study we make the key assumptions that carbon accumulation rates are equal to sedimentation rates, and carbon accumulation is exclusively from plant growth. From this assumption, unsupported ^{210}Pb can be used as a proxy to estimate net carbon accumulation rates in the organic horizon of the active layer.

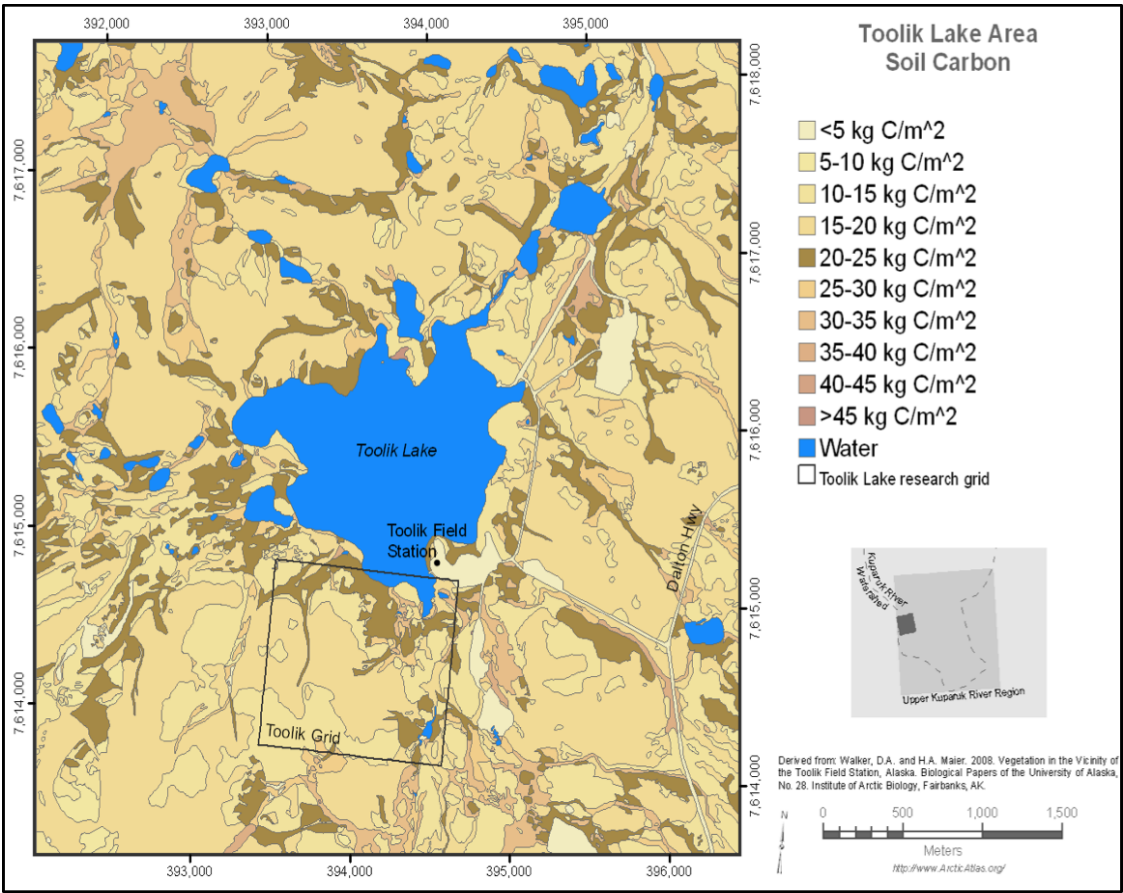


Figure 11: Map of Toolik Lake Area and the approximate soil carbon inventory (Toolik Field Station, UAF, 2012). Our experimental location is within the “Toolik Grid” square on the map where total soil carbon inventory ranges from 20-35 kg C/m^2 .

3.3 Application of ^{210}Pb to Determine Net Carbon Uptake Rates with a Modified Model

Sedimentation rate determinations from unsupported ^{210}Pb activity profiles in lake sediments (Robbins, 1978) assume a constant rate of supply of ^{210}Pb to the sediment-water interface. It is useful for determining average sedimentation rate in systems where this rate may vary substantially from year to year. In this work, we make the analogy between sediment accumulation rate in a lake and carbon accrual by plant growth at the surface of the soil organic horizon in the permafrost active layer. Deposition of ^{210}Pb is generally correlated with the annual precipitation amount (Beks et al., 1998). Because the 1994 snow fence caused substantial changes in the annual accumulation of precipitation across the experimental site, ^{210}Pb deposition rates would have been affected, and an increase in unsupported ^{210}Pb accumulation would thus be expected to have occurred leeward of the snow fence after 1994. Therefore, we developed a modified CIC approach (Fig. 12) to estimate mass accumulation rates from the measured ^{210}Pb profiles, and used it to estimate these rates, along with initial ^{210}Pb activities, both pre-1994 and post-1994 core segments to obtain evidence on the effect of snow depth on net C uptake in the soil organic horizon of the active layer.

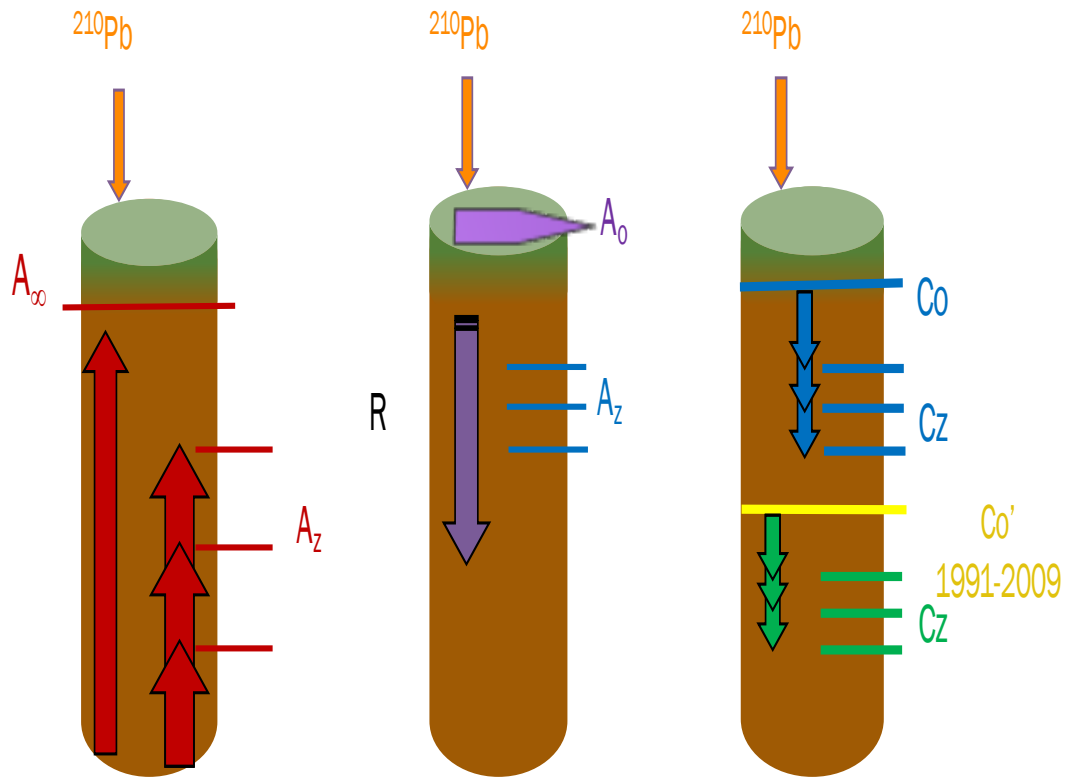


Figure 12: Diagrams representing the three different sedimentation rate models considered in this study. **A)** Diagram representing how a CRS model uses ^{210}Pb deposition and $\ln(A_0/A_z)$ to calculate sedimentation rates. **B)** Diagram representing how a CIC model uses ^{210}Pb deposition for calculating sedimentation rates. **C)** The modified CIC model created in this study to calculate the carbon accumulation rate in the Toolik snow fence cores using the $\ln(C_0/C_z)$ and $\ln(C_0'/C_z)$ approach derived from the CIC intersection value found to calculate the C_0' , ^{210}Pb initial activity. $\ln(C_0/C_z)$ and $\ln(C_0'/C_z)$ values were also later used to date the core segments.

Sediment age using the Constant Initial Concentration model (CIC) assumes the initial concentration of ^{210}Pb in the sediment is constant. Using the method of Appleby (2001)

$$C_z = C_0 * e^{-\lambda t}$$

Equation 1

where C_0 is the unsupported ^{210}Pb activity (Bq/kg dry mass) at the sediment-water interface, the top of the core, λ is the decay constant of ^{210}Pb (0.03114 yr), and C_z is the unsupported ^{210}Pb activity (Bq/kg dry mass) at section depth z . The age of a section in years can be found using

$$t = \frac{1}{\lambda} \ln\left(\frac{C_0}{C_z}\right) \quad \text{Equation 2}$$

and sedimentation rate (r) (g/cm²/year) is

$$r = \lambda M \quad \text{Equation 3}$$

where M is the slope of the line of cumulative carbon dry mass vs. $\ln(C_0/C_z)$.

The first step in developing our modified CIC model is based on the observation of a substantial change in slope in plots of cumulative carbon dry mass vs. $\ln C_0/C_z$ (Fig. 13; Appendix II), which we hypothesized was the result of the snow fence installation, representing changes in post-snow fence mass accumulation and ^{210}Pb deposition rates. Therefore, a new data analysis approach was developed to test the hypothesis of changing ^{210}Pb deposition rates corresponding to changing carbon accumulation rates, with the ^{210}Pb profiles.

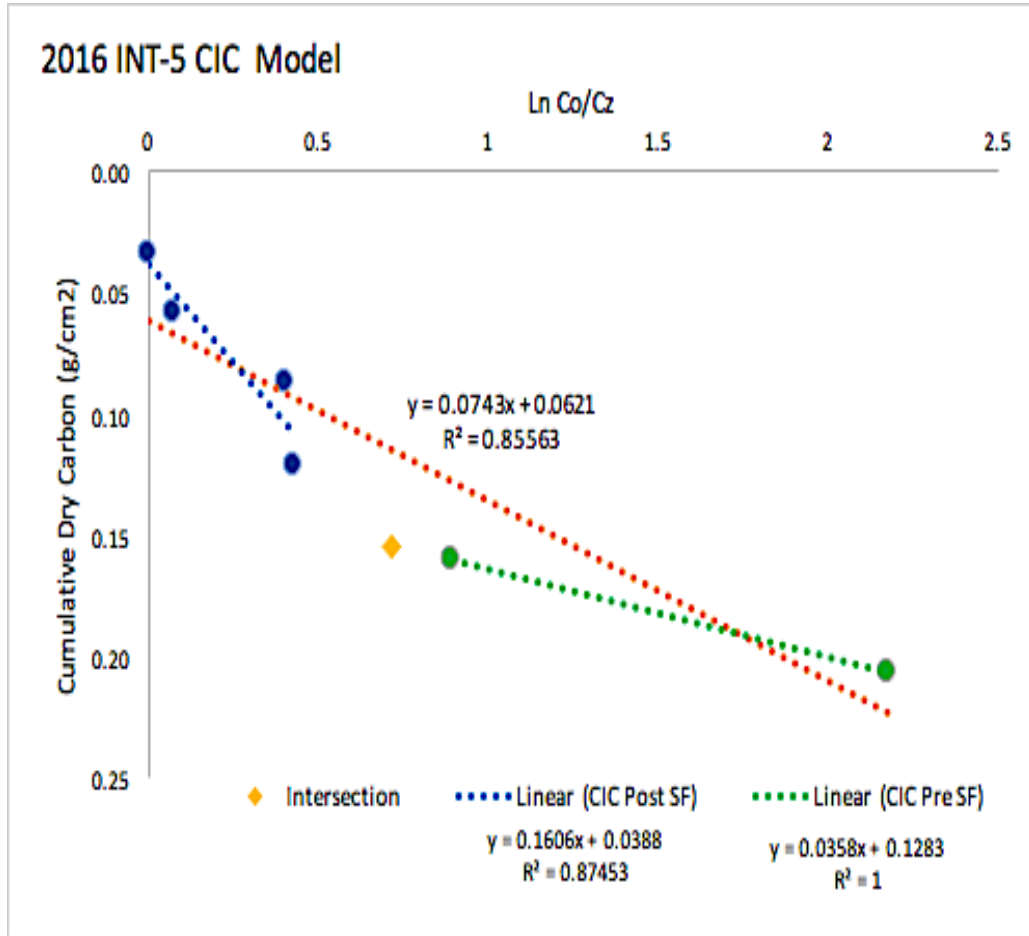


Figure 13: Graph of the standard CIC model created for INT-5 in a first attempt to calculated carbon accumulation rate in Toolik snow fence cores. The orange trendline and corresponding equation show the standard CIC model of the core. Due to the distinct correlation and our knowledge of the changing ²¹⁰Pb deposition, the intersection point approach and modified CIC model was then created. The original CIC graphs created for the other core locations can be found in the Appendix II.

The highest excess ²¹⁰Pb value specific to each core was defined as the initial ²¹⁰Pb activity, which is referred to as Co (Fig. 12). The core segments were dated from the top down using the core-specific Co value and the segment-specific ²¹⁰Pb activity,

which is referred to as Cz (Fig. 12). The new Co/Cz ratio at each segment was divided by the ^{210}Pb decay constant, and the calendar date profile for the entire core was thus determined. Once this was completed for each core, it was apparent that the calendar date associated with the change in slope corresponded to 1994 (within error) for every core we analyzed that showed a significant change in slope. The only cores not showing a change in slope were 2016 CTL-2, 2016 CTL-4, 2012 CTL-2 and 2016 LOW-2 (Appendix II). The CTL cores are controls, from sites outside the influence of the snow fence, and the absence of a change in slope on their cumulative carbon dry mass vs $\ln \text{Co/Cz}$ plots supports our hypothesis that these changes in slope were effects of the snow fence installation.

We first attempted to determine an appropriate value of Co that could be applicable for the pre-snow fence ^{210}Pb deposition in order to date the older, deeper soil by taking the average of the highest excess ^{210}Pb activities of all the 2016 and 2012 control (CTL) cores. However, because of local heterogeneity and apparent influence of snow fence on one of the most distant control sites (CTL-5), the average Co value thus determined had a large standard deviation. Therefore, this method did not yield useful results.

Instead, we found the intersection point of the two intersecting slopes on the cumulative carbon dry mass vs $\ln \text{Co/Cz}$ plot for each core (Fig. 13) This point was dated using the top-down, core-specific CoCz value approach described above. Based on the values of $\ln \text{Co/Cz}$ and cumulative dry carbon determined for the intersection point, we made the assumption that the initial activity of excess ^{210}Pb for the lower portion of the two-slope data array, which was termed Co', was equal to the Cz value of that point in the upper portion of the two-slope data array (Fig. 12). Co' was then

used as the initial ^{210}Pb activity for pre-snow fence segments below the intersection point (Fig. 14; Appendix II).

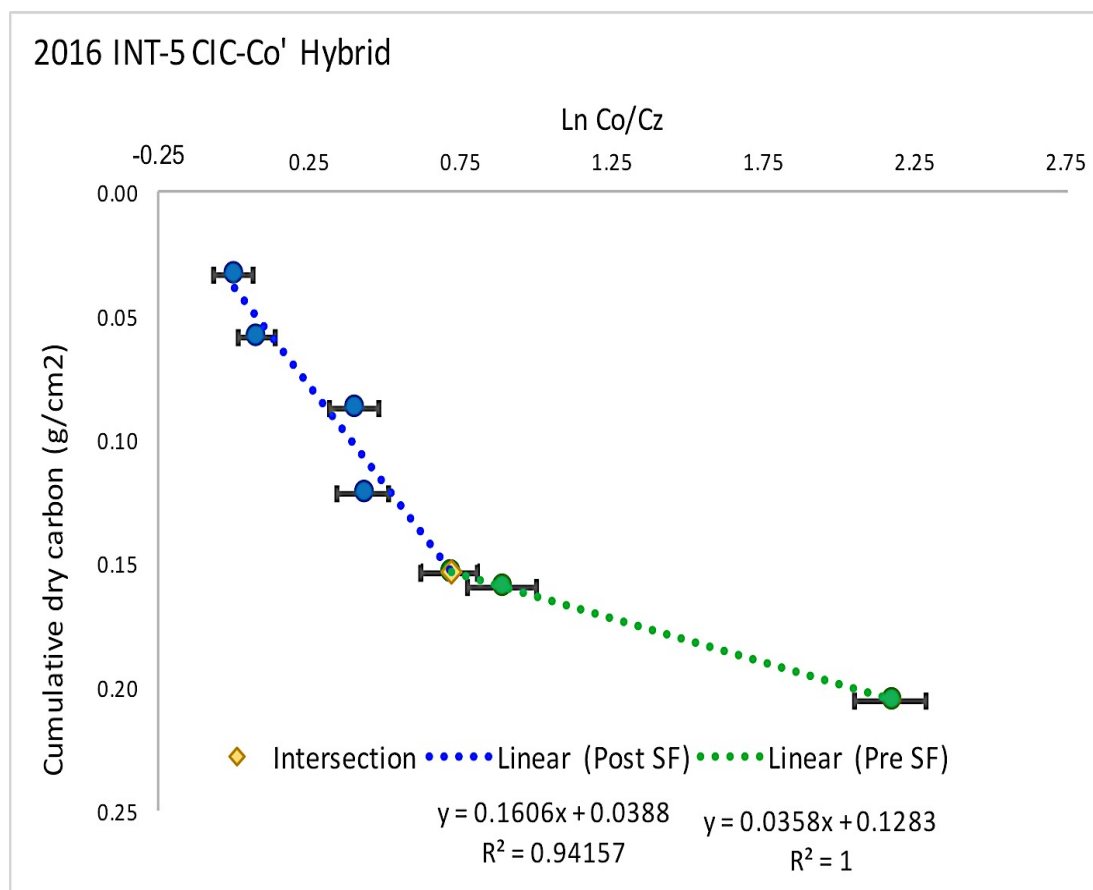


Figure 14: Graph of the modified CIC model created in this study to calculate the carbon accumulation rates in the experiment cores that had significant changes in ^{210}Pb deposition due to the installation of the 1994 snow fence. The modified CIC graphs created for the other core locations can be found in Appendix II. Note that the slope of the linear trendlines changed and the R^2 for all modified CIC models show a closer linear correlation than their standard CIC counterparts (Appendix II).

3.4 Age Calculations

Age calculations followed the two-stage CIC approach described above. $\ln(C_o/C_z)$ values were multiplied by the $1/\lambda$ (decay constant for ^{210}Pb) to calculate the apparent age of each core segment (in years). These values were then subtracted from the year of core collection to determine average calendar year of segment accumulation. If a canopy cover was detected in the core, these segments were excluded from $\ln(C_o/C_z)$, and thus the age calculation, and the segment immediately underlying the canopy was assumed to be the year before collection (Table??). Core segments were dated down the core profile by this technique until, and including, the intersection point described above (Fig. 14; Appendix II). After the intersection point, $\ln(C_o'/C_z)$ was then used to perform age calculations in a similar manner (Fig. 12). $\ln(C_o'/C_z)$ values were multiplied by the $1/\lambda$ (decay constant for ^{210}Pb) to calculate the core segment age (in years). These ages, however, were then subtracted from the calculated year of the intersection point, to determine apparent calendar year of segment accumulation from pre- snow fence ^{210}Pb deposition. Calculated calendar year dates of the segments were then graphed against their cumulative dry carbon values, and a representation of the amount of change in carbon accumulation rates can be seen from the two contrasting slopes of data arrays in each core (Fig. 15; Appendix II).

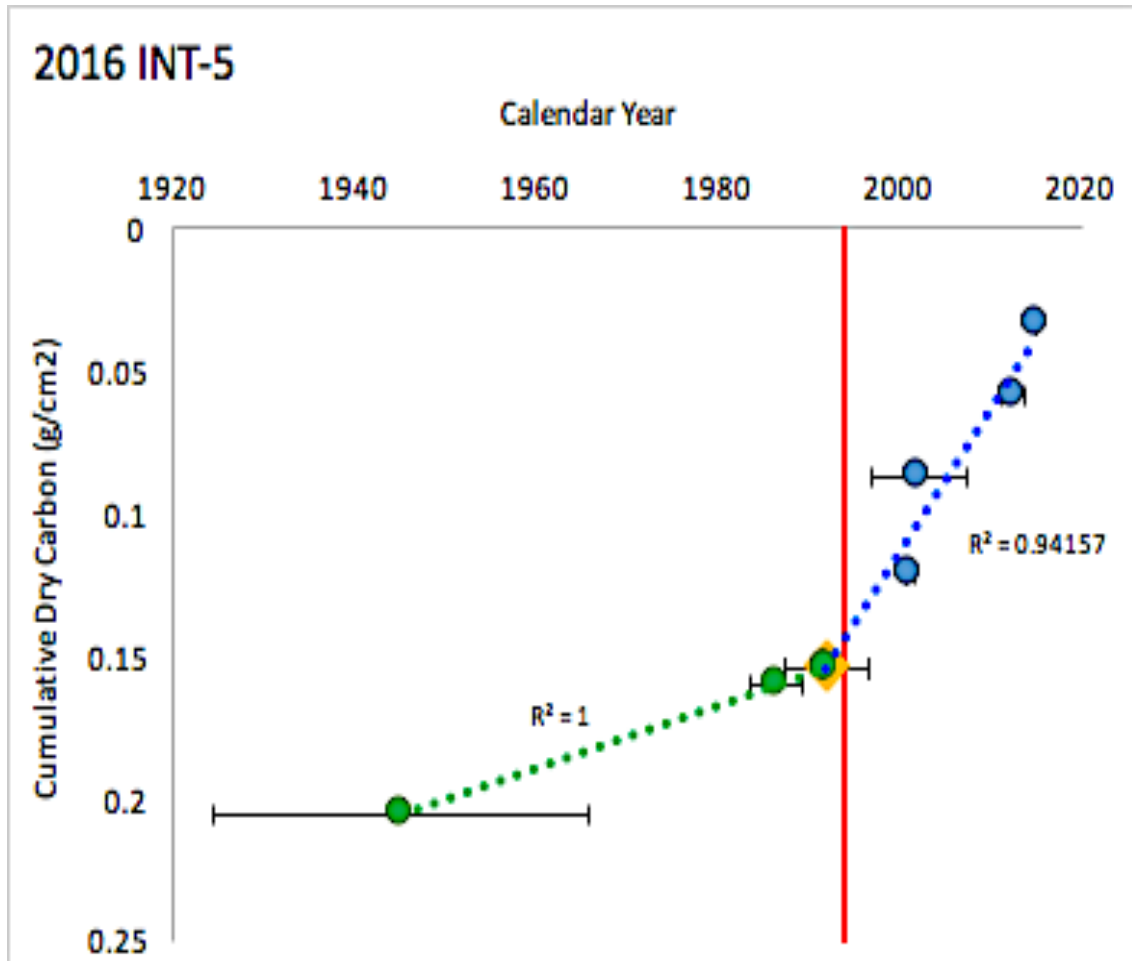


Figure 15: Graph of INT-5 calculated calendar year vs. cumulative dry carbon mass with the date of the snow fence installation represented by the vertical red line. For cores showing changes in ²¹⁰Pb deposition, post- snow fence dated core segments are shown in blue, pre- snow fence dated core segments are shown in green, and the calculated intersection point founded in the CIC graphs is shown in yellow. The calculated age graphs created for the other core locations are located in Appendix II.

Chapter 4

DISCUSSION

4.1 Toolik Soils and Organic Carbon

Toolik soils are classified as moist acidic tussock tundra in the continuous permafrost region of Alaska (Walker et al., 2003). Based on the classification scheme developed by Walker (1983, 1985), moist acidic tussock tundra occurs where the soil is saturated in a portion of the active layer throughout the growing season, but standing water is absent or present for only a part of the growing season. Tussock tundra is a common type of moist tundra on the Foothills, and is dominated by tussock cottongrass (*Eriophorum vaginatum*), dwarf shrubs, mosses, and lichens.

The soils around Toolik Lake consist of a dense, compressed mat of roots and organic matter that overlies mineral soils, with a relatively thin active layer due to the dense insulating organic mat and moderate soil moisture content. The soils have a pH ranging from ~4.3-6.2, Summer Warmth Index of approximately 26.4°C, recorded thaw depth of 42-50 cm, a total biomass of approximately 429-583 g/m², and soil H₂O of ~14-20 vol% (Walker et al., 2003).

Arctic soils contain large organic matter stocks, making them a significant component of the global soil carbon inventory. The northern permafrost zone is

estimated to contain 1024 Pg C when organic matter is stored deep (up to 3 m) in the permafrost profile, which would be approximately equivalent to 460 ppm of atmospheric CO₂ if it was all released to the atmosphere as CO₂ (Vogel et al., 2009). The Alaskan Arctic North Slope region is composed mainly of two tundra types, wet sedge tundra and moist tussock tundra (Kwon et al., 2006). Specifically, the tussock tundra region in Alaska, which includes Toolik Lake, holds between 7 and 27 kg/m² of soil organic carbon (SOC), with root litter dominating C input and SOC storage in this environment (Sullivan et al., 2007). Moist acidic tundra, like that at Toolik, is composed of a mixture of deciduous evergreen and graminoid species, with the main period of plant growth occurring in the summer period (June 1st-August 31st). The organic mat thickness ranges from <5 to >40 cm thick, but averages ~15-20cm, with a summer thaw depth of 40-60cm (Shaver et al., 2006).

4.2 ⁷Be: Short-Term Soil Tracer

Beryllium-7 is a natural cosmogenic radionuclide produced in the upper atmosphere by cosmic ray spallation of nitrogen and oxygen (Mabit et al., 2008). Although seasonal variations have been shown to affect the deposition of ⁷Be, the short half-life of ⁷Be (53.3 days) makes it an excellent short-term soil tracer. ⁷Be is readily fixed by surface vegetation cover, and is rarely found at depths greater than 3 cm in most areas (Mabit et al., 2008). If ⁷Be is found at depths greater than 3 cm, it is likely that there is downward movement of soil particles in the area, possibly caused by various factors such as fissures, bioturbation, or soil tilling (Mabit et al., 2008). Because of the relatively constant deposition of ⁷Be, and its short half-life,

^7Be is usually used to investigate soil erosion processes that occur over a short timescale. However, in this study ^7Be is used to help identify the vegetation canopy and support that there is little to no bioturbation or downward soil movement in the field site.

Some 2016 samples had significant, detectable values for ^7Be , such as CTL-5, INT-5, INT-3, LOW-2, and DEEP-4 (Fig. 9; Table 1; Appendix II). The presence of ^7Be in the cores was useful, in combination with excess ^{210}Pb values, to better identify the canopy layer and exclude some of the uppermost segment(s) from the two-stage CIC model calculations (Fig. 12; Fig 14; Table 1; Appendix II).

4.3 ^{137}Cs : Widely Used Soil Tracer

Cesium-137 is a widely used, medium-term soil tracer with a half-life of 30.2 years. ^{137}Cs is a ‘man-made’ radionuclide, created as a product of thermonuclear weapons testing and nuclear accidents. The nuclear weapons testing took place from 1950 to the early 1970’s, with a global peak in ^{137}Cs production by above-ground testing during 1963 (Mabit et al., 2008). Near-constant ^{137}Cs activities in the uppermost section of the soil profile typically reflects the influence of bioturbation processes; consequently, ^{137}Cs can provide evidence for of soil redistribution and mobility from a number of processes (Mabit et al., 2008). In undisturbed soils, or soils with little Cs mobility, ^{137}Cs activities typically increase with depth to a peak activity, below which they decrease exponentially with depth (Mabit et al., 2008). Therefore, the ^{137}Cs peak in undisturbed soils is a good tracer of sediment accumulation rates.

The moist-acidic Alaskan Arctic continuous permafrost soils researched in this study had ^{137}Cs peaks at various depths (Fig. 9; Table 1; Table 1; Appendix II). The

majority of the ^{137}Cs peaks were not concordant with ^{210}Pb dates at 1963. This can be due to several factors such as unconsidered sources of ^{137}Cs deposition or ^{137}Cs mobility in the soil profile. ^{137}Cs deposition from other atmospheric nuclear events (i.e. Chernobyl) was an initial possible explanation for the unexpected location of the ^{137}Cs peaks in these cores. The Chernobyl nuclear meltdown event in 1986 released Cs having a $^{137}\text{Cs}/^{134}\text{Cs}$ ratio of 2.5 at the time of the accident (Baskaran et al., 1991). In some areas of the Arctic, the Chernobyl accident contributed significantly to ^{137}Cs deposition, but no attempt has been made to provide a prediction of the radiocaesium deposition resulting from this event due to the inhomogeneous nature of the single deposition event (Wright et al., 1999). A previous study attempted to calculate levels of ^{137}Cs in Alaskan soil, plant, and wildlife samples and found that the majority of Chernobyl-derived radiocaesium concentrations were below detectable levels (Baskaran et al., 1991). As a result of the prominent ^{137}Cs peaks in the Toolik samples and research founded in previous studies, it is unlikely that the Chernobyl event affected the unexpected position of our ^{137}Cs peaks.

Another possible explanation for the unexpected location of the ^{137}Cs peaks in these cores is that the originally deposited ^{137}Cs peak was mobilized in the soil profile, potentially from freeze-thaw cryoturbation, vegetation uptake, or localized subsurface hydrologic effects including desorption caused by the acidic pH (< 5.5) of the soil pore water (Gough et al., 2000). Some studies conducted after the Chernobyl accident indicated that vertical migration of radioactive Cs was mostly slow, and most radioactive ^{137}Cs was present in the upper soil layers (e.g., Almgren and Isaksson 2006). However, in the Russian Arctic, ^{137}Cs was found to be slightly mobile (Usacheva and Semenov, 2014). Movement of ^{137}Cs in the soils was significantly

found to be from organic matter movement to subsoil by cryoturbation, due to freeze-thaw cycles, and windfalls (Usacheva and Semenov, 2014). Thaw-induced consolidation and compaction of the active layer was shown to be a relatively dominant geomorphological agent in Alaska, especially under deeper snow, and an intensification over time of thaw settlement and consolidation of the active layer can create initial stages of thermokarst development (Blanc-Betes et al., 2016), and therefore likely contribute to ^{137}Cs mobility as well. Vegetation is also a possible catalyst of ^{137}Cs peak mobilization. Some vegetation, especially immature plants, in K- and N-limited soils uptake ^{137}Cs (Ogura et al., 2014). In addition, subsurface hydrologic effects, such as snow melt runoff and leaching due to freeze-thaw temporal active layer melting yield mildly acidic pore water, can also be a factor in the mobility of the ^{137}Cs in the Toolik cores.

4.4 ^{210}Pb : Radionuclide Used for Estimation of Soil Mass Accumulation Rate

The majority of ^{210}Pb in our core profile, especially the upper ~12cm of focus, is unsupported ^{210}Pb (Table 1). Highest values of unsupported ^{210}Pb values ranged from 399 Bq/kg to 1305 Bq/kg, with an average highest value of 623 Bq/kg of unsupported ^{210}Pb (Table 1). When comparing core location, higher unsupported ^{210}Pb values were associated with higher snow depth zones. The highest unsupported ^{210}Pb value of 1305 Bq/kg is in DEEP-4. The INT and CTL cores had similar peak unsupported ^{210}Pb values, with the INT cores being slightly higher than the CTLs (Table 1).

The highest value of unsupported ^{210}Pb is normally located at the surface of the soil profile (Mabit et al., 2008). In some cores, the highest value of unsupported ^{210}Pb was not located in the upper-most segment of the collected core. These cores included

INT-5, INT-3, DEEP-4, and CTL-4 (Table 1). The majority of these cores had detectable ^7Be data that correlated with less-than-maximum unsupported ^{210}Pb values, with the exception of CTL-4 which had no detectable ^7Be data. Therefore, segments are considered to almost exclusively be comprised of the canopy layer (Fig. 5), or vegetation growth, of 2016 and the highest unsupported ^{210}Pb which underlies these segments is considered the surface of the soil profile. Since the majority of ^{210}Pb in the Toolik experimental site (Table 1), and likely the moist acidic continuous permafrost zone of Alaska, is from atmospheric deposition, the unsupported ^{210}Pb values can be used to find accumulation rates.

4.5 Carbon Accumulation Rates

Adjusted CIC models were created using the method described in the results section (Fig. 12; Fig. 14; Table 1; Appendix II). 2016 CTL-2, 2016 CTL-4, and 2012 CTL-2 show relatively consistent carbon accumulation rates both pre- and post- snow fence installation (Table 1; Appendix II). Carbon accumulation rates for 2016 CTL-2, 2016 CTL-4, and 2012 CTL-2 range from $0.95 \pm 0.16 \text{ mg C cm}^{-2}\text{y}^{-1}$ to $1.53 \pm 0.13 \text{ mg C cm}^{-2}\text{y}^{-1}$, averaging a carbon accumulation rate of $1.18 \text{ mg C cm}^{-2}\text{y}^{-1}$ (Table 2). Although the carbon accumulation rates of 2016 CTL-2, 2016 CTL-4, and 2012 CTL-2 do not seem to be much affected by the installation of the snow fence, they may show slight effects, particularly less drastic minimum soil temperatures, that are not caused by the snow fence and are representative of natural global climate variation. LOW-2 shows a slight snow fence effect on the carbon accumulation rate (Table 1; Appendix II), with a post- snow fence carbon accumulation rate of $4.32 \pm 0.71 \text{ mg C cm}^{-2}\text{y}^{-1}$, pre- snow fence carbon accumulation rate of $2.56 \pm 0.56 \text{ mg C cm}^{-2}\text{y}^{-1}$, and

Post:Pre accumulation rate ratio of 1.69, falling within error of the CTL carbon accumulation rates (Table 2).

Cores from the experimental location under deeper snow depth, i.e. INT and DEEP, showed strongly varying carbon accumulation rates compared to other localities (Appendix II; Table 2). Carbon accumulation rates for INT-5 show a post-snow fence carbon accumulation rate of $4.99 \pm 0.72 \text{ mg C cm}^{-2} \text{ y}^{-1}$, pre-snow fence carbon accumulation rate of $1.11 \pm 0.25 \text{ mg C cm}^{-2} \text{ y}^{-1}$, and Post:Pre accumulation rate ratio of 4.49 (Table 2). Carbon accumulation rates for INT-3 show a post-snow fence carbon accumulation rate of $5.48 \text{ mg C cm}^{-2} \text{ y}^{-1}$, pre-snow fence carbon accumulation rate of $1.17 \pm 0.14 \text{ mg C cm}^{-2} \text{ y}^{-1}$, and Post:Pre accumulation rate ratio of 4.70 (Table 2). Similarly, DEEP-4 showed varying carbon accumulation rates compared to other localities (Table 2). Carbon accumulation rates for DEEP-4 show a post-snow fence carbon accumulation rate of $4.61 \pm 0.01 \text{ mg C cm}^{-2} \text{ y}^{-1}$, pre-snow fence carbon accumulation rate of $0.86 \pm 0.12 \text{ mg C cm}^{-2} \text{ y}^{-1}$, and Post:Pre accumulation rate ratio of 5.38 (Table 2). INT and DEEP carbon accumulation rates post-snow fence were significantly higher than CTL and LOW rates, suggesting a strong correlation between increased snow depth and increased carbon accumulation rates (Appendix II; Table 2). Some 2016 cores showed unexpected results. For instance, the adjusted CRS model for 2016 CTL-5 shows an effect of the snow fence on carbon accumulation at this location (Appendix II; Table 2). Based on our data, a carbon accumulation rate of $5.96 \pm 1.01 \text{ mg C cm}^{-2} \text{ y}^{-1}$ was calculated for post-snow fence installation, and a carbon accumulation rate of $0.45 \pm 0.13 \text{ mg C cm}^{-2} \text{ y}^{-1}$ was calculated for pre-snow fence (Appendix II; Table 2). This unexpected effect may be due to CTL-5 being affected by

the snow drift of the snow fence, or perhaps snowmelt runoff contribution of unsupported ^{210}Pb carried by SOC particles, which will be discussed further below.

The stored terrestrial soil carbon in the Toolik snow fence grid area ranges from approximately 20-35 kg C m⁻²(Fig. 11). Based on our control carbon accumulation rates, the average carbon accumulation in the area is 0.012 kg C m⁻²y⁻¹. Based on our data, an intermediate snow increase of +20-45% will result in approximately 4.6x faster carbon accumulation, at least over a period of 20 years (Table 2). This would then change the current carbon accumulation rate from approximately 0.012 kg C m⁻²y⁻¹ to approximately 0.054 kg C m⁻²y⁻¹. Based on our data, a deep snow increase of +70-100% will result in approximately 5.4x faster carbon accumulation rate, at least over a period of 20 years (Table 2). This would then change the current carbon accumulation rate from approximately 0.012 kg C m⁻²y⁻¹ to approximately 0.054 kg C m⁻²y⁻¹. Roughly based on this data, an increase in snow depth will result in a somewhat immediate increase in net carbon accumulation rate in the soil organic horizon. The increased accumulation rate may cause the moist acidic arctic permafrost to, at least temporarily, be more of a carbon sink than it is currently. However, biotic interactions will likely change the magnitude, extent, and long-term net effect of the temporarily increased sink due to carbon accumulation in the soil organic horizon by deeper thawing that will expose frozen SOC to microbial degradation that promotes methanogenesis and CH₄ release to the atmosphere (Fig. 2).

4.6 Effect of Snow Depth on Ground Thermal Regime

Snow is a leading factor in insulating the ground from heat loss in the winter, generally resulting in higher mean annual ground temperatures (Fig. 2). This is

especially true at higher latitudes where stable snow cover lasts an extended period of time (Zhang, 2004). However, the magnitude of the effect of seasonal snow cover on the ground thermal regime is dependent on the timing, duration, accumulation, melting processes, structure, density, and thickness of the snow.

Based on a soil thermal regime study in other parts of Alaska, it was concluded that snow depth has a direct effect on the soil surface energy balance from the date of the active layer freeze-up to the date when snow depth reaches maximum, with variations in timing and duration of snow cover having minimal effect on the active layer thickness (Zhang, 2004). In Arctic Alaska, it has been found that there is an overall net positive impact on soil surface temperature, with an average temperature difference value between air and ground surface of 4-9 °C (Zhang, 2004). A sensitivity study was done using the average snow and climatic conditions along the Alaskan Arctic that indicated changes in the thermal conductivity of snow cover have a significant impact on the ground surface, active layer, and permafrost temperatures (Zhang et al., 1997). Seasonal snow cover has also been found to have extreme impacts specifically on continuous permafrost temperatures, specifically during the 8-9-month winter on the North Slope of Alaska, with larger implications for ecosystems and thus global cycling of nutrients (Zhang et al., 1997; Sturm et al., 2001).

In addition to an increased growing season, increased snow depth would lead to increased snow melt, resulting in wetter soil and potentially leaching and deeper storage of water-extractable organic matter (Delarue et al., 2011). Understanding saturation conditions of soil is pertinent to understanding the carbon cycle, and therefore should be considered for future work in this region (Abbott et al., 2012; Delarue et al., 2011).

4.7 Active Layer and Thermodynamics in Alaskan Continuous Permafrost Zone

The active layer is a layer of soil at the surface in areas of permafrost that thaws seasonally. Active layer thickness is affected by two opposing trends in the climate gradient: (1) warmer temperatures promoting deeper thaw and causing denser plant canopies, and (2) the resulting denser plant canopies and thicker soils counteracting the warmer temperature thaw (Walker et al., 2003). However, the active layer is generally expected to increase in thickness with warmer climate projections.

The temporal pattern of soil moisture and temperature in the active layer ranges greatly season to season (Hinzman et al., 1990). In control soils, the active layer near Toolik Lake, AK has been found to cool to the 0°C isotherm within a few days of sustained freezing air temperatures, once the onset of soil freezing began. During the winter, the soil layer is insulated by the snow and therefore remains at warmer temperatures than the air temperatures (Fig. 16). In the summer, the organic rich section of the active layer remains lower than air temperature, likely because of the large heat sink in the underlying permafrost. The active layer is structured by the thermal and hydrological regimes (Hinzman et al., 1990). The amount of moisture in the soil profile directly affects the depth and rate of freezing and thawing, and is amplified if the water is moving (Hinzman et al., 1990). The thermophysical properties of the active layer are determined primarily by density and moisture content, therefore the most important factor determining the temperature field in the active layer is the soil moisture regime (Fig. 16) (Hinzman et al., 1990).

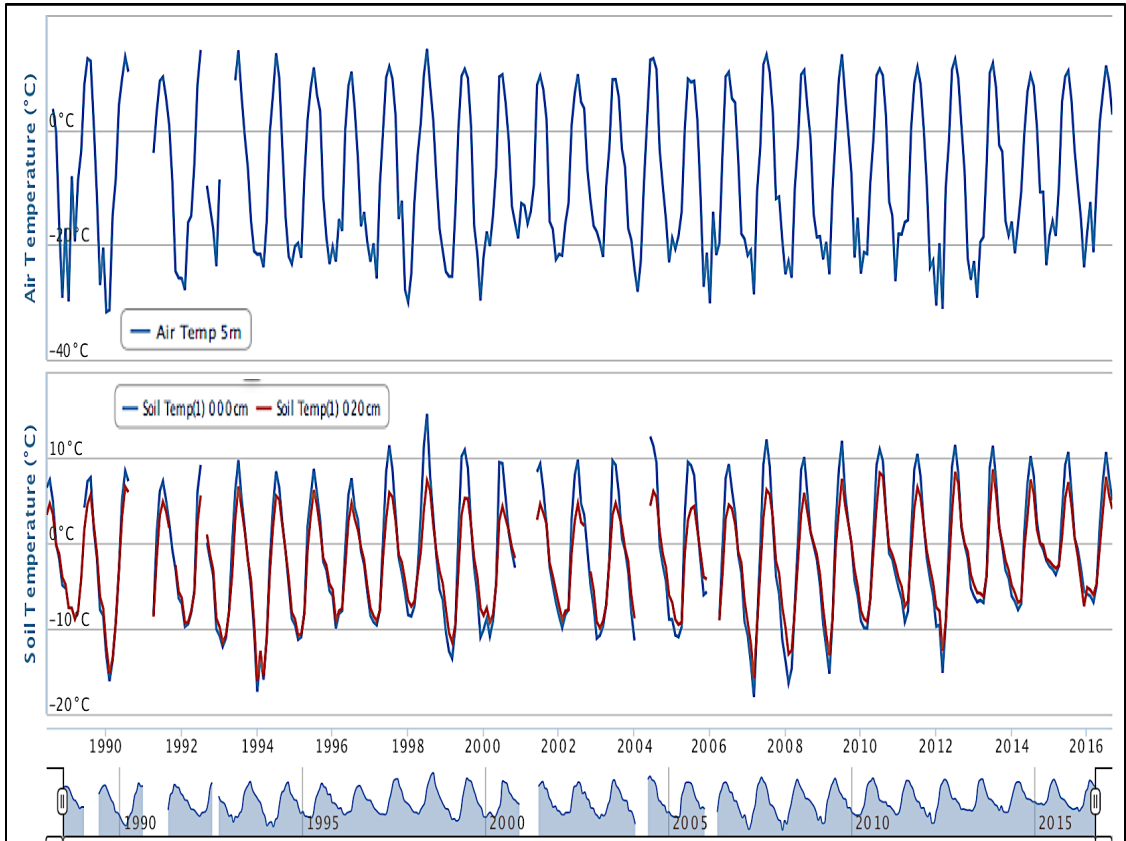


Figure 16: Graphs of daily recorded air temperature at 5m (°C) (upper graph), and soil temperature at 0cm and 20cm depth (°C) (lower graph), from 1998-2016 at the Toolik Field Station at a control site outside of but near the snow fence area. The last ~10 years show little variation in the minimum/ maximum air temperatures, but during this time the minimum soil temperatures appear to be steadily increasing, indicating a general winter warming of the soils in the area outside the snow fence plot (Modified from UAF).

The volume of moisture content in the organic soil can vary up to 60%, and on average the mineral soil remains near saturation throughout the year (Hinzman et al., 1990). In the near-surface organic soils (0-10cm), the pores are large and once these pores are empty, a relatively small amount of moisture remains. In the deeper mineral

soils (20-25cm), there is much more fine grained material and more of the water is adsorbed. The distinct stratification in the soils strongly affects the soil's thermal and hydrologic regimes (Hinzman et al., 1990). During the spring runoff event, subsurface water only flows through the top 10 cm of organic soil, and most downslope flow occurs just above the organic/mineral interface (Hinzman et al., 1990).

At the onset of spring melt, most pores in the mineral soil are filled with ice. Upon thawing, the thermal conductivity of the saturated organic soil decreases by approximately 50%. After thawing, the thermal conductivity of the saturated mineral soil decreases by approximately 30% (Hinzman et al., 1990). Thermal conductivity, regardless of temperature or moisture content, is lower in the organic soil than the mineral soil (Hinzman et al., 1990).

A process likely to affect the data in this study is snowmelt runoff. The process of snowmelt runoff is a result of the large differences in the mineral and organic layers' bulk density, porosity, and hydraulic conductivity. Snowmelt in the area was typically found to last approximately 10 days or less. Therefore, snowmelt runoff was always completed before the active layer thawed below 10cm, resulting in subsurface drainage only in the top 10cm (Hinzman et al., 1990). The radionuclide profiles and dating in this study focuses on the top ~16cm of the soil profile, with the majority of radionuclide activity occurring in the top 10cm.

4.8 Active Layer and Ecosystem Implications

Projected changes of precipitation in Arctic regions will influence local ecosystems as well as global carbon cycling. Changes in local ecology composition,

biomass, and productivity can occur directly as a result of warmer air and soil temperatures, or indirectly through changes in soil resources, such as water and nutrient availability (Fig. 2) (Schuur et al., 2007). Warmer air and soil temperatures stimulate increased heterotrophic decomposition and nutrient release from soil organic matter (Schuur et al., 2007).

As mentioned above, previous studies found that snow insulation can have considerable effects on soil temperatures in Arctic regions. Increased snow insulation affects the rates of soil cooling/warming and frequency of freeze/thaw cycles, having significant effects on soil-dwelling microorganisms (Fig. 2). For example, warmer soils could result in a positive feedback to climate change by increasing SOC availability under deeper snow, thus accelerating SOC decomposition and therefore ecosystem respiration (Schaefer et al., 2011).

Biotic effects on the Arctic carbon cycle are extremely complex and site specific. For example, previous studies have found strong links of zonal vegetation to active-layer thickness across northern Alaska. Active layer thickness is affected by two opposing trends in the climate gradient: (1) warmer temperatures promoting deeper thaw and causing denser plant canopies, and (2) the resulting denser plant canopies and thicker soils counteracting the warmer temperature thaw (Walker et al., 2003). Certain factors expected to remain constant throughout climate change need to be considered when trying to understand biotic implications and active layer thickness predictions in this region. In tussock-tundra, like that at Toolik, Walker found soil accumulation did not increase as strongly with temperature and that the biomass in

these areas is likely limited by cold wet soils rather than air temperature. Therefore, although climate change predicts temperature warming in the Arctic, it is the associated prediction of increased precipitation that will have the larger effect on Arctic vegetation, and thus drive the Arctic tundra carbon budget, affecting the global carbon cycle.

At the same experimental snow fence from where we collected our cores, an observed shift in vegetation community from predominantly bryophytes (mosses) and lichens to more grasses and woody shrubs was reportedly coincident with enhanced winter CO₂ respiration and N mineralization in soils experiencing deeper snow cover (Jones et al., 1998; Walker et al., 1999). However, in a previous study performed by Miller et al., 2013, the distribution and chemistry of five of the dominant vegetation species at the snow fence plot at Toolik, were observed to cover approximately 80% of the plots in August 2012. Control, Intermediate, and Low snow depth locations were composed of statistically indistinguishable distributions of the five major species with a decreasing order of dominance from 32-36% *E. vaginatum*, 17-27% *Sphagnum spp.*, 13-16% *B. nana*, 3-5% *S. pulchra*, and 1-4% *C. bigelowii*. The locations in the Deep snow depth showed significantly higher *Sphagnum* and *C. bigelowii* cover, and significantly lower *E. vaginatum* and *B. nana* cover than all other zones.

An increase in carbon accumulation rates, particularly within the deeper snow depth localities, is synonymous with an increase in vegetative growth in this environment (Landis et al., GCA, 2016). Therefore, in addition to observed shifts recorded in vegetation communities, an overall shift towards a higher abundance of

vegetation is to be expected with increased snow depth locations.

Chapter 5

SUMMARY AND CONCLUSIONS

5.1 Arctic Carbon Cycling

Terrestrial Arctic annual mean surface air temperatures are predicted to rise by between 2 and 9°C by 2100, depending on greenhouse gas emissions to the global atmosphere, and thus the ground temperatures are predicted to rise as well (Chapman and Walsh, 2007). The magnitude of simulated ground warming does not directly correlate to the degree of surface warming however (Lawrence and Slater, 2009).

Recent studies have reported that thermal profiles of permafrost and northern latitude temperature records across northern Alaska have risen 2-4°C over the last few decades (Kwon et al., 2006). Some studies have shown that carbon is lost quite quickly when permafrost thaws (Zimov et al., 2006). Experiments involving incubated permafrost soils concluded that permafrost carbon is quite decomposable when thawed. Thawing of permafrost can be self-sustaining due to changes in surface energy balance and the heat released by soil respiration that add heat and continue the thawing process (Zimov et al., 2006). Conservative measurements of in situ

respiration of recently unthawed vegetated loess averages $2.3\text{-}5.3 \text{ g C m}^2\text{d}^{-1}$ with an observed burst of respiration rates associated with initial thaw and annual freeze-thaw events (Zimov et al., 2006).

Based on our results, in general deeper snow accumulation will result in increased carbon accumulation rates in the soil organic horizon. This will in turn result in an increase in the sink strength for carbon, at least for approximately two decades as we have observed in Toolik. The increase in carbon accumulation rates will lead to an increase in active layer thickness. The deepening of the active layer in combination with cryoturbation could potentially result in the exchange of soil material between the surface and the base of the active layer, surface buried old frozen carbon and/or buried younger carbon in anoxic conditions (Michaelson et al., 1996). Organic carbon buried by this mechanism can eventually be incorporated into permafrost, especially if accretion of mineral or organic soil at the surface occurs simultaneously (Schuur et al., 2008). During a typical annual cycle, the active layer thins in response to temporal cooling affects and thick layers of segregated ice develop at the top of the permafrost (Shur and Jorgenson, 1998). When climate is favorable to permafrost conditions, the soil below the active layer will typically maintain a perennially frozen state within a few years (Shur and Jorgenson, 2007). If the active layer thins in continuous permafrost zones, most of the initial mineral active layer becomes part of the upper permafrost and is accompanied by

accumulation of aggradation ice, ultimately preserving or even expanding permafrost SOC (Shur and Jorgenson, 2007).

However, with increased snow accumulation rates, an observed increase in carbon accumulation rates results in a thickening the active layer. Thickening of the active layer in a continuous permafrost zone is associated with permafrost warming and degradation, talik formation, development of thermokarsts, lateral permafrost thawing, etc. (Zhang et al., 2005). Therefore, there is believed to be long-term effects of increased snow accumulation resulting in permafrost degradation, ultimately resulting in a positive feedback loop regarding the carbon cycle and climate change. As summer seasons lengthen, soil respiration rates increase, and previously frozen carbon degrades at depth, this short-term increase in carbon accumulation will then eventually change the most acidic continuous permafrost region of Alaska to a net source of carbon.

5.2 Future Work

With climate models and predictions constantly varying, base data in Arctic regions in particular is critical for future interpretation of how climate change will affect the globe. This study aims to provide carbon accumulation rates in various snow depths, increased and reduced, to aid in future Arctic climate studies. Interactions in this environment are extremely complex. Future work in the 1994

snow fence experimental region should include studies on site-specific CO₂ and CH₄ emissions, lateral transport of DOC/DIC in soil pore water, shallow subsurface hydrology, and specific biotic reactions to the various changes in the specific soil moisture/temperature.

REFERENCES

- Anisimov OA, Shiklomanov NI, Nelson FE. 1997. Global warming and active-layer thickness: results from transient general circulation models. *Global and Planetary Change* 15:61–77.
- Appleby PG. 2001. Chronostratigraphic Techniques in Recent Sediments. *Tracking Environmental Change Using Lake Sediments Developments in Paleoenvironmental Research* 1:171–203.
- Blanc-Betes ME. 2017. Impacts of Changes in Winter Precipitation on C Stocks and Fluxes in Arctic Tussock Tundra. PhD Thesis submitted to University of Illinois at Chicago.
- Blanc-Betes E, Welker JM, Sturchio NC, Chanton JP, Gonzalez-Meler MA. 2016. Winter precipitation and snow accumulation drive the methane sink or source strength of Arctic tussock tundra. *Global Change Biology* 22:2818–2833.
- Beks J, Eisma D, Plicht JVD. 1998. A record of atmospheric ²¹⁰Pb deposition in The Netherlands. *Science of The Total Environment* 222:35–44.
- Bockheim JG. 2007. Importance of Cryoturbation in Redistributing Organic Carbon in Permafrost-Affected Soils. *Soil Science Society of America Journal* 71:1335.
- Bockheim JG, Hinkel KM, Nelson FE. 2003. Predicting Carbon Storage in Tundra Soils of Arctic Alaska. *Soil Science Society of America Journal* 67:948.
- Callaghan TV, Johansson M, Brown RD, Groisman PY, Labba N, Radionov V, Barry RG, Bulygina ON, Essery RLH, Frolov DM, et al. 2011. The Changing Face of Arctic Snow Cover: A Synthesis of Observed and Projected Changes. *Ambio* 40:17–31.
- Carvalhais N, Forkel M, Khomik M, Bellarby J, Jung M, Migliavacca M, Mu M, Saatchi S, Santoro M, Thurner M, et al. 2014. Global covariation of carbon turnover times with climate in terrestrial ecosystems. *Nature* 514:213–217.

- Cohen J, Screen J, Furtado J, Barlow M, Whittleston D, Coumuo D, Francis J, Dethloff K, Entekhabi D, Overland J, et al. 2014. Recent Arctic Amplification and Extreme Mid-latitude Weather. *Nature Geoscience* 7:627–637.
- Deng J, Li C, Frohling S, Zhang Y, Bäckstrand K, Crill P. 2014. Assessing effects of permafrost thaw on C fluxes based on multiyear modeling across a permafrost thaw gradient at Stordalen, Sweden. *Biogeosciences* 11:4753–4770.
- Gough L, Shaver GR, Carroll J, Royer DL, Laundre JA, 2000. Vascular plant species richness in Alaskan arctic tundra: the importance of soil pH. *Journal of Ecology* 88: 54-66.
- Hinkel KM, Outcalt SI, Nelson FE. 1990. Temperature variation and apparent thermal diffusivity in the refreezing active layer, Toolik Lake, Alaska. *Permafrost and Periglacial Processes* 1:265–274.
- Hinzman LD, Bettez ND, Bolton R, Chapin FS, Dyrgerove M, Fastie C, Griffith B, Hollister R, Hope A., et al. 2005. Evidence and Implications of Recent Climate Change In Northern Alaska and Other Arctic Regions. *Climate Change* 72:251–298. Jorgenson MT, Shur YL, Pullman ER. 2006. Abrupt increase in permafrost degradation in Arctic Alaska. *Geophysical Research Letters* 33.
- Hugelius G, Strauss J, Zubrzycki S, Harden JW, Schuur EAG, Ping C-L, Schirmermeister L, Grosse G, Michaelson GJ, Koven CD, et al. 2014. Estimated stocks of circumpolar permafrost carbon with quantified uncertainty ranges and identified data gaps. *Biogeosciences* 11:6573–6593.
- Iversen CM, Sloan VL, Sullivan PF, Euskirchen ES, Mcguire AD, Norby RJ, Walker AP, Warren JM, Wulfschleger SD. 2014. The unseen iceberg: plant roots in arctic tundra. *New Phytologist* 205:34–58.
- Kaste JM, Heimsath AM, Bostick BC. 2007. Short-term soil mixing quantified with fallout radionuclides. *Geology* 35:243–246.
- Landis JD, Renshaw CE, Kaste JM. 2016. Beryllium-7 and lead-210 chronometry of modern soil processes: The Linked Radionuclide aCcumulation model, LRC. *Geochimica et Cosmochimica Acta* 180:109–125.
- Landis JD, Renshaw CE, Kaste JM. 2014. Quantitative Retention of Atmospherically Deposited Elements by Native Vegetation Is Traced by the Fallout Radionuclides ⁷Be and ²¹⁰Pb. *Environmental Science & Technology* 48:12022–12030.

- Lawrence DM, Koven CD, Swenson SC, Riley WJ, Slater AG. 2015. Permafrost thaw and resulting soil moisture changes regulate projected high-latitude CO₂ and CH₄ emissions. *Environmental Research Letters* 10.
- Lawrence DM, Slater AG. 2009. The Contribution of Snow Condition Trends to Future Ground Climate. *Climate Dynamics* 34:969–981.
- McGuire AD, Christensen TR, Hayes D, Herault A, Euskirchen E, Kimball JS, Koven C, Lafleur P, Miller PA, Oechel W, et al. 2012. An assessment of the carbon balance of Arctic tundra: comparisons among observations, process models, and atmospheric inversions. *Biogeosciences* 9:3185–3204.
- McGuire D, Anderson L, Christensen T, Dallimore S, Guo L, Hayes D, Heimann M, Lorenson T, Macdonald R, Roulet N. 2009. Sensitivity of the Carbon Cycle in the Arctic to Climate Change. *Ecological Monographs* 79:523–555.
- Natali SM, Schuur EAG, Trucco C, Pries CEH, Crummer KG, Lopez AFB. 2011. Effects of experimental warming of air, soil and permafrost on carbon balance in Alaskan tundra. *Global Change Biology* 17:1394–1407.
- Nowinski NS, Taneva L, Trumbore SE, Welker JM. 2009. Decomposition of old organic matter as a result of deeper active layers in a snow depth manipulation experiment. *Oecologia* 163:785–792.
- Pries CEH, Schuur EAG, Vogel JG, Natali SM. 2013. Moisture drives surface decomposition in thawing tundra. *Journal of Geophysical Research: Biogeosciences* 118:1133–1143.
- Povinec P, Gera M, Holý K, Hirose K, Lujaniené G, Nakano M, Plastino W, Sýkora I, Bartok J, Gažák M. 2013. Dispersion of Fukushima radionuclides in the global atmosphere and the ocean. *Applied Radiation and Isotopes* 81:383–392.
- Shaver GR, Giblin AE, Nadelhoffer KJ, Thieler KK, Downs MR, Laundre JA, Rastetter EB. 2006. Carbon turnover in Alaskan tundra soils: effects of organic matter quality, temperature, moisture and fertilizer. *Journal of Ecology* 94:740–753.
- Shaver GR, Billings WD, Chapin FS, Giblin AE, Nadelhoffer KJ, Oechel WC, Rastetter EB. 1992. Global Change and the Carbon Balance of Arctic Ecosystems. *American Institute of Biological Sciences* 42:433–441.
- Schuur EAG, McGuire AD, Schadel C, Grosse G, Harden JW, Koven CD, Kuhry P, Lawrence DM, Olefeldt D, Romanovsky VE, et al. 2015 Apr 9. climate change and the permafrost carbon feedback. *Nature*:171–179.

- Schuur EAG, Vogel JG, Crummer KG, Lee H, Sickman JO, Osterkamp TE. 2009. The effect of permafrost thaw on old carbon release and net carbon exchange from tundra. *Nature* 459:556–559.
- Wahren C-HA, Walker MD, Bret-Harte MS. 2004. Vegetation responses in Alaskan arctic tundra after 8 years of a summer warming and winter snow manipulation experiment. *Global Change Biology* 11:537–552.
- Walker MD, Walker DA, Welker JM, Arft AM, Bardsley T, Brooks PD, Fahnestock JT, Jones MH, Losleben M, Parsons AN, et al. 1999. Long-term experimental manipulation of winter snow regime and summer temperature in arctic and alpine tundra. *Hydrological Processes* 13:2315–2330.
- Welker JM., Fahnestock JT., Jones MH. 2000. Annual CO₂ Flux in Dry and Moist Arctic Tundra: Field Responses to Increase in Summer Temperatures and Winter Snow Depth. *Climate Change* 44:139–150.
- Wijk MTV, Clemmensen KE, Shaver GR, Williams M, Callaghan TV, Chapin FS, Cornelissen JHC, Gough L, Hobbie SE, Jonasson S, et al. 2003. Long-term ecosystem level experiments at Toolik Lake, Alaska, and at Abisko, Northern Sweden: generalizations and differences in ecosystem and plant type responses to global change. *Global Change Biology* 10:105–123.
- Zimov SA, Davydov SP, Zimova GM, Davydova AI, Schuur EAG, Dutta K, Chapin FS. 2006. Permafrost carbon: Stock and decomposability of a globally significant carbon pool. *Geophysical Research Letters* 33.

APPENDIX I

TABLES OF DATA MEASUREMENTS AND CALCULATIONS

Table 1: Data measurements of depth corrected for compaction (cm), soil bulk density (g/cm³), wt. % Carbon, carbon (g/cm³), and radionuclide activity (Bq/kg) and corresponding errors (Bq/kg).

Sample name	Corrected Depth (cm)	Dry Bulk Density (g/cm ³)	wt. % C dry mass	C (g/cm ³)	TOTAL Pb-210 (Bq/kg)	Pb-210 Error (Bq/kg)	Excess Pb-210 (Bq/kg)	137-Cs (Bq/kg)	137-Cs Error (Bq/kg)	7-Be (Bq/kg)	7-Be Error (Bq/kg)
CTL5 0-1	0.66	0.016	39.35	0.006	428.2	29.1	398.9	9.3	2.5	16.9	1.5
CTL5 1-2	1.97	0.031	46.41	0.015	369.8	22.3	340.6	12.1	1.7	9.7	1.6
CTL5 2-3	3.28	0.046	44.35	0.020	378.3	19.5	349.1	15.2	1.5	5.0	1.0
CTL5 3-4	4.59	0.036	43.41	0.016	376.7	20.6	347.5	20.3	1.6		
CTL5 4-5	5.90	0.046	41.73	0.019	364.4	28.9	335.2	39.4	2.7		
CTL5 5-6	7.21	0.044	41.76	0.019	316.4	17.0	287.2	54.4	1.9		
CTL5 6-7	8.52	0.045	39.78	0.018	258.7	14.9	229.4	93.1	1.9		
CTL5 7-8	9.83	0.066	26.40	0.017	218.7	15.5	189.5	198.9	2.6		
CTL5 8-9	11.14	0.113	10.73	0.012	156.4	14.1	127.2	285.5	2.8		
CTL5 9-10	12.45	0.371	4.72	0.018	57.8	5.4	28.6	113.3	1.0		
CTL5 10-11	13.76	0.608	2.72	0.017	30.6	5.4		10.1	0.6		
CTL5 11-12	15.07	0.962	2.36	0.023	24.4	5.3					
CTL5 12-13	16.38	0.950	2.35	0.022	39.2	4.6					
CTL5 13-14	17.69	0.726	2.23	0.016	20.6	5.7					
CTL5 14-14.5	18.67	1.154	1.80	0.021	31.3	4.4					
LOW2 0-1	0.56	0.023	46.36	0.011	513.7	34.2	487.6	10.2	2.4	158.6	27.9
LOW2 1-2	1.67	0.040	46.83	0.019	513.3	12.3	487.2	29.9	1.0	58.6	8.8
LOW2 2-3	2.79	0.048	47.16	0.023	433.3	10.3	407.2	52.9	1.0	11.2	7.6
LOW2 3-4	3.90	0.050	47.08	0.024	321.2	14.6	295.1	77.0	2.0	26.3	12.6
LOW2 4-5	5.01	0.059	47.09	0.028	270.9	15.9	244.8	139.5	2.4		
LOW2 5-6	6.13	0.070	47.06	0.033	274.5	14.7	248.4	196.6	2.6		
LOW2 6-7	7.24	0.086	46.73	0.040	214.7	11.3	188.6	203.5	2.0		
LOW2 7-8	8.36	0.087	45.10	0.039	177.6	9.6	151.5	161.9	1.7		
LOW2 8-9	9.47	0.108	40.78	0.044	134.4	10.2	108.3	81.1	1.4		
LOW2 9-10	10.59	0.157	29.24	0.046	69.5	5.4	43.4	15.9	0.6		
LOW2 10-11	11.70	0.284	23.87	0.068	23.2	5.6		3.7	0.5		
LOW2 11-12	12.81	0.361	20.14	0.073	21.4	6.3		2.5	0.6		
LOW2 12-13	13.93	0.436	18.49	0.081	23.4	4.8		1.4	0.4		
LOW2 13-14	15.04	0.660	3.78	0.025	28.2	4.0					
LOW2 14-15	16.16	0.806	6.64	0.054	29.1	3.5					
LOW2 15-16	17.27	0.469	10.13	0.047	31.5	5.4					
CTL4 0-1	0.53	0.023	43.01	0.010	562.0	19.1	536.6	276.5	2.9		
CTL4 1-2	1.59	0.067	42.83	0.029	464.8	27.0	439.4	261.4	4.1		
CTL4 2-3	2.64	0.074	40.72	0.030	237.1	14.5	211.6	199.1	2.6		
CTL4 3-4	3.70	0.064	39.97	0.026	165.5	18.0	140.1	129.0	3.2		
CTL4 4-5	4.76	0.107	31.40	0.034	91.3	11.2	65.8	53.1	1.4		
CTL4 5-6	5.81	0.221	19.04	0.042	49.0	6.0	23.6	19.2	0.8		
CTL4 6-7	6.87	0.677	3.12	0.021	26.8	5.9					
CTL4 7-8	7.93	1.129	2.01	0.023	29.8	3.3					

CTL4 8-9	8.99	1.142	1.70	0.019	24.0	3.3					
CTL4 9-10	10.04	1.124	1.75	0.020	21.2	5.7					
INT5 0-1	0.53	0.002	44.07	0.001	446.4	42.9	409.9	10.3	4.4	305.6	35.7
INT5 1-2	1.58	0.031	44.44	0.014	449.9	17.0	413.3	10.3	1.2	59.5	12.4
INT5 2-3	2.64	0.045	42.01	0.019	513.9	22.5	477.4	29.4	1.8		
INT5 3-4	3.69	0.057	43.72	0.025	478.6	19.6	442.1	50.5	1.8		
INT5 4-5	4.74	0.064	44.35	0.029	355.5	21.1	319.0	93.2	2.7		
INT5 5-6	5.80	0.079	43.68	0.034	347.1	22.5	310.6	119.4	3.7		
INT5 6-7	6.85	0.089	42.96	0.038	232.6	15.0	196.0	166.6	2.9		
INT5 7-8	7.91	0.112	41.06	0.046	90.9	4.5	54.4	84.4	0.8		
INT5 8-9	8.96	0.134	38.48	0.052	47.5			45.4	1.3		
INT5 9-10	10.01	0.223	25.42	0.057	47.0			14.2	0.9		
INT5 10-11	11.07	0.475	11.2	0.053	31.5						
INT5 11-12	12.12	0.670	7.16	0.048	26.1						
INT5 12-13	13.18	0.806	6.24	0.050	32.5						
INT5 13-14	14.23	0.921	5.42	0.050	37.2						
INT5 14-15	15.28	0.897	5.7	0.051	34.0						
DEEP4 0-1	0.55	0.035	8.55	0.003	1147.0	23.3	1116.7	6.6	1.6	174.6	1.1
DEEP4 1-2	1.64	0.083	40.36	0.033	1197.1	21.5	1166.8	14.1	1.5	19.9	0.8
DEEP4 2-3	2.73	0.105	39.86	0.042	1335.1	22.0	1304.8	23.3	1.7	4.8	0.8
DEEP4 3-4	3.82	0.129	39.99	0.052	951.5	26.2	921.2	74.7	3.1	61.3	1.1
DEEP4 4-5	4.91	0.111	33.03	0.037	533.2	21.5	502.9	202.4	3.5		
DEEP4 5-6	6.00	0.355	12.93	0.046	125.2	8.8	94.9	100.2	1.4		
DEEP4 6-7	7.09	0.906	3.31	0.030	35.6	5.7		11.1	0.6		
DEEP4 7-8	8.18	1.183	1.62	0.019	28.2	5.6					
DEEP4 8-9	9.27	1.273	1.74	0.022	32.7	3.9					
DEEP4 9-10	10.36	1.391	1.69	0.024	30.5	5.4					
DEEP4 10-11	11.45	1.142	1.61	0.018	27.9	5.9					
DEEP4 11-12	12.55	0.986	1.75	0.017	30.8	5.9					
DEEP4 12-13	13.64	0.943	2.20	0.021	19.8	5.1					
DEEP4 13-14	14.73	0.832	2.43	0.020	30.6	5.0					
DEEP4 14-15	15.82	0.973	2.63	0.026	22.6	6.5					
DEEP4 15-16	16.91	1.253	2.67	0.033	44.4	7.2					
INT3 0-1	0.56	0.030	45.41	0.013	474.8	22.2	443.9	19.2	2.1	131.3	1.4
INT3 1-2	1.67	0.061	42.84154732	0.026	711.8	28.3	680.9	88.3	3.7	27.0	1.4
INT3 2-3	2.79	0.065	42.91534722	0.028	612.2	45.4	581.4	122.4	6.8		
INT3 3-4	3.90	0.075	44.93135413	0.034	311.5	12.1	280.6	98.4	1.5		
INT3 4-5	5.01	0.062	46.28740621	0.029	187.2	11.7	156.4	83.3	1.4		
INT3 5-6	6.13	0.082	42.23249685	0.035	121.1	18.2	90.2	64.4	2.5		
INT3 6-7	7.24	0.086	42.67319316	0.037	51.2	17.0	20.4	31.4	2.1		
INT3 7-8	8.36	0.092	43.32725543	0.040	6.5	9.3		0.8	1.0		
INT3 8-9	9.47	0.098	42.6502588	0.042	21.5	12.7		23.7	1.5		

INT3 9-10	10.59	0.162	30.3297518	0.049	35.3	10.4		23.8	1.3		
INT3 10-11	11.70	0.218	23.67048478	0.052	36.0	10.0		12.5	1.1		
INT3 11-12	12.81	0.346	15.18164174	0.053	32.3	4.1		5.3	0.4		
INT3 12-13	13.93	0.627	7.753730483	0.049	32.5	6.1					
INT3 13-14	15.04	0.852	5.342246327	0.045	35.4	5.1					
INT3 14-15	16.16	0.764	7.033727169	0.054	40.4	5.6					
INT3 15-16	17.27	0.463	11.1227446	0.052	38.0	3.8					
CTL2 0-1	0.54	0.036	36.74	0.013	403.5	12.2	373.6	6.4	1.0		
CTL2 1-2	1.63	0.092	39.61	0.022	503.4	20.5	473.5	39.9	2.1		
CTL2 2-3	2.72	0.201	22.67	0.025	264.9	10.5	235.1	158.3	1.9		
CTL2 3-4	3.81	0.457	9.46	0.024	92.8	3.7	63.0	87.4	0.7		
CTL2 4-5	4.90	0.956	7.24	0.036	55.7	5.9	25.8	59.4	1.0		
CTL2 5-6	5.99	1.654	3.45	0.024	45.3	4.9	15.5	14.9	0.6		
CTL2 6-7	7.07	2.360	2.28	0.016	24.6	3.0		1.7	0.3		
CTL2 7-8	8.16	3.355	2.05	0.020	25.5	3.7					
CTL2 8-9	9.25	4.376	1.82	0.019	29.4	4.4					
CTL2 9-10	10.34	5.442	1.92	0.020	32.6	4.9					
CTL2 10-11	11.43	6.450	1.77	0.018	38.9	5.5					
CTL2 11-12	12.51	7.388	1.84	0.017	29.1	3.2					
CTL2 12-13	13.60	8.292	1.97	0.018	26.2	2.6					
CTL2 13-14	14.69	9.195	2.08	0.019	33.5	2.9					
CTL2 14-15	15.78	10.216	2.08	0.021	24.2	5.1					
INT1 0-1	0.61	0.029	46.66	0.014	322.4	16.4	268.1				
INT1 1-2	1.83	0.063	44.64	0.015	489.5	14.5	435.1				
INT1 2-3	3.05	0.117	43.38	0.023	530.2	11.5	475.9	13.7	1.0		
INT1 3-4	4.27	0.172	42.53	0.023	489.1	13.9	434.8	20.7	1.3		
INT1 4-5	5.48	0.230	43.06	0.025	328.4	10.0	274.0	27.7	1.1		
INT1 5-6	6.70	0.288	44.97	0.026	262.8	12.5	208.4	31.9	1.4		
INT1 6-7	7.92	0.347	42.98	0.025	237.7	10.8	183.4	63.2	1.5		
INT1 7-8	9.14	0.404	43.9	0.025	260.8	17.9	206.5	123.6	2.9		
INT1 8-9	10.36	0.462	42.72	0.025	238.9	8.6	184.5	244.9	2.0		
INT1 9-10	11.58	0.528	41.53	0.027	172.6	7.8	118.2	317.2	1.9		
INT1 10-11	12.80	0.598	39.48	0.028	116.3	13.1	61.9	159.0	2.7		
INT1 11-12	14.02	0.664	38.49	0.025	59.0	6.7		84.7	1.2		
INT1 12-13	15.23	0.753	34.05	0.030	49.7	7.3		25.2	0.9		
2012CTL-2 0-1	1.20	0.024	35.81	0.009	105.8	9.5	57.8	8.3	0.9		
2012CTL-2 1-2	1.80	0.047	40.72	0.019	379.6	35.0	331.6	15.3	3.3		
2012CTL-2 2-3	2.76	0.043	40.05	0.017	427.8	22.8	379.8	21.9	2.2		
2012 CTL-2 3-4	3.72	0.046	39.16	0.018	495.0	23.2	447.0	21.9	2.2		
2012CTL-2 4-5	4.92	0.053	40.35	0.021	643.0	19.6	595.0	22.4	1.7		
2012CTL-2 5-6	6.00	0.038	39.27	0.015	386.2	17.5	338.2	91.5	2.2		
2012CTL-2 6-7	7.20	0.046	38.32	0.018	269.2	13.1	221.2	153.3	2.1		

2012CTL-2 7-8	8.28	0.061	35.63	0.022	226.7	11.5	178.7	149.1	1.8		
2012CTL-2 8-9	9.12	0.088	22.71	0.020	34.0	5.5	149.1	149.1	1.8		
2012CTL-2 9-10	10.32	0.217	7.92	0.017	51.7	6.0		12.7	0.6		
2012CTL-2 10-11	11.82	0.543	3.98	0.022	50.0	5.8		3.5	0.5		
2012CTL-2 11-12	13.62	0.578	2.84	0.016	41.6	6.7					
2012CTL-2 12-13	15.42	0.627	2.72	0.017	67.3	16.7					
2012CTL-1 0-1	0.62	0.039	41.10	0.016	232.0	34.8	185.9	65.3	10.1		
2012CTL-1 1-2	1.85	0.035	39.38	0.014	140.1	18.6	94.0	11.5	1.9		
2012CTL-1 2-3	3.08	0.034	40.80	0.014	203.5	15.5	157.4	19.6	1.6		
2012 CTL-1 3-4	4.31	0.041	40.39	0.016	233.0	17.1	186.9	17.7	1.7		
2012CTL-1 4-5	5.54	0.043	41.56	0.018	184.1	12.1	137.9	25.4	1.3		
2012CTL-1 5-6	7.08	0.060	41.86	0.025	190.1	9.9	143.9	61.1	1.4		
2012CTL-1 6-7	8.31	0.043	39.88	0.017	205.7	20.5	159.6	162.7	3.7		
2012CTL-1 7-8	9.54	0.068	39.69	0.027	182.8	17.9	136.6	172.1	3.3		
2012CTL-1 8-9	10.77	0.066	38.28	0.025	211.4	12.2	165.2	140.2	2.2		
2012CTL-1 9-10	12.31	0.070	33.16	0.023	138.0	13.7	91.9	86.9	2.1		
2012CTL-1 10-11	13.54	0.055	33.56	0.018	105.2	10.6	59.0	62.3	1.5		
2012CTL-1 11-12	14.77	0.038	31.78	0.012	126.1	12.8	79.9	60.9	1.7		
2012CTL-1 12-13	16.00	0.046	29.04	0.013	81.0	10.5	34.9	45.2	1.4		

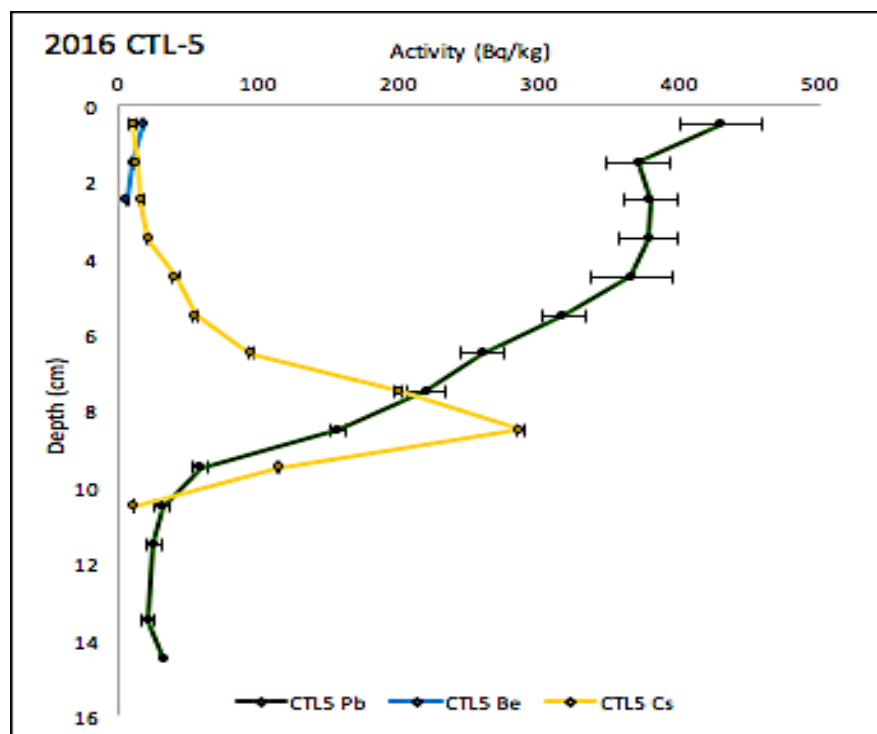
Table 2: Table showing the post/pre or unaffected carbon accumulation rates and corresponding error

SAMPLE NAME	Post SF seed rate (mgC/yr)	Error for Post SF seed rate (mgC/yr)	Pre SF seed rate (mgC/yr)	Error for Pre SF seed rate (mgC/yr)	Accumulation rate ratio (post/pre seed rates for non-changing slopes (mgC/yr)/Error for non-changing seed rates (mgC/yr)	Pre SF seed rate (mgC/yr)	Error for Pre SF seed rate (mgC/yr)	Accumulation rate ratio (post/pre seed rates for non-changing slopes (mgC/yr)/Error for non-changing seed rates (mgC/yr)
CT1-5	5.955	1.008	0.454	0.131	13.123	/	/	/
CT1-4	/	/	/	/	/	1.576	0.134	0.134
CT1-2	/	/	/	/	/	1.054	0.205	0.205
2012 CT1-2	/	/	/	/	/	0.948	0.161	0.161
LOW-2	4.324	0.713	2.558	0.538	1.690	/	/	/
INT-5	4.992	0.718	1.113	0.248	4.466	/	/	/
INT-3	5.480	0.0004	1.166	0.138	4.701	/	/	/
DEEP-4	4.613	0.013	0.858	0.174	X	/	/	/

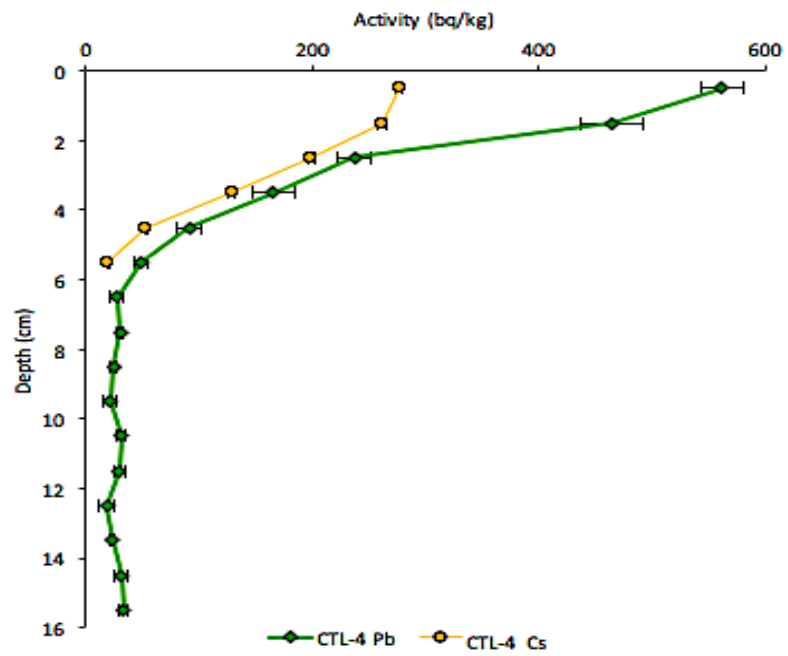
APPENDIX II

GRAPHS CREATED FOR ALL CORES ANALYZED

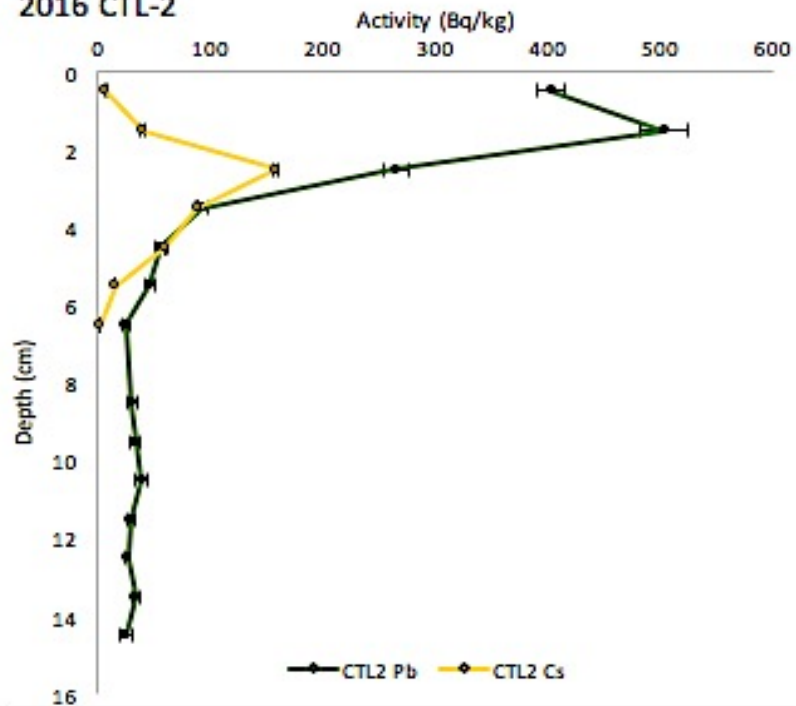
2016 Core Radionuclide Profiles vs. depth: Radionuclide profiles of 2016 cores counted on a high purity Ge gamma spectrometer. All radionuclide activities were measured in Bq/kg dry mass. ^{210}Pb is represented in green, ^{7}Be is represented in blue, and ^{137}Cs is represented in yellow.

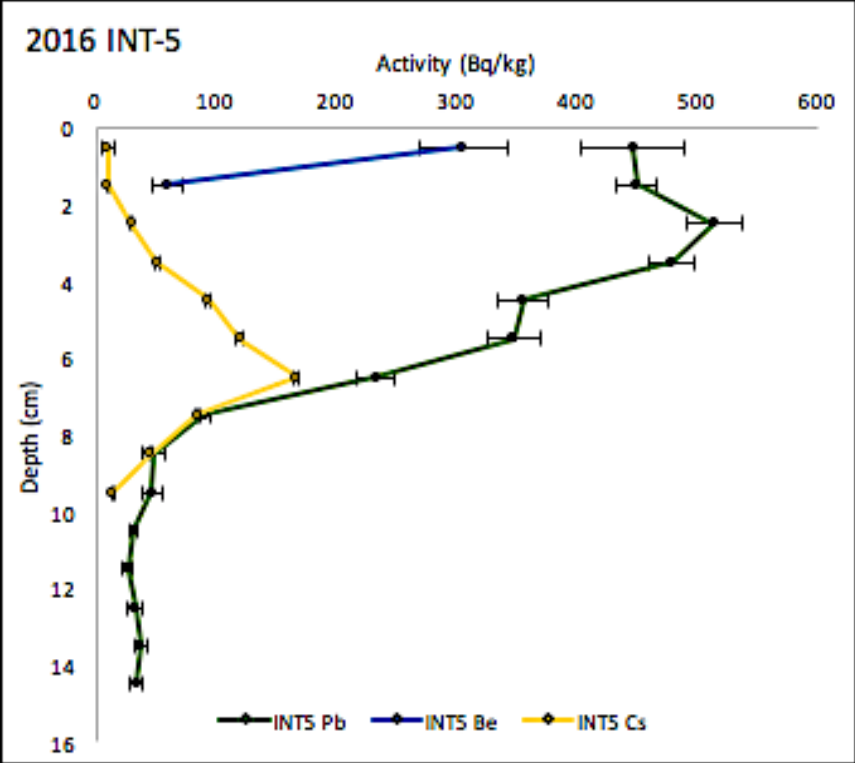
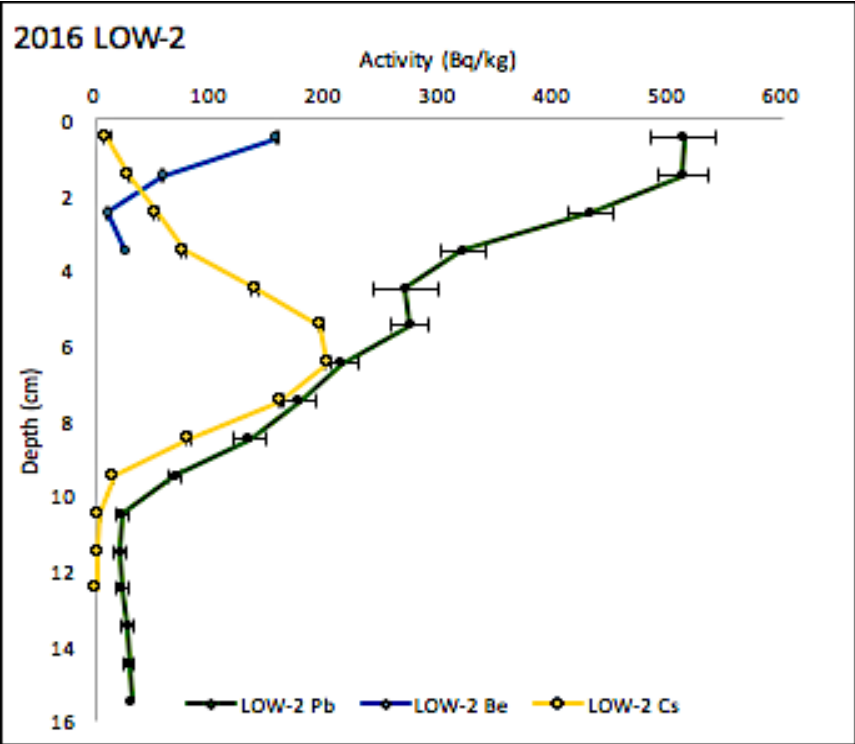


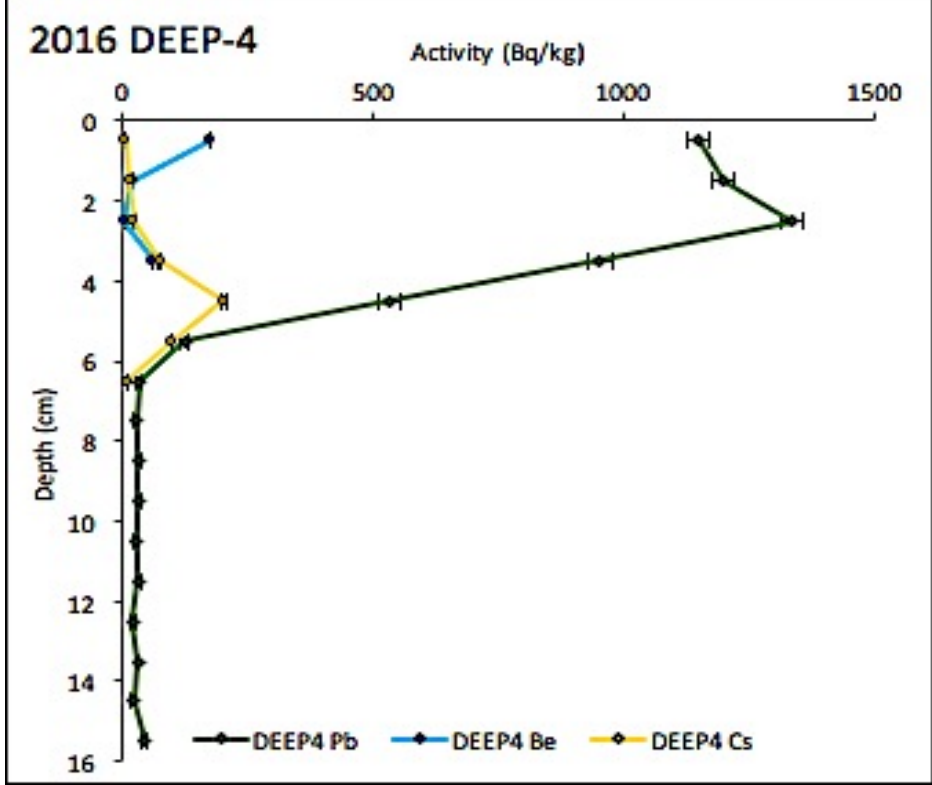
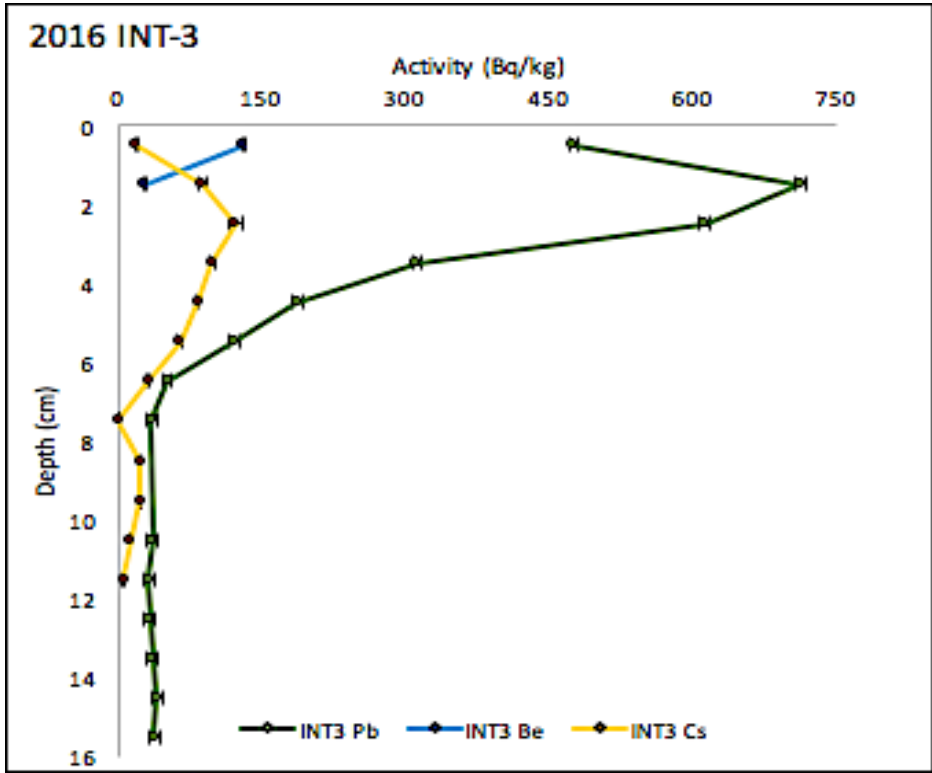
2016 CTL-4



2016 CTL-2

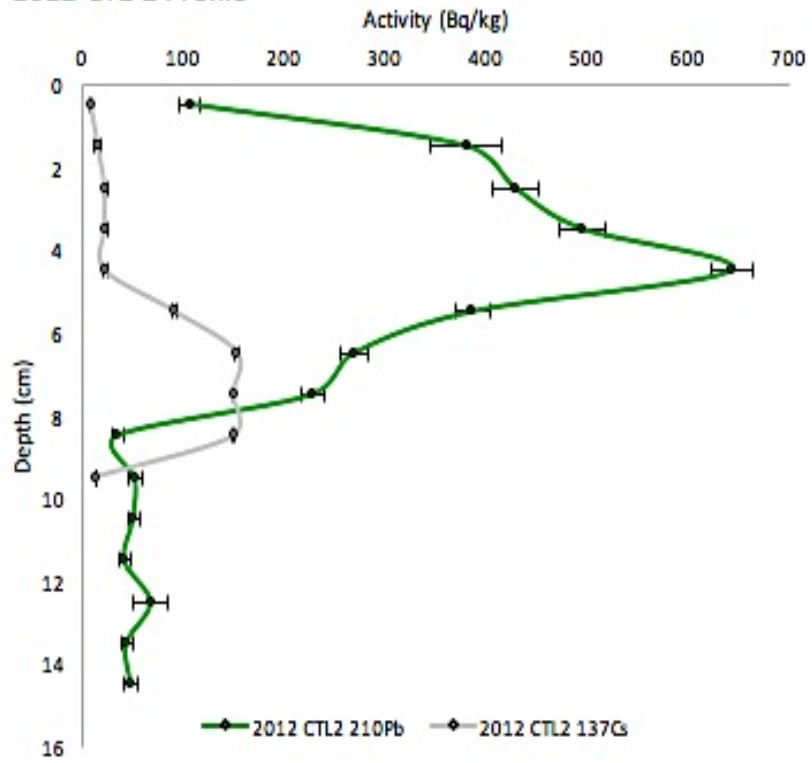




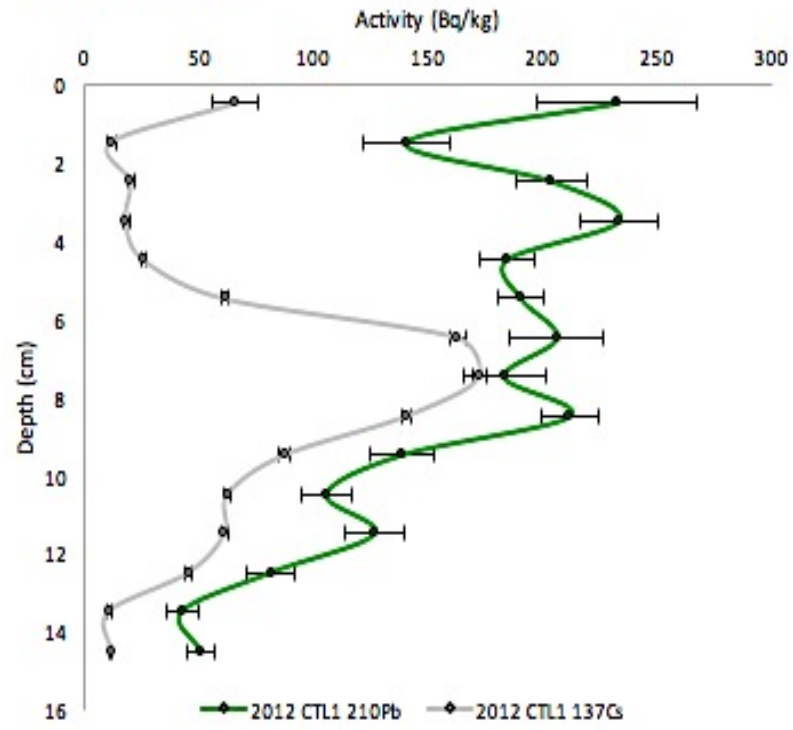


2008 and 2012 Core Radionuclide Profiles vs. depth: Radionuclide profiles of 2008 and 2012 cores counted on a high purity Ge gamma spectrometer. All radionuclide activity was measured in Bq/kg dry mass. ^{210}Pb is represented in green, and ^{137}Cs is represented in gray.

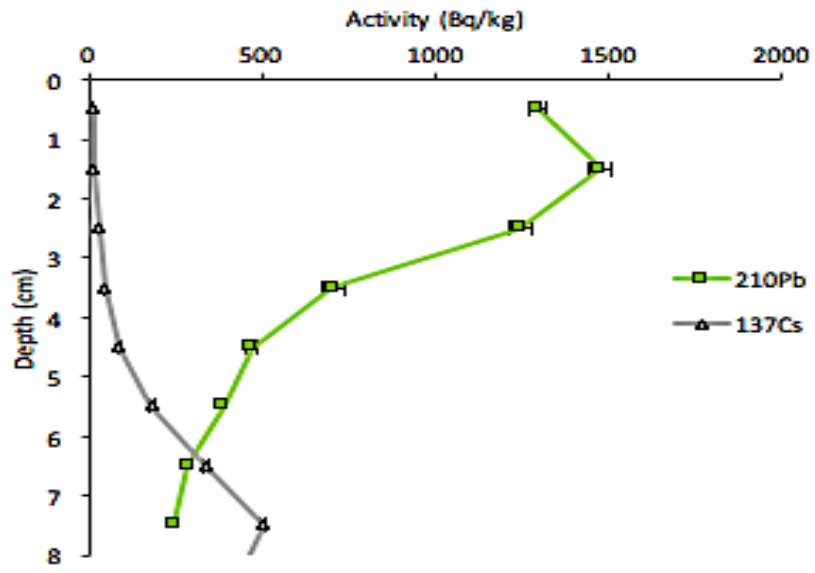
2012 CTL-2 Profile

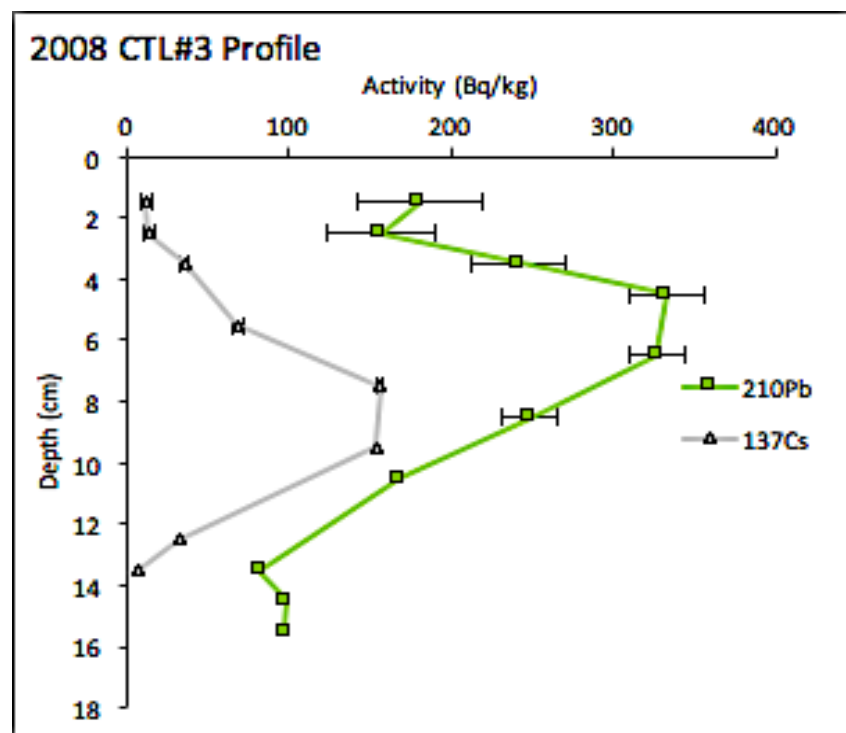
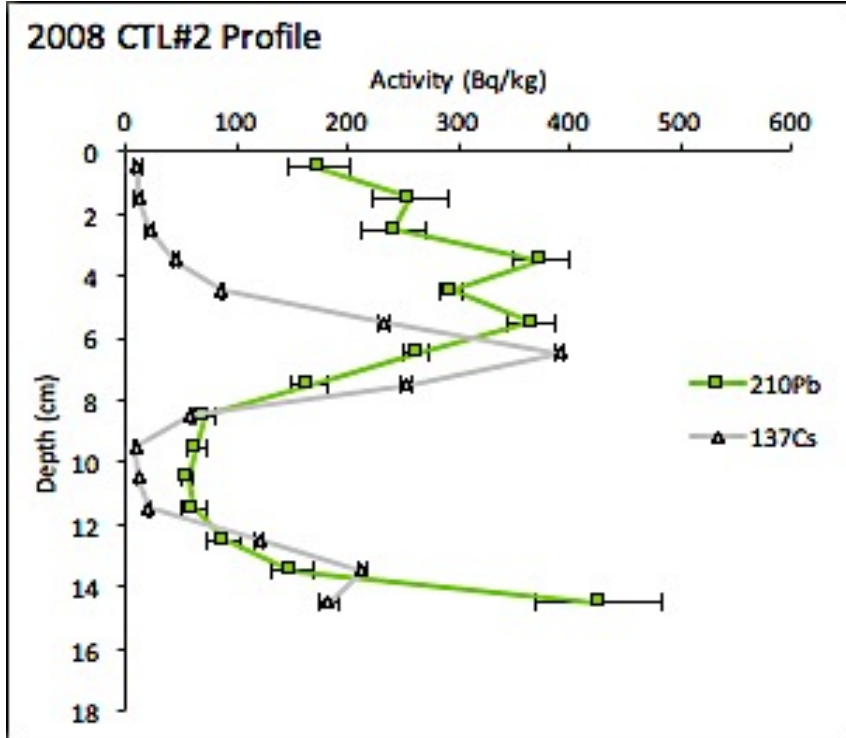


2012 CTL-1 Profile

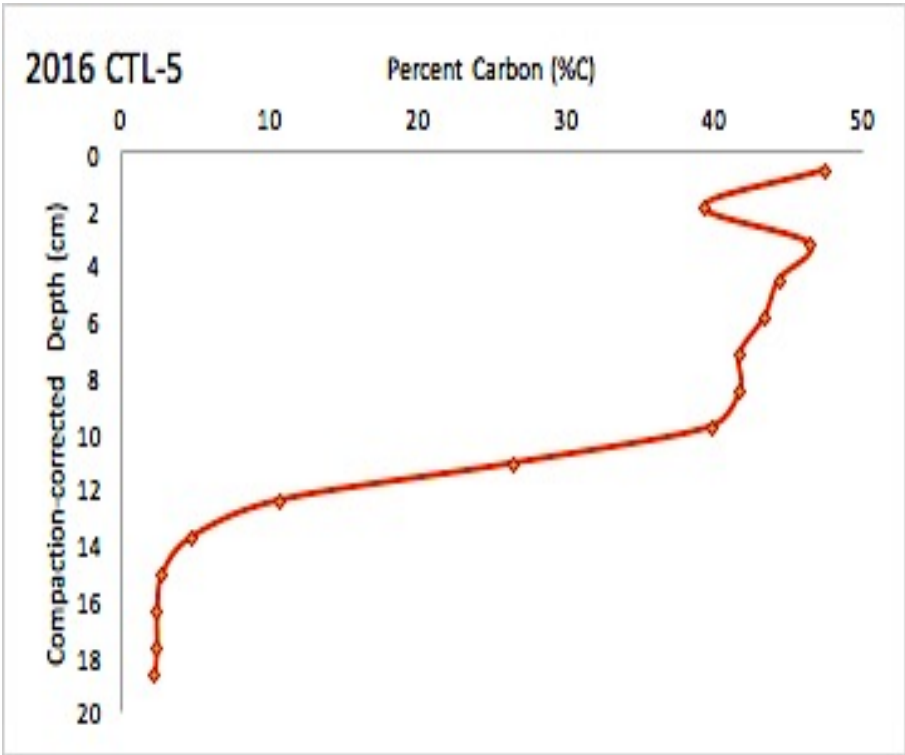


2008 CTL#1 Profile

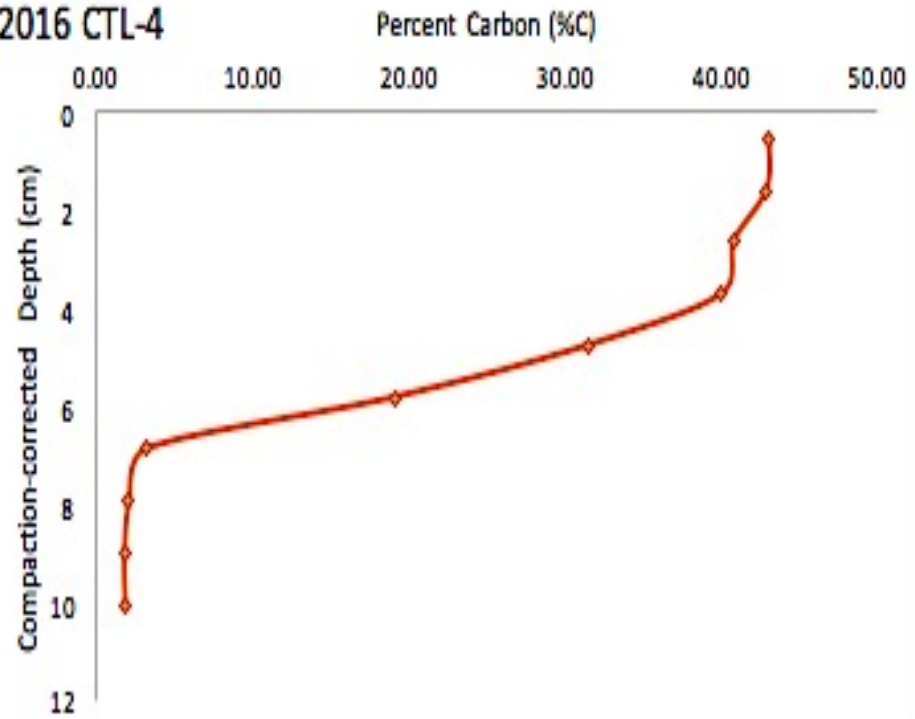




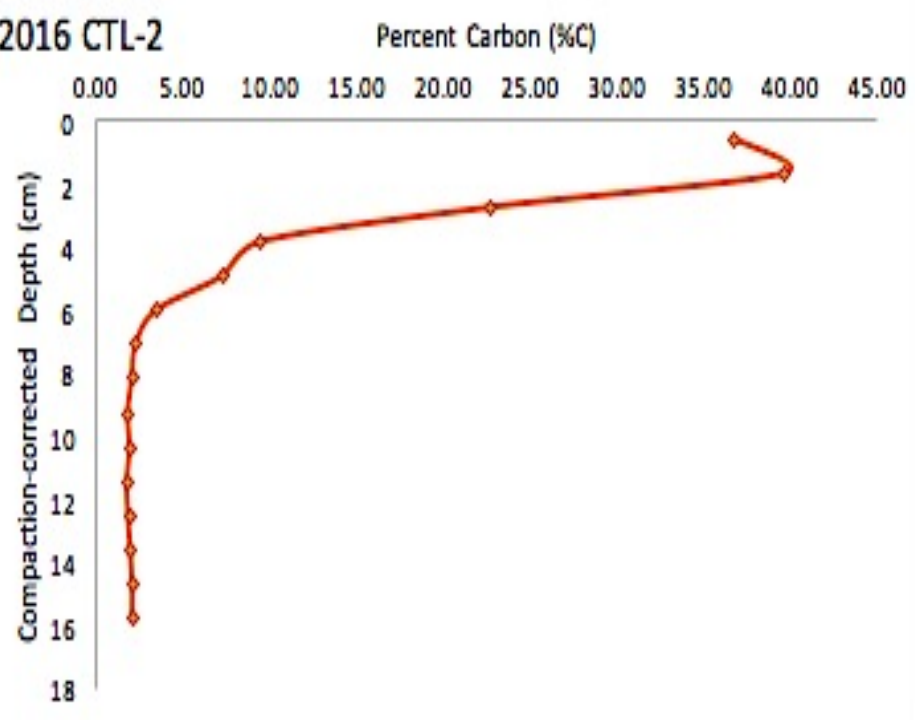
2016 Cores wt. % Carbon vs. Depth (cm): Graphs of 2016 cores percent carbon with depth. Wt. % carbon is calculated on dry mass basis with relative errors of 2%, and significantly decreases with depth, where biologically-driven carbon decomposition and respiration is likely occurring. All cores, despite snow depth location had similar %C vs depth graphs.

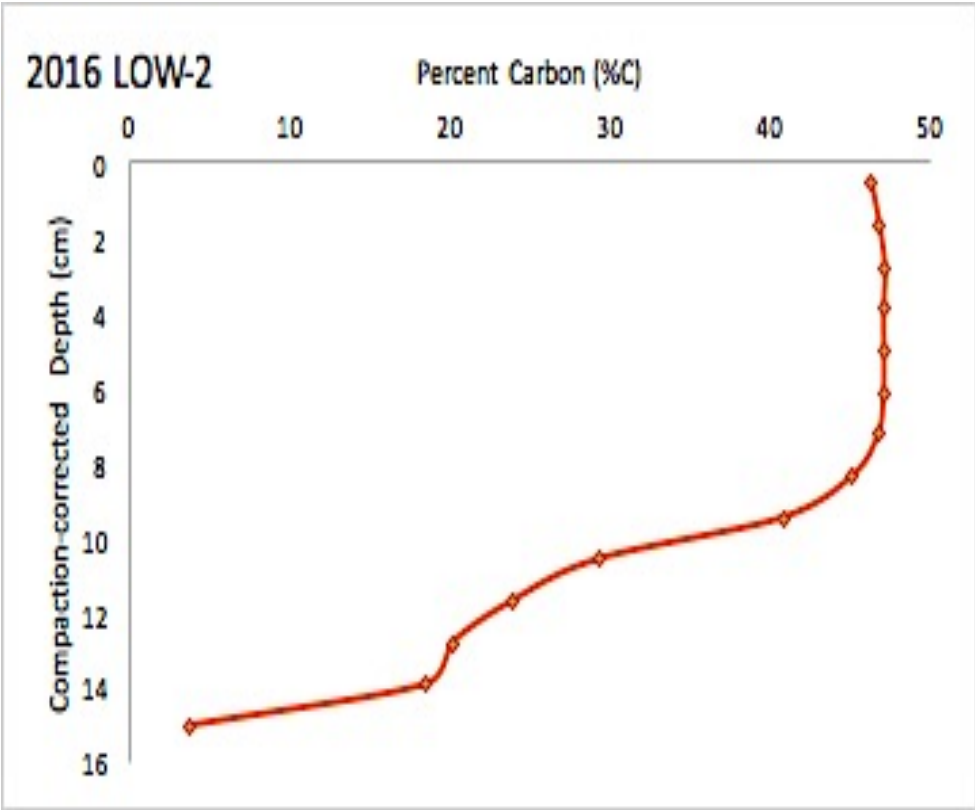


2016 CTL-4



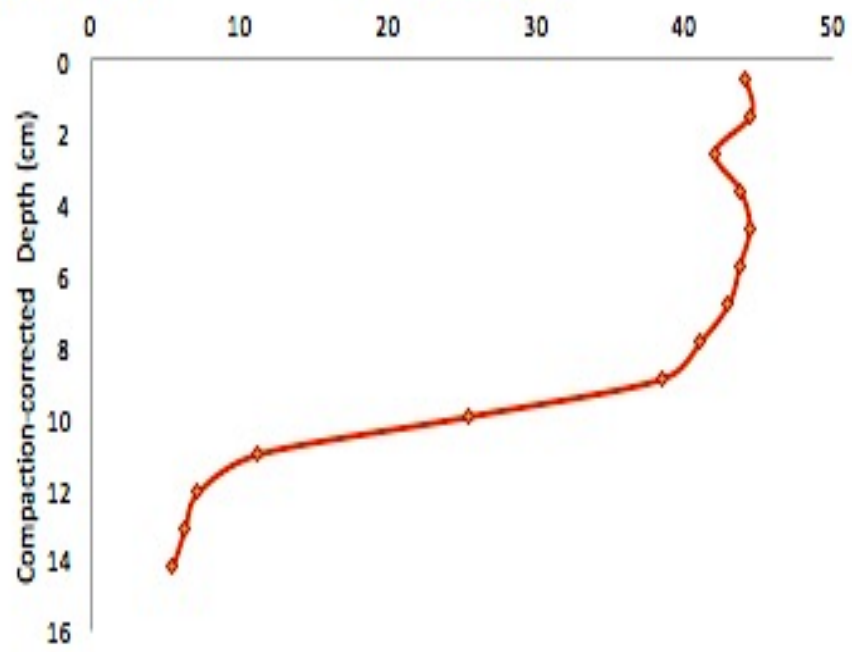
2016 CTL-2





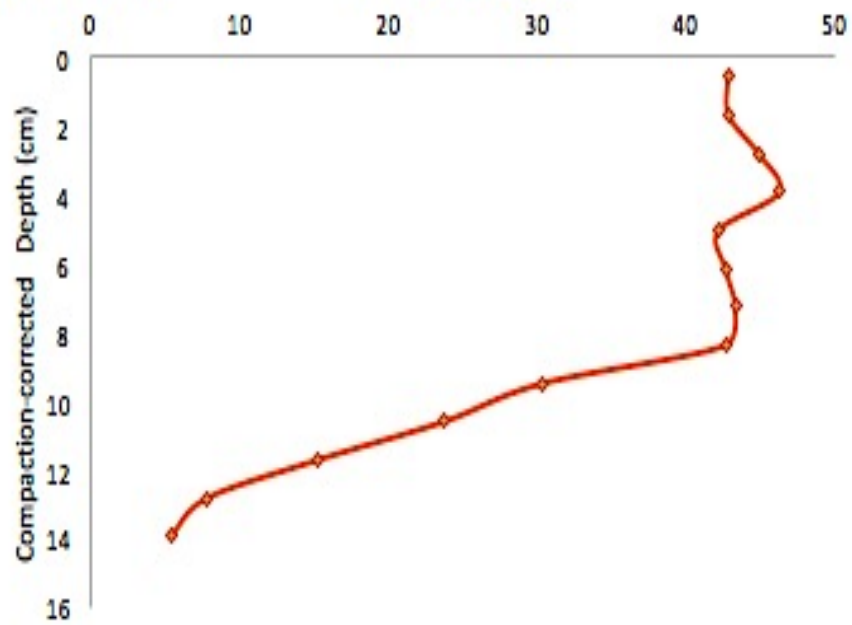
2016 INT-5

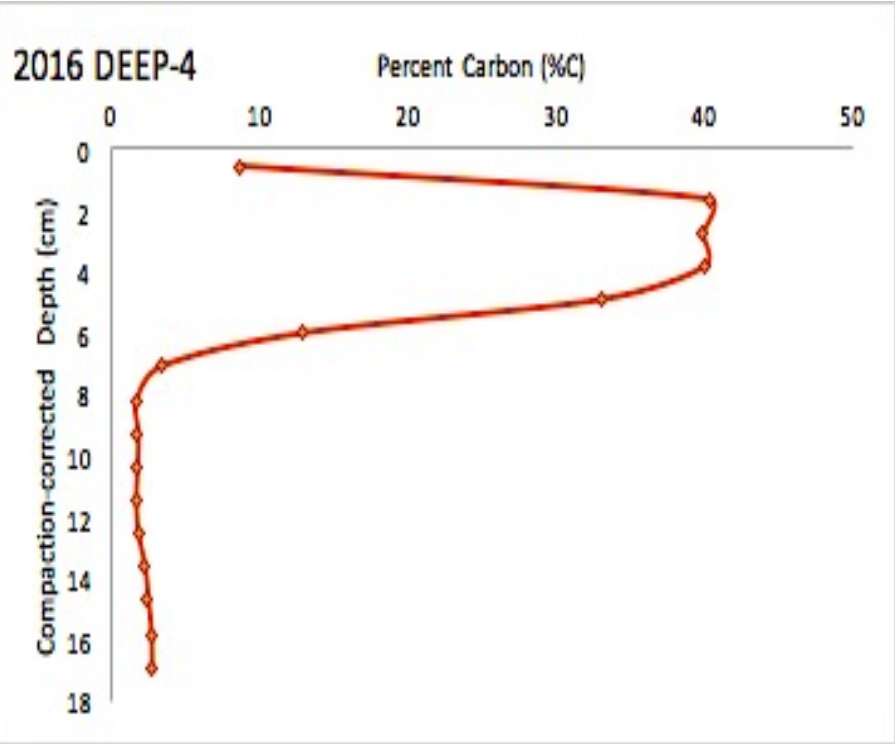
Percent Carbon (%C)



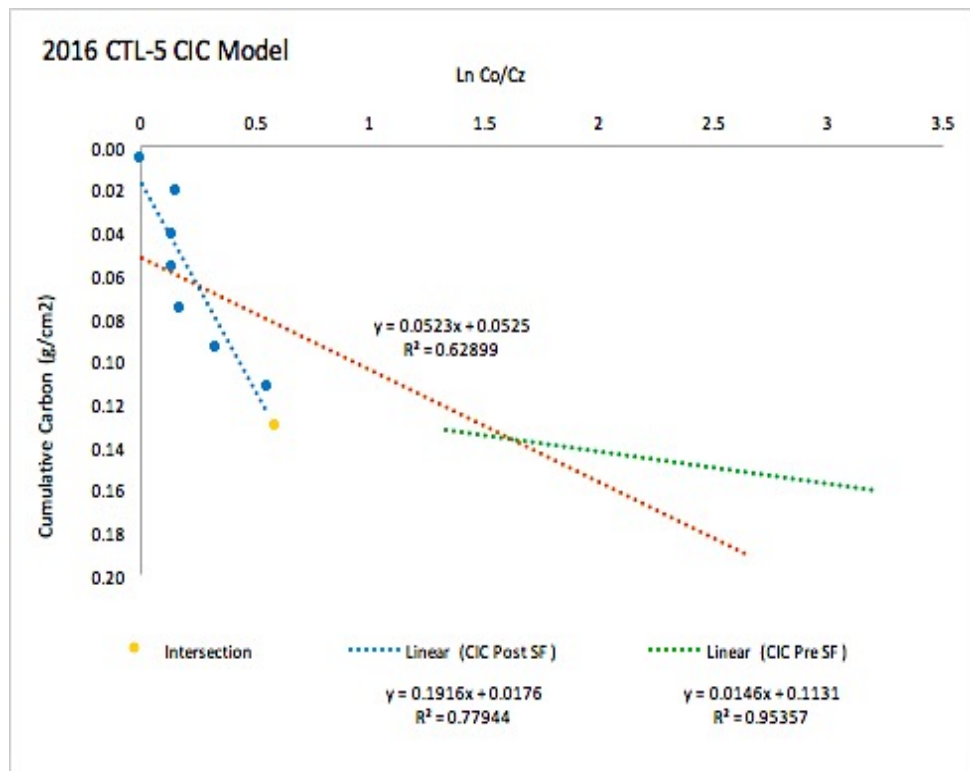
2016 INT-3

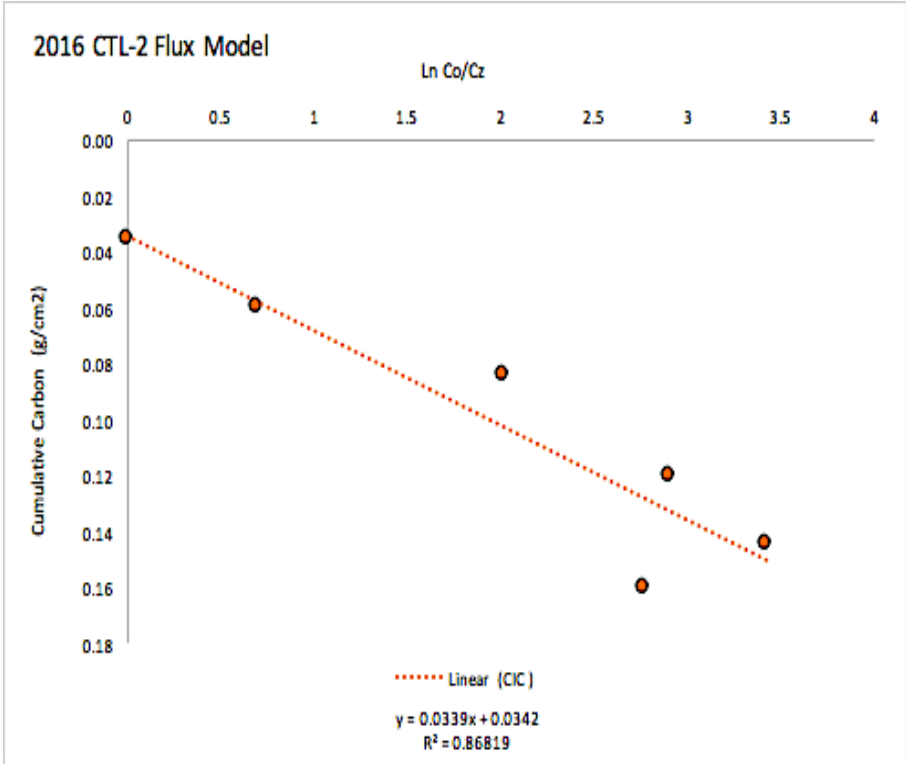
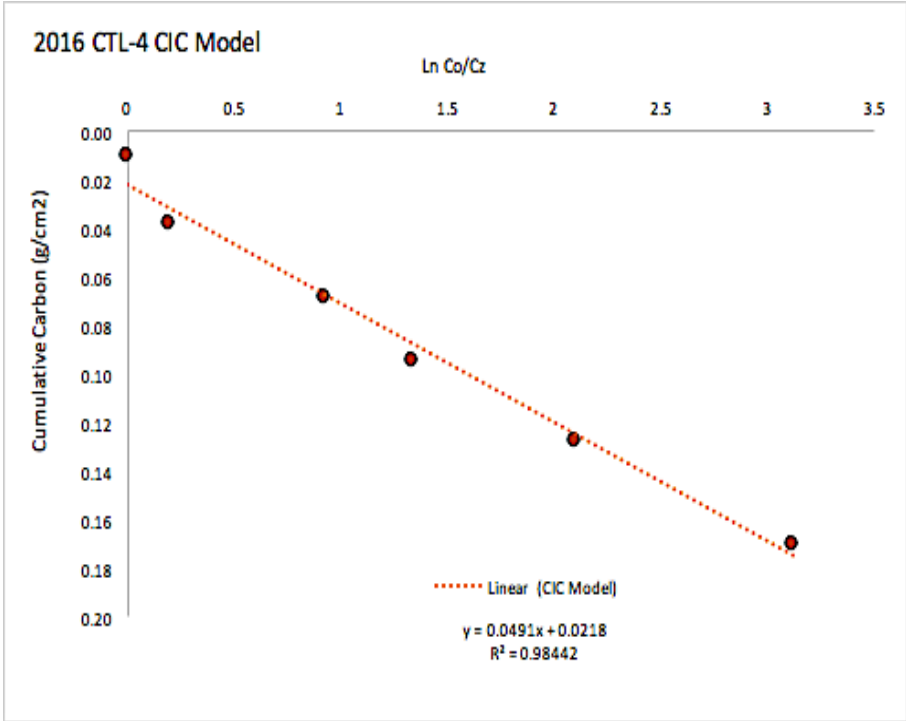
Percent Carbon (%C)

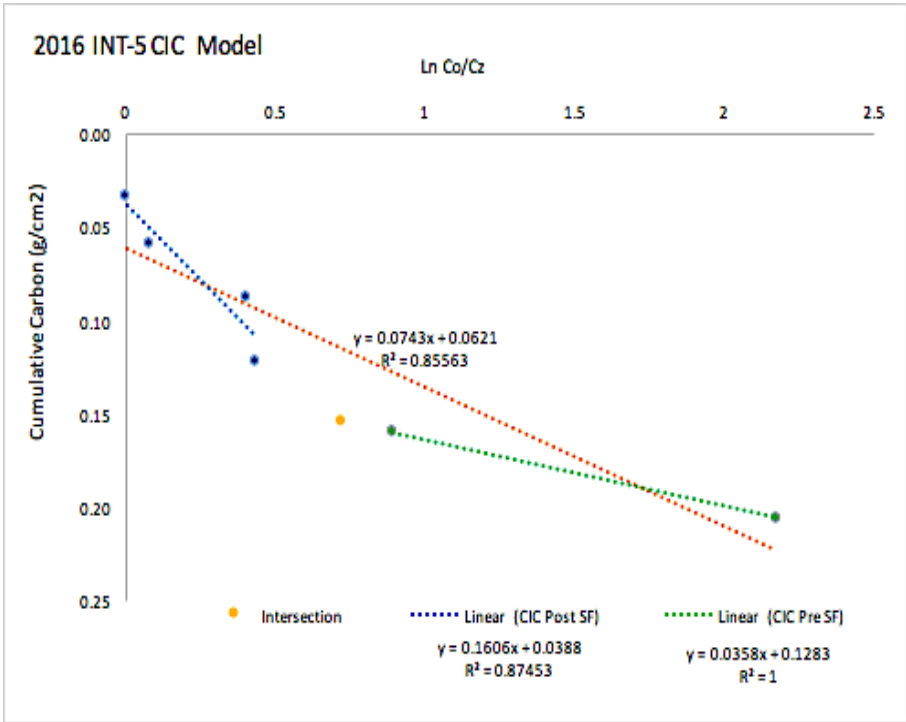
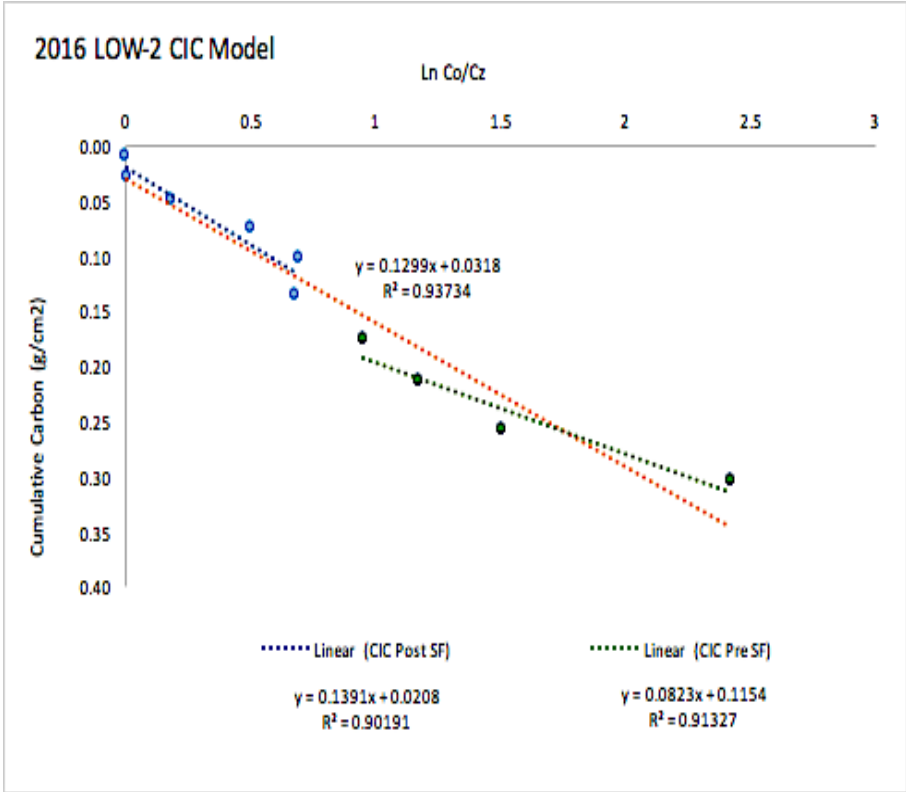


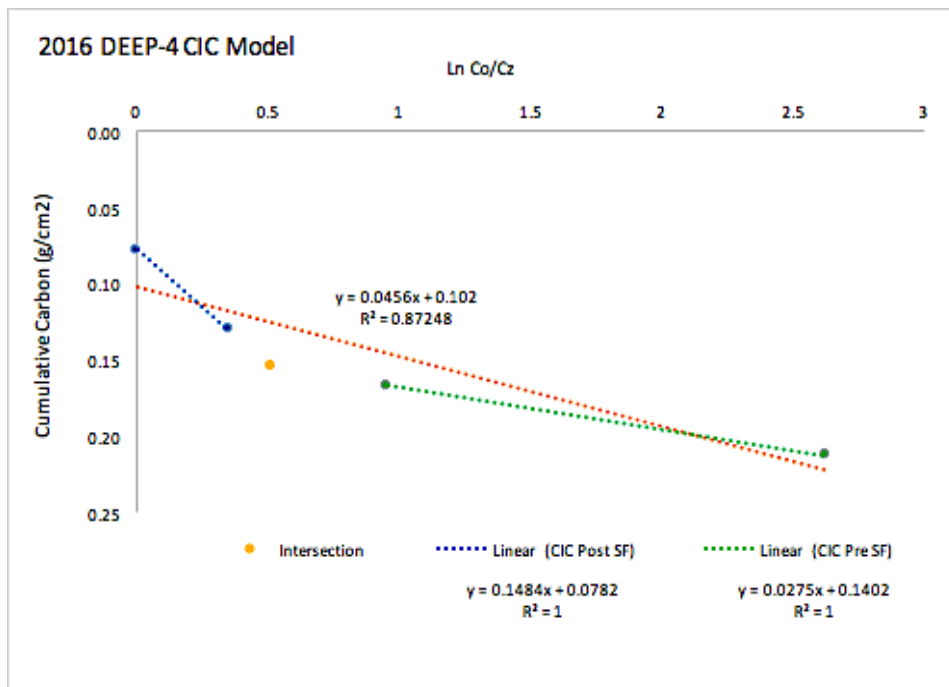
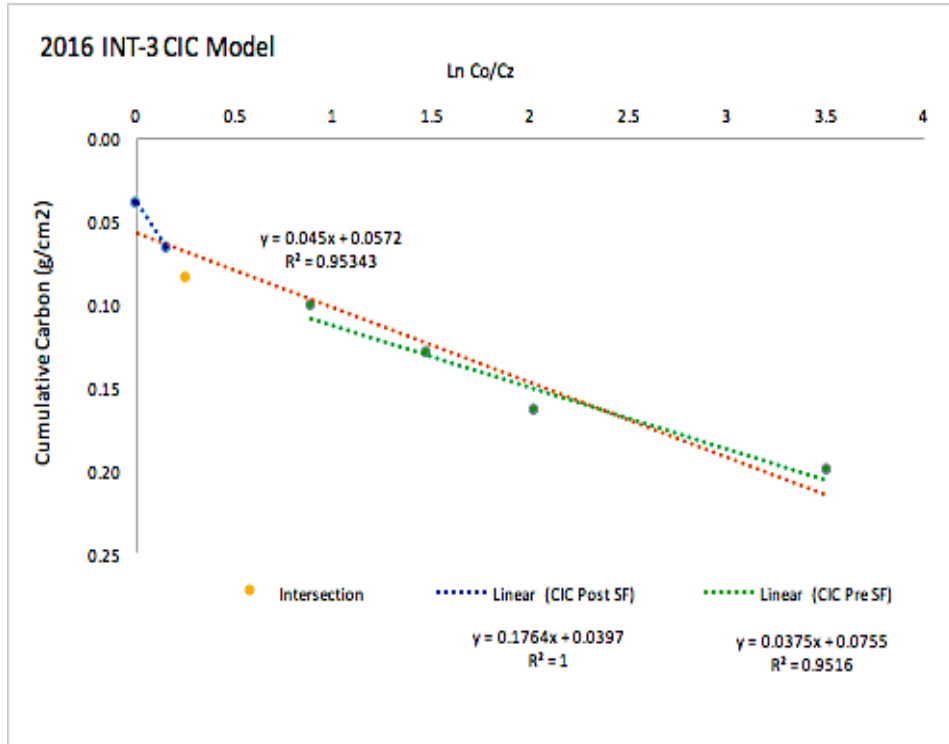


2016 Cores Intersection CIC Graphs: Graphs of the standard CIC models created for cores in a first attempt to calculate carbon accumulation rate in Toolik snow fence cores. The orange trendline and corresponding equation show the standard CIC model of the core. Due to the distinct correlation and our knowledge of the changing ^{210}Pb deposition in some cores, the intersection point approach and modified CIC model was then created (see results). Post- snow fence represented in blue, pre- snow fence represented in green.



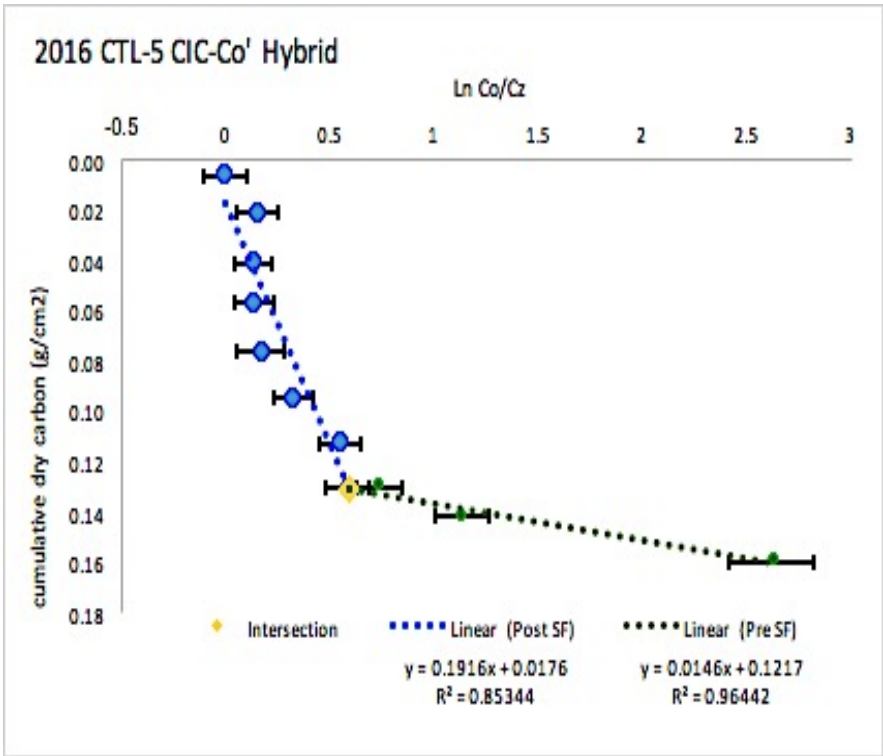


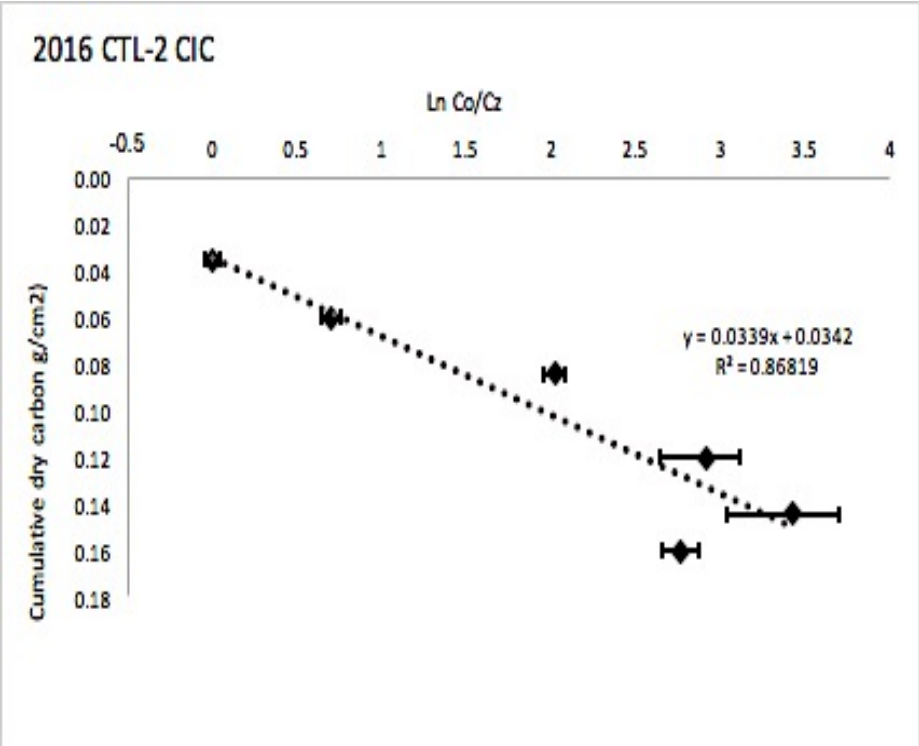
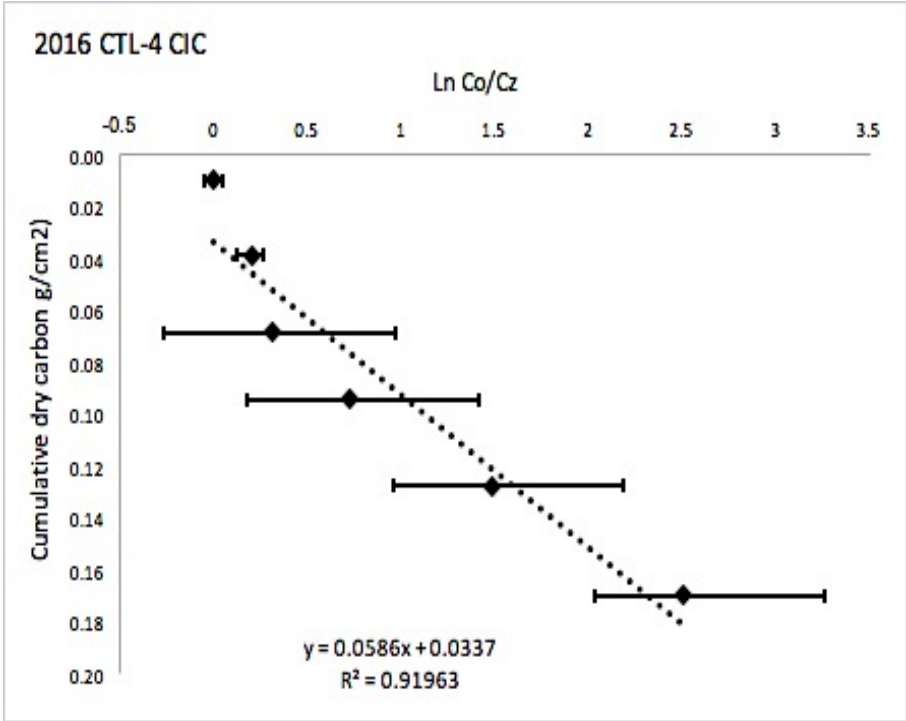


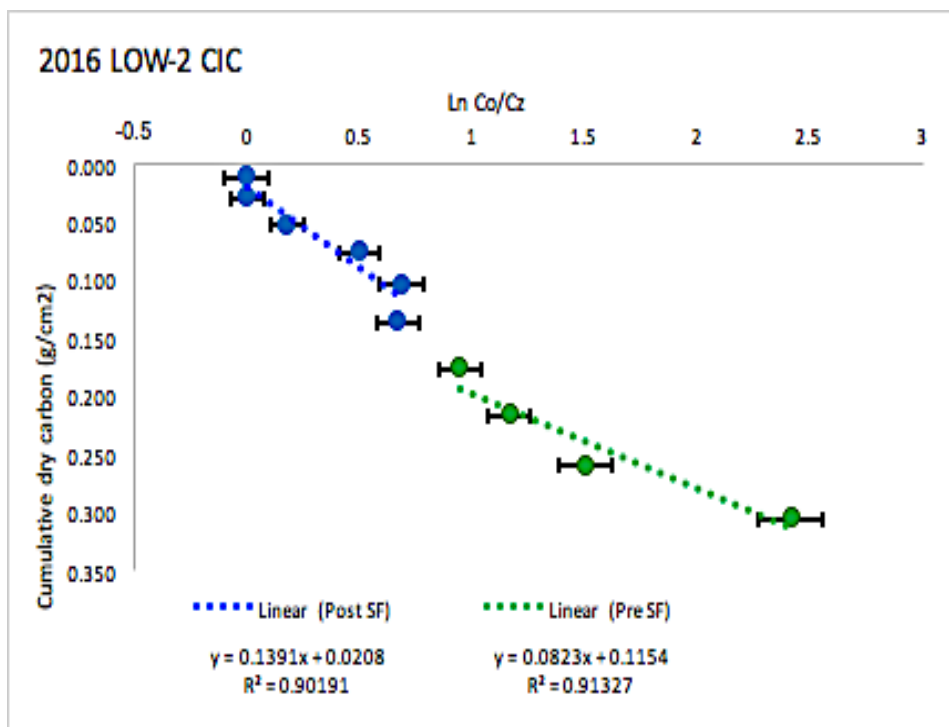
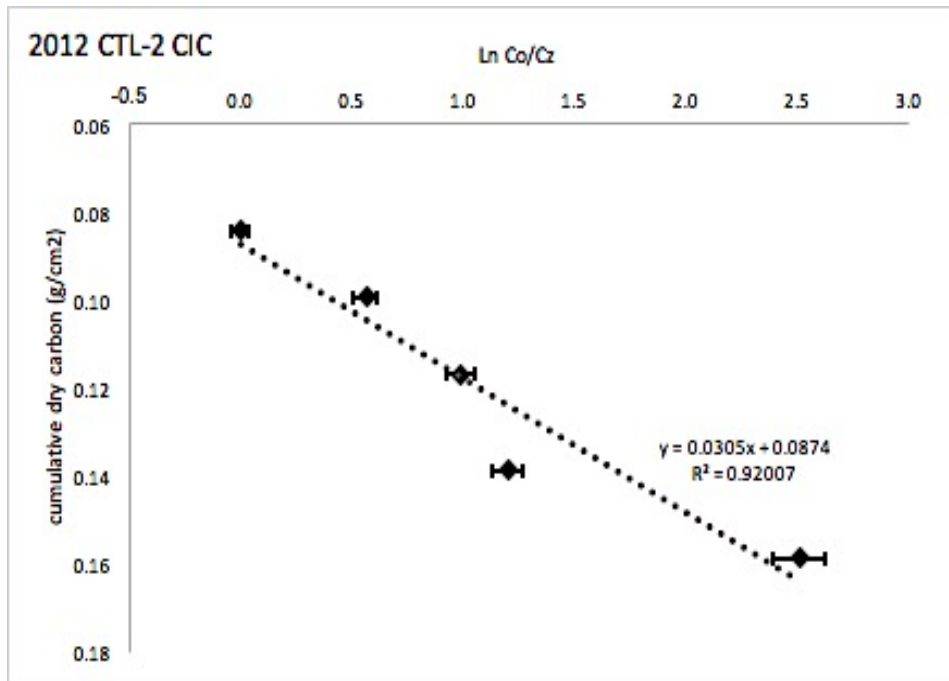


2016 and 2012 Finalized Adjusted CIC-Co' Hybrid graphs and CIC Models:

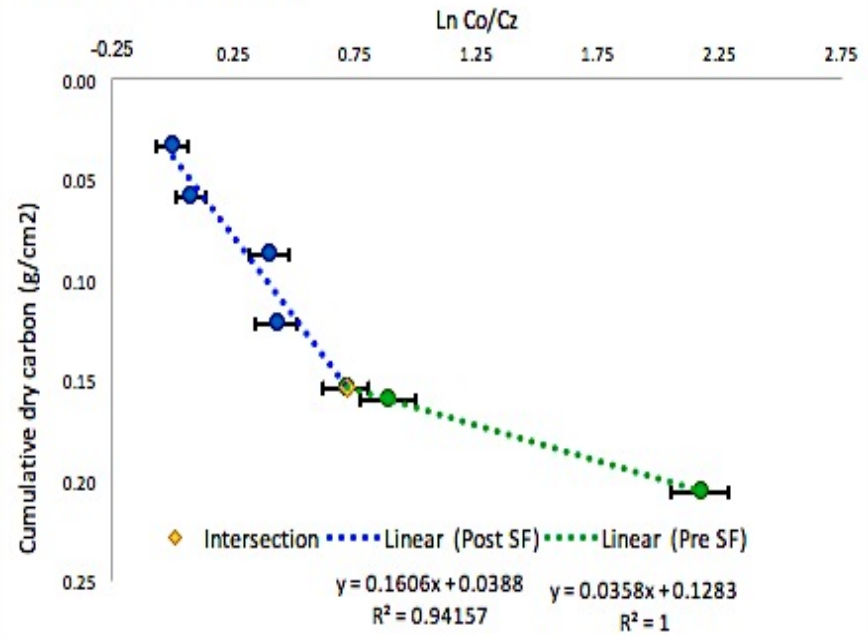
Graphs of the modified CIC model created in this study to calculate the carbon accumulation rates in the experiment cores that had significant changes in ²¹⁰Pb deposition due to the installation of the 1994 snow fence. Post- snow fence represented in blue, pre- snow fence represented in green, calculated intersection point shown in yellow.



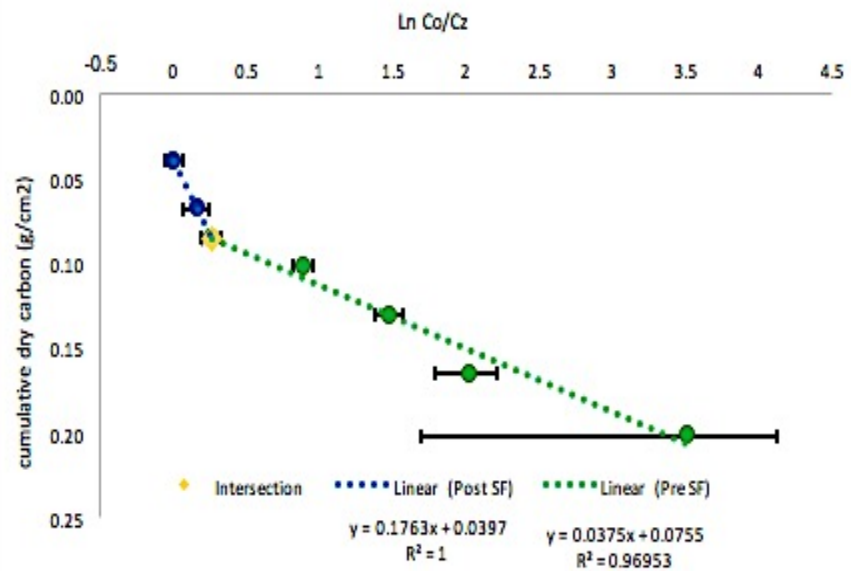




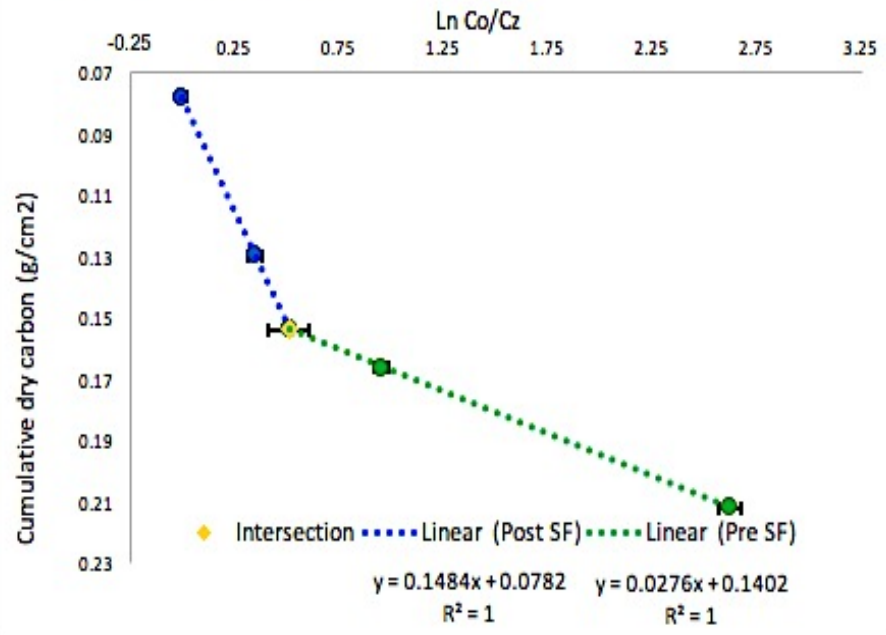
2016 INT-5 CIC-Co' Hybrid



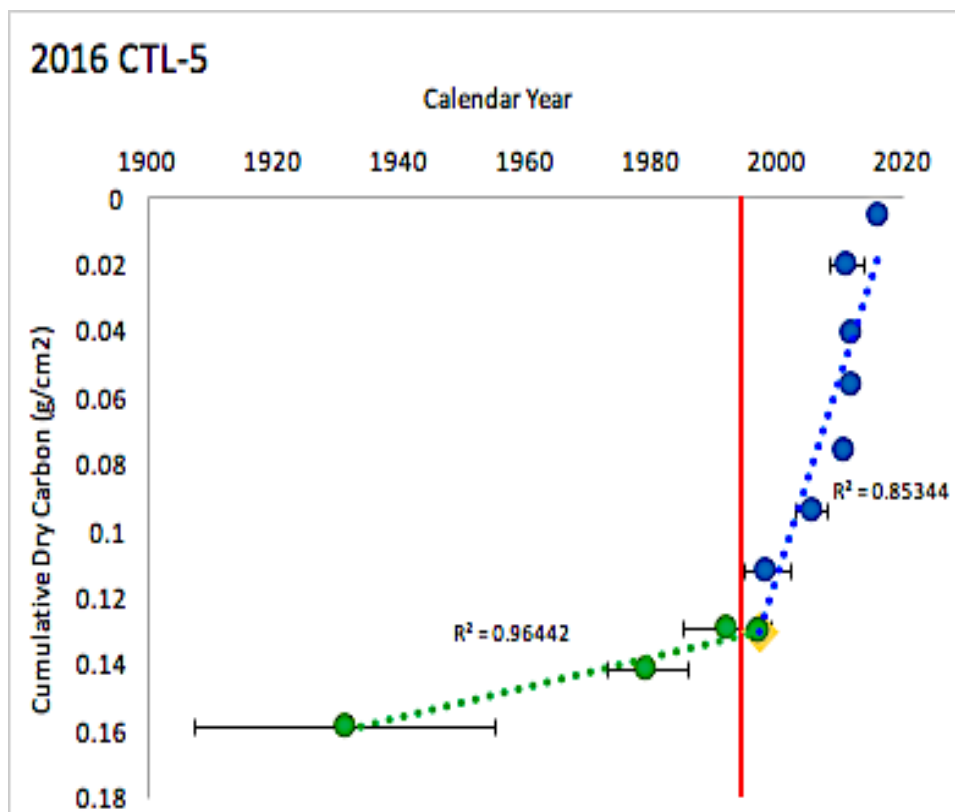
2016 INT-3 CIC-Co'-Hybrid

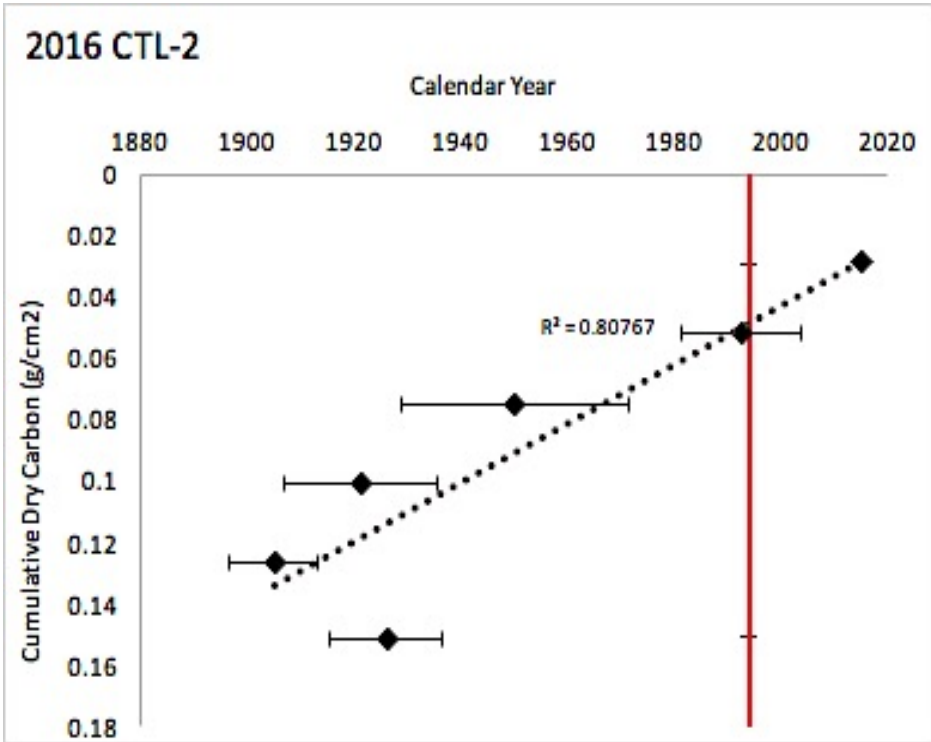
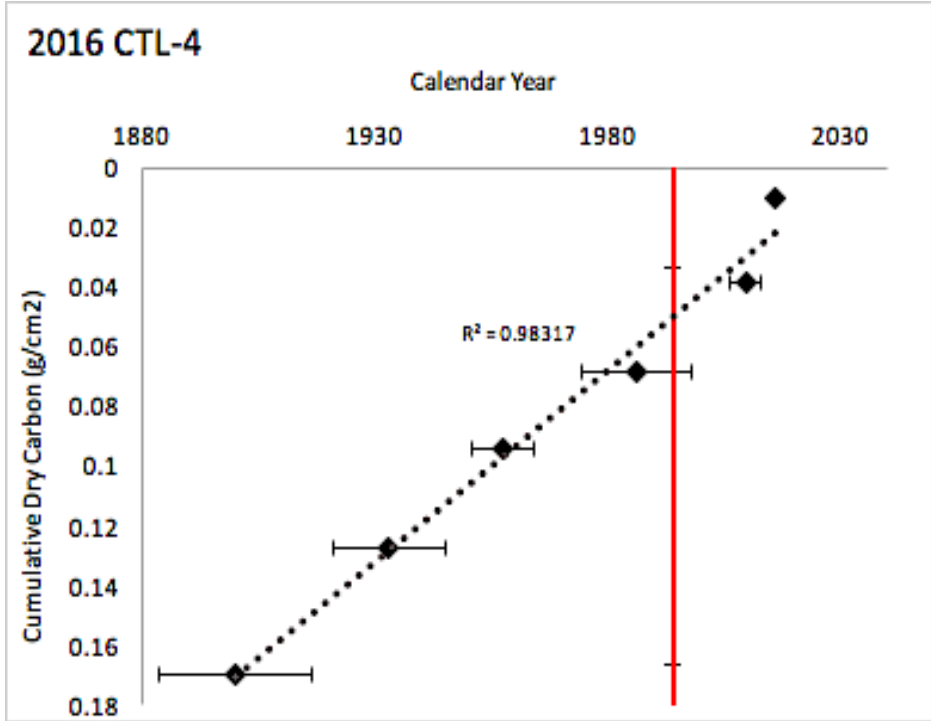


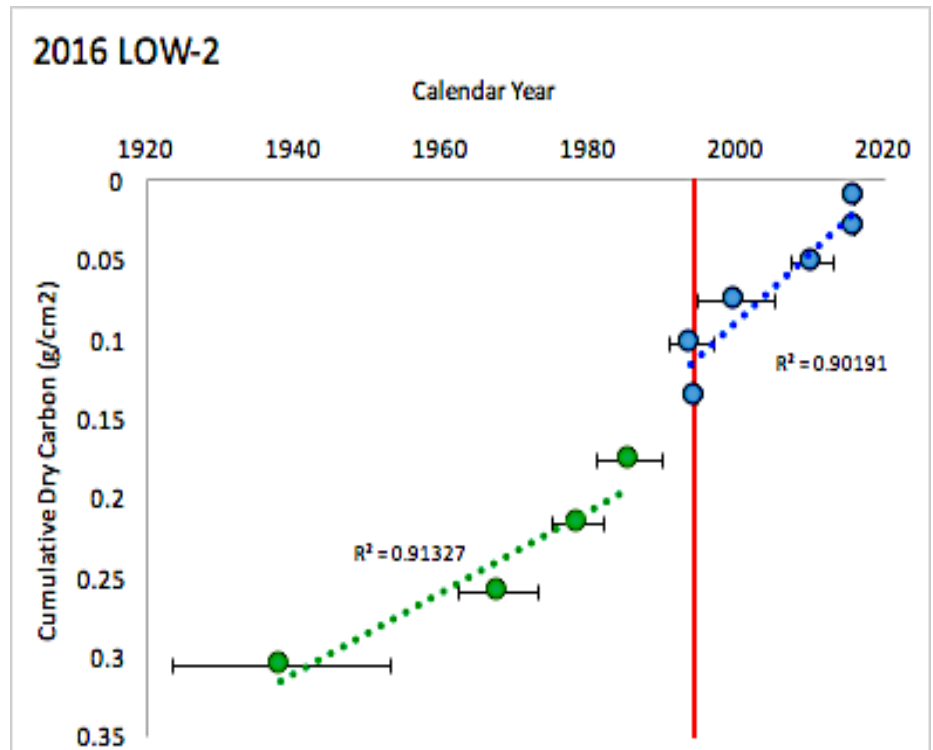
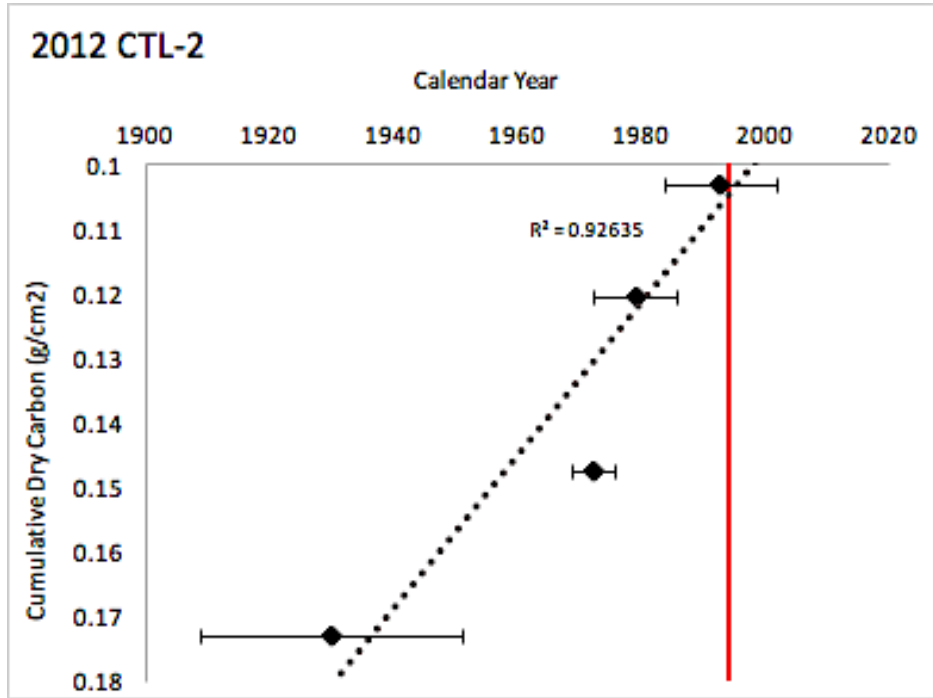
2016 DEEP-4 CIC-Co¹-Hybrid

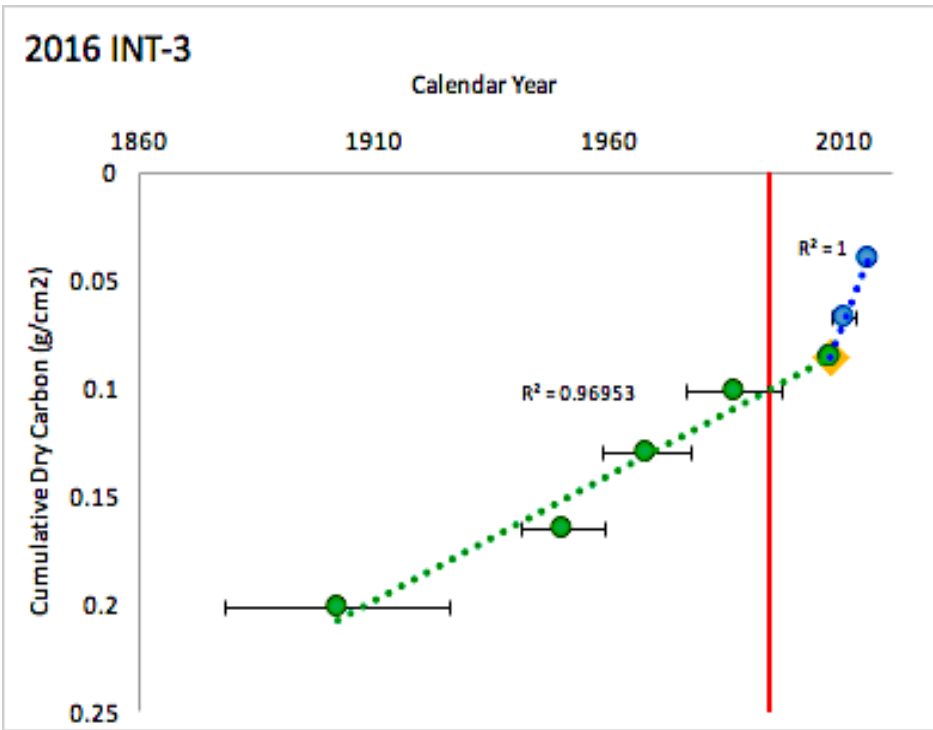
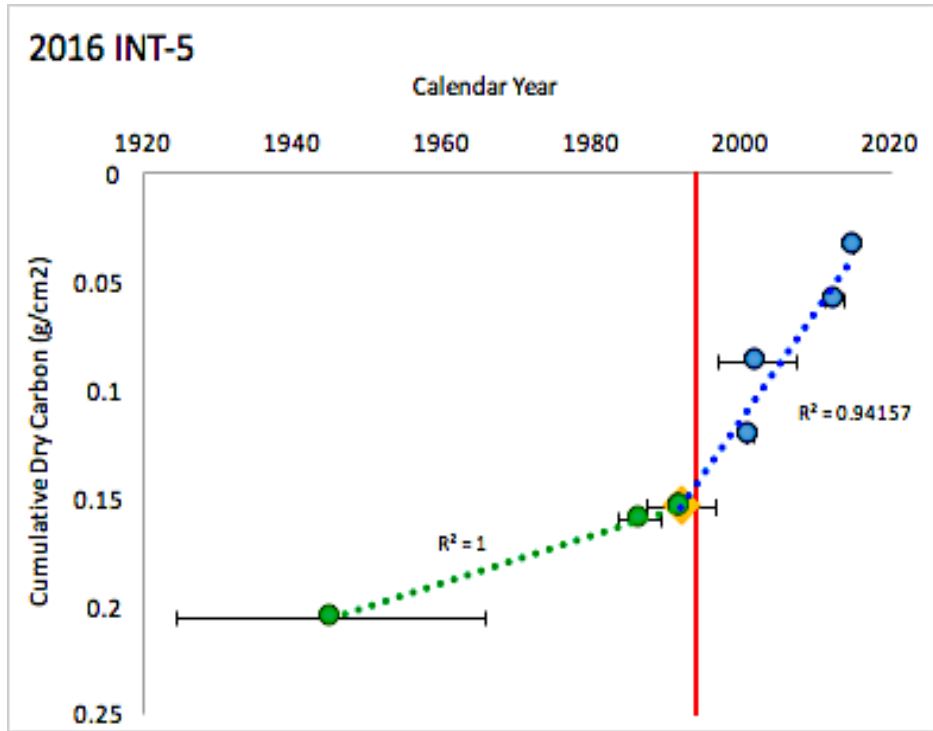


2012 and 2016 Core Age Calculation Graphs: Graphs of calculated calendar year vs. cumulative dry carbon mass with the date of the snow fence installation represented by the vertical red line. For cores showing changes in ^{210}Pb deposition, post- snow fence dated core segments are shown in blue, pre- snow fence dated core segments are shown in green, and the calculated intersection point founded in the CIC graphs is shown in yellow









2016 DEEP-4

